NASA TECHNICAL NOTE

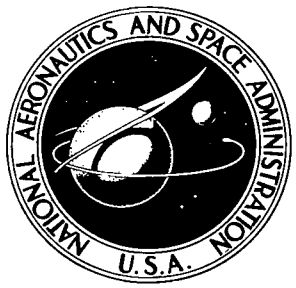

NASA TN D-6163

EXPERIMENTAL PERFORMANCE AND COMBUSTION STABILITY OF A FULL-SCALE DUCT BURNER FOR A SUPERSONIC TURBOFAN ENGINE

by J. Robert Branstetter, Albert J. Juhasz, and Peter W. Verbulecz

Lewis Research Center
Cleveland, Ohio 44135

NATIONAL AERONAUTICS AND SPACE ADMINISTRATION • WASHINGTON, D. C. • MARCH 1971

1. Report No.	2. Government Accession No.	3. Recipient's Catalog No.
NASA TN D-6163		

4. Title and Subtitle: EXPERIMENTAL PERFORMANCE AND COMBUSTION STABILITY OF A FULL-SCALE DUCT BURNER FOR A SUPERSONIC TURBOFAN ENGINE

5. Report Date: March 1971

6. Performing Organization Code:

7. Author(s): J. Robert Branstetter, Albert J. Juhasz, and Peter W. Verbulecz

8. Performing Organization Report No.: E-5679

9. Performing Organization Name and Address:
Lewis Research Center
National Aeronautics and Space Administration
Cleveland, Ohio 44135

10. Work Unit No.: 720-03

11. Contract or Grant No.:

12. Sponsoring Agency Name and Address:
National Aeronautics and Space Administration
Washington, D. C. 20546

13. Type of Report and Period Covered: Technical Note

14. Sponsoring Agency Code:

15. Supplementary Notes:

16. Abstract

A 67.7-in. (172-cm) diameter flight-weight annular diffuser and combustor assembly for the fan stream of a duct-burning turbofan underwent numerous modifications to achieve a highly efficient geometry and stable combustion. The apparatus was tested in a connected-pipe facility at conditions simulating those of a supersonic transport plane. Two zones of fuel injection provided overall fuel-air ratios of 0 to 0.050. Air entered the upstream combustion zone by means of ram-scoops. Much effort was devoted to means of combating combustion instability (70 to 470 Hz) encountered at many test conditions. These efforts, only partially successful, are described along with other performance results.

17. Key Words (Suggested by Author(s))	18. Distribution Statement
Duct burners; Combustion chambers; Combustion efficiency; Combustion stability; Performance tests; Duct-burning turbofan engines; Supersonic transports; Fuel combustion	Unclassified - unlimited

19. Security Classif. (of this report)	20. Security Classif. (of this page)	21. No. of Pages	22. Price*
Unclassified	Unclassified	84	$3.00

*For sale by the National Technical Information Service, Springfield, Virginia 22151

CONTENTS

EXPERIMENTAL PERFORMANCE AND COMBUSTION STABILITY OF A FULL-SCALE DUCT BURNER FOR A SUPERSONIC TURBOFAN ENGINE

by J. Robert Branstetter, Albert J. Juhasz, and Peter W. Verbulecz

Lewis Research Center

SUMMARY

A 67.7-inch (172-cm) diameter flight-weight annular diffuser and combustor assembly for the fan stream of a duct-burning turbofan engine underwent numerous modifications to achieve a highly efficient geometry and stable combustion. The apparatus was tested in a connected-pipe facility at conditions simulating those of a supersonic transport plane. Two zones of fuel injection provided overall fuel-air ratios of 0 to 0.050. Air entered the upstream combustion zone by means of ram-scoops. Much effort was devoted to means of combating combustion instability (70 to 470 Hz) encountered at many test conditions. These efforts, only partially successful, are described along with other performance results.

A configuration evolved which provided smooth combustion at three prescribed, simulated flight conditions. Combustion efficiencies were as follows: 92 percent at transonic climb, 99 percent at cruise approach, and 91 percent at cruise. The addition of a set of air scoops improved the mixing process and raised the efficiency 3 to 4 percent at transonic climb and cruise conditions; however, combustion oscillations existed at the cruise-approach condition when the scoops were present.

After 200 hours of hot testing and 200 hours of cold flowing, the hardware showed no evidence of hot-spot damage or metal fatigue. Furthermore, the test apparatus was subjected hundreds of times to combustion instability, which often produced violent and noisy apparatus vibrations for periods of several seconds each.

Four separate methods of combating the pressure oscillations by means of acoustic damping liners were unsuccessful. Tests showed the combustion instability could not be linked to apparatus-facility interface, or to the bleed diffuser and centerbody cavity. The report describes factors that promoted combustion stability.

INTRODUCTION

A survey of four types of gas-turbine engines deemed suitable for powering supersonic commercial aircraft is contained in reference 1. The survey shows that a duct-burning turbofan engine, in which about one-half the total air is burned in the fan duct and exhausted directly to the atmosphere is a competitive engine. An annular combustor that receives duct air was developed and tested (ref. 2). The combustor showed good performance but was subject to pressure oscillations which could cause severe damage.

The purpose of the work described in this report was to eliminate this instability and still retain the generally good performance demonstrated in reference 2. To achieve this goal a number of changes were made (combustor hardware, fuel manifolding, absorption liners, decoupling of combustor and test apparatus, etc.). Most attempts were unsuccessful, but one modification (Model B-NOTURB) evolved which gave good performance and still allowed operation at all key test conditions without encountering instability.

The design, fabrication, and initial evaluation of the combustor are described in reference 2. The test apparatus included a diffuser and a combustor sized for an engine whose total airflow is 600 pounds per second (270 kg/sec) at sea-level static conditions. The combustor had flight-weight liners capable of confining near-stoichiometric flames. The burned gases passed into a short-length, adjustable-area, water-cooled nozzle. The apparatus was tested in a connected-pipe facility at the Lewis Research Center. Combustion efficiency, pressure loss, wall temperatures, and hardware durability were satisfactory. However, the apparatus exhibited combustor pressure oscillations (also called combustion instability) at numerous locations in the envelope of simulated flight conditions. These oscillations were judged to be of sufficient amplitude that damage to the combustor hardware would result from extended periods of operation. The instability problem is described in the next several paragraphs.

At most test conditions, the pressure oscillations occurred at fuel-air ratios that were smaller than those required for maximum thrust augmentation. The oscillation frequency ranged from 70 to 470 hertz. In an attempt to eliminate this instability problem, numerous changes were made to the combustor liners, fuel injectors, and inlet piping. Two acoustic tailpipe liners were tested. Certain of these hardware changes produced changes in the frequency of the oscillations and in the fuel and airflow rates at which the oscillations occurred. However, no single hardware combination eliminated the oscillations at all test conditions of interest.

Reference 2 cites numerous cases of metal fatigue and failure brought on by mechanical vibration. Pressure oscillations greater than about 100 hertz produced hardware vibrations that were audible. For a given pressure amplitude, the sound level and

accelerometer-measured casing vibrations increased greatly as the frequency of the oscillations increased. When combustion instability was present, a small increase in fuel flow rate sometimes produced a drastic increase in pressure amplitude.

The object of the work reported herein was to eliminate combustion instability in the existing duct burner while maintaining good combustion efficiency and low combustor pressure loss. No drastic changes to the combustor were undertaken. Rather, the basic design concepts set forth in reference 2 were adhered to. The diffuser and combustor were kept closely matched. Two combustion zones were employed. Changes that were made include modifications to the fuel and air entries, the use of large acoustical absorbers, the isolation of the inlet ducting of the test facility, and the investigation of a diffuser bypass bleed. The extent to which the hardware modifications suppressed combustor pressure oscillations is shown on stability maps. Performance data for the combustor configuration providing the greatest margin of improvement are shown in detail. ASTM A-1 fuel was used throughout the program.

APPARATUS

Facility

A diagram of the test facility and a view of the combustor through the open access cover are presented in figures 1 and 2, respectively. The combustion air, after being heated in a natural-gas-fired, tube-type heat exchanger, flows through the measuring orifice (fig. 1) at about 10 atmospheres pressure. A choked butterfly valve regulates the flow. A perforated cylinder (fig. 1) disperses the air into the inlet plenum. Further downstream, a venturi guides the air into the annular diffuser, which in turn discharges into the annular combustion chamber. The combustion products, upon leaving the annular exhaust nozzle, spill into a cylindrical water-cooled exit section where they are quenched by water sprays. The quenched mixture passes through a butterfly valve, is further quenched, and then passes through the exhausters.

The safety shroud (fig. 1) serves a dual role. It is a frame for supporting the test apparatus and also a safety barrier. A fan provides purge air around the test combustor to reduce the possibility of an explosion or fire in the event of an accidental spillage of fuel. Gravity drains remove accidental liquid spillage.

Three independent and nearly identical supply systems bring fuel to the test site. Each system contains, in sequence, a displacement pump, a bypass-type pressure regulator, a throttle valve, a flow-rate measuring station, and a positive shutoff valve. A cooler maintains the fuel in all three systems at a near-ambient temperature. Maxi-

mum working pressure is 70 atmospheres. The three systems are located immediately outside the building which houses the test apparatus.

Test Apparatus

Test hardware is presented in figures 3 to 10. The components shown therein are for the Model B configuration. This configuration provided the best test results. Component variations of particular interest are presented in later sections of the report.

The diffuser is a one-piece assembly, consisting of inner and outer casings joined together by two sets of radial struts. An inlet dome bolted to the forward end of the inner casing guides the air into the diffuser. Figures 1 and 3 show the two casings and dome but do not show the struts. The upstream struts consist of four equally spaced fairings that also serve to carry water, fuel, and instrumentation leads into the centerbody cavity. These upstream fairings are much larger than the eight downstream struts (one of which is shown in fig. 5). The forward section of the primary combustor liner (fig. 6) is pinned to the downstream struts. The entire centerbody of the combustor, including the water-cooled inner walls of the exhaust nozzle is cantilevered from the downstream flange of the inner diffuser wall (fig. 5). The inner walls of the diffuser contain a bleed passage (figs. 3 and 5) which itself is a diffuser. The air entering the bleed is eventually returned to the aft portion of the combustor.

At the flow venturi (fig. 3) instruments measure the airflow rate. Throat area is 662 square inches (4270 cm^2). (This flow-measuring station provides a check on the airflow orifice described later.) The distance from venturi to burner snout is 40 inches (100 cm). The inner and outer exit diameters of the annular passage at the diffuser exit are 47.0 and 67.7 inches (119.5 and 172.0 cm), respectively. These casing diameters are essentially the same as those of the combustor (see fig. 3). The diffuser bleed flow area is 117 square inches (755 cm^2) measured at the lip.

The combustor primary liner (fig. 6) is an integral unit containing snout, swirlers, firewall, and number 1 and 2 scoops. Total length is 14 inches (36 cm). The liner accepts two surface discharge spark ignitors located 180^o apart. Each ignitor is supplied by a 20-joule exciter capable of generating 48 spark discharges per minute.

The secondary liner assemblies (figs. 7 to 9), which contain the number 3 scoops, support the trailing edge of the primary liner. Turbulators (number 4 scoops) are located immediately downstream of the zone 2 fuel bars. The circumferential arrangement of the four sets of scoops is shown in figure 8. Tests were conducted both with and without the turbulators (i.e., Model B-TURB and Model B-NOTURB).

The tailpipe liners (fig. 3) are about 36 inches (91 cm) long. Liner cooling is handled differently on the inner and outer wall. For the film-cooled inner liner (fig. 9)

the bleed diffuser provides air for the bypass and cooling louvers. The upstream, or bypass, louver is relatively large and air from this part is assumed to enter into the combustion process. The inner liner is structurally supported by a perforated cylinder that also supports the inner exhaust nozzle wall attached to its downstream flange (fig. 9).

The convection-cooled outer liner is composed of 60 sets of panels mounted in tracks (figs. 3 and 10). The filler plates increase the cooling air velocity, thereby enhancing the cold-side heat-transfer coefficient. Both inner and outer liners contain acoustical absorbers on the upstream portion of the walls.

The exhaust nozzle (fig. 11), which is attached to the tailpipe casings, is described in the instrumentation section.

Fuel at ambient temperature is introduced in two zones. Zone 1 consists of 40 concentric dual-orifice nozzle assemblies (see figs. 4 to 6). The 40 nozzle assemblies are served by two independent fuel systems. The 40 inner (primary) nozzles are connected to a common manifold which is supplied by one of the fuel systems. The 40 outer (secondary) nozzles are arranged such that 20 nozzles (located in every other nozzle assembly) are connected to a common manifold supplied by the second fuel system. The other 20 secondary nozzles are connected to a third manifold which is joined to the second fuel system by means of a remote shutoff valve. Hence, the zone 1 manifolds provide five fuel injection arrangements as follows:

(1) Forty primary nozzles
(2) Forty primary and 20 secondary nozzles
(3) Forty primary and 40 secondary nozzles
(4) Twenty secondary nozzles
(5) Forty secondary nozzles

} Maximum allowable pressure, 30 atmospheres, because the nozzle design calls for primary fuel pressure to help seat an internal seal

The zone 1 nozzles are fixed-area swirlers producing thin hollow cone sprays having an included angle of 90°. The atomizer heads are designed to direct combustion air over the nozzle face to help keep the face clean. The nozzles are designed for a large turndown ratio. At 60 atmospheres pressure (maximum design pressure) each inner (primary) nozzle injects fuel at a rate of 180 pounds per hour (82 kg/hr) and each outer (secondary) nozzle injects 800 pounds per hour (363 kg/hr). The spacing of 4.5 inches (11 cm) between nozzle assemblies was chosen for reasons of combustion efficiency, cost, complexity, weight, and lean blowout limits (ref. 2).

The zone 2 fuel injection system furnishes the additional fuel necessary to attain large values of fuel-air ratio. This system consists of two concentric rings on which the zone 2 nozzles are mounted at approximately 1.4-inch (3.36-cm) spacing. The outer ring consists of 10 spray bars (segments) with a total of 140 nozzles. The inner ring is made up of four spray bars with a total of 112 nozzles. All spray bars are supplied by a

common fuel system, with fuel entering the inner ring by means of supply lines through an upstream diffuser strut and the centerbody cavity. All zone 2 nozzles (fig. 7) have fixed-area, swirl-type ports and are aimed 15° inward from the walls. The total spray angle is 90°. Each nozzle provides a flow of 180 pounds per hour (82 kg/hr) at 60 atmospheres pressure (maximum design pressure).

Instrumentation

Airflow rate is measured by a sharp-edged orifice with flange pressure taps (fig. 1). Also, the flow rate is measured with a venturi at the diffuser inlet. The location of the venturi (station 2), along with other major instrumentation stations, is shown in figure 3. Fixed position pressure and temperature sensors used at stations 2, 4, and 5 are shown in figure 12. Eight pressure rakes are located at each station along with eight static-pressure taps distributed on the wall circumference. Flow rate through the diffuser bleed is measured at station 3 (fig. 4) by two sets of total head and wall static-pressure sensors. In the tailpipe, flow measurements in the bypass louver (fig. 9) and behind the outer liner panels are obtained with pitot-static tubes.

Two vane-type flowmeters are series-mounted in each of the three fuel supply systems. Pressure transducers are located on the fuel manifolds. A similar, but less elaborate, sensing system measures water flow to the exhaust nozzle. Temperatures of the entering fuel and entering and exiting water are sensed with thermocouples. Chromel-Alumel thermocouples sense firewall and tailpipe liner temperatures.

The annular exhaust nozzle (fig. 11) consists of inner and outer casings and 20 variable-position plugs, permitting variation of flow area from 960 to 1500 square inches (6194 to 9677 cm^2). The nozzle thus can be used as a sonic choke for a wide range of operating conditions. Changes to the flow area are accomplished by adding or removing nozzle plug spacers on 18 of the plugs prior to a test run. Remote-control positioning of the remaining two plugs provides flow area trimming capability during a test run. All surfaces exposed to the combustion products are water-cooled. Eight ports located circumferentially in the outer nozzle casing are used to insert water-cooled pressure and temperature sensors into the gas stream. For normal operation, the choked nozzle being used to determine average total gas temperature, each of the eight ports is used to insert an eight-point total-pressure rake into the stream. When local radial temperature profiles are desired in addition to average total temperature, water-cooled radial traversing temperature probes (fig. 13) are installed through two of these ports, with the remaining six ports occupied by eight-point total-pressure rakes. The sensing elements on the aspirated traversing temperature probes are iridium/60-percent-iridium - 40-percent-rhodium thermocouples. The two probe assemblies

are traversed simultaneously and the radial movement is remotely controlled.

The instrumentation described thus far has been of the steady-state measuring type. Dynamic pressure sensors are located 90° apart on the circumference both in the diffuser and in the primary liner. Also, two to four dynamic pressure sensors can be mounted at other selected places depending on the purpose of a given test; however, at least one sensor is kept in the inlet plenum to monitor "noise." All sensors are flush with either casing or tailpipe liner walls. Casing vibration is measured by a vertically mounted accelerometer located on the diffuser-exit outer flange.

A portion of the instrumentation, including airflow and fuel-air ratio obtained by an on-line analog computer, is continuously displayed in the control room so the test operator can set the data points and monitor test apparatus behavior. All the dynamic instrumentation outputs are displayed in the control room. Also, high-speed strip charts are available for recording the dynamic data.

Most of the steady-state data are recorded by the CADDE automatic data recording and processing system (fig. 14 and refs. 3 and 4). These raw (signal level type) data are processed by a conversion program which yields data in engineering units and also calculates averages and makes elementary terminal calculations such as airflow rate and Mach number. The raw data are also sent back to the control room by means of a flexowriter and facsimile plotter, thereby permitting rough calculations to be made during the testing.

PROCEDURE

Test Procedure

The combustor described in the APPARATUS section was evaluated at each airflow condition listed in table I. Other combustor configurations examined during the investigation were tested at one or several of the tabulated airflow conditions. The procedure for mapping combustion instability differed from the procedure for obtaining combustion efficiency data.

Stability tests were conducted as follows: A given airflow condition (table I) was established. After ignition, the fuel flow rate was gradually increased. Constant burner pressure was maintained by the manually controlled exhaust butterfly valve. (For these tests the exhaust nozzle was not choked.) The output of the dynamic pressure sensors was visually observed and recorded on a strip chart.

The criterion used for defining combustion instability was a periodic pressure fluctuation having a peak-to-peak amplitude approximately 5 percent, or greater, of the combustor pressure. As soon as an instability of this amplitude was observed, the dy-

namic data were recorded on strip charts and the fuel flow rate on each of the three fuel systems was noted. Immediately thereafter, the fuel flow rate was reduced in order to minimize possible damage to the test apparatus.

The procedure for constructing a "typical" combustion instability map is described with the aid of figure 15. The example assumes the presence of both primary and secondary flow in zone 1 (fig. 4). The primary fuel is ignited and the flow rate is increased until a fuel-air ratio of 0.006 is achieved (point 1 on fig. 15). The primary fuel flow is held constant for the remainder of the test. Then, secondary fuel is injected and the flow rate is gradually increased until combustion instability occurs (point 2). Another point on the instability map is obtained in a two-step sequence. The flow rate of secondary fuel is reduced an arbitrary amount until point 3 is reached. Then zone 2 fuel is introduced and its flow rate is increased to point 4, where instability occurs. The region between points 2 and 4 is mapped by reducing zone 2 fuel flow rate an arbitrary amount until point 5 is attained, increasing secondary fuel flow rate to point 6, and finally increasing zone 2 fuel rate to point 7, another point of unstable burning. Maps were not always as simple as the "typical" map of figure 15. Hence, the test operator adjusted the size of the arbitrary step changes to fit the particular needs of the moment.

Combustion efficiency data were obtained with the exhaust nozzle choked. Hence, the nozzle flow area had to be tailored to a particular value dependent on both airflow condition (table I) and fuel flow rate. Data for a modest range of fuel-air ratios could be gathered by trimming the nozzle area with the two variable-position plugs. Otherwise, airflow had to be stopped and plug spacers (fig. 11) installed or removed to suit. Test conditions were held essentially constant throughout the 20 seconds required to automatically record the data. These data were used for all performance calculations.

Data Analysis Procedure

The results obtained from the conversion program (see APPARATUS section) were submitted as inputs to a digital computer program which was used for the performance computations. Pertinent equations, definitions, and flow constants are described in the next paragraphs. (Symbols are shown in appendix A. An error analysis is contained in appendix B.)

The duct reference Mach number M_{ref} was obtained by iteration from

$$M_{ref} = \frac{W_a}{A_{ref} P_4} \times \sqrt{\frac{\mathscr{R}_4 T_4}{\gamma_4 g_c}} \times \left(1 + \frac{\gamma_4 - 1}{2} \times M_{ref}^2\right)^{\frac{\gamma_4+1}{2(\gamma_4-1)}} \qquad (1)$$

where A_{ref} is total annular area bounded by the inner and outer combustor-casing walls and W_a is the airflow rate entering the diffuser. The value of A_{ref} used in the equation is 1863 square inches (12 019 cm^2).

At the choke condition the actual total temperature at the nozzle throat is

$$T_5 = \left(\frac{C_d A_5 P_5}{W_t}\right)^2 \frac{\gamma_5 g_c}{\mathcal{R}_5 \left(\frac{1+\gamma_5}{2}\right)^{\frac{\gamma_5+1}{\gamma_5-1}}} \tag{2}$$

where A_5 is the nozzle area adjusted for thermal growth. The discharge coefficient C_d was fixed at 0.985, a value experimentally determined in reference 2. The gas properties were evaluated at static temperature.

The ideal total temperature at the nozzle throat is determined from a theoretical combustion subroutine included in the computer program. The calculations assume equilibrium combustion and isentropic expansion through the nozzle.

Combustion efficiency is defined as

$$\eta = \left(\frac{T_5 + \Delta T_L - T_4}{T_{5,\,ideal} - T_4}\right) \times 100 \tag{3}$$

where ΔT_L is a temperature loss occurring in the convergent section of the nozzle and is computed from the enthalpy rise of the nozzle cooling water. (One-half of the water enthalpy rise was assumed to occur in the convergent section of the nozzle.) The adjustment to η resulting from the presence of ΔT_L was nearly always less than 1 percent.

Diffuser pressure loss is defined as

$$\frac{(P_2 - P_4) \times 100}{P_2} \tag{4}$$

and combustor pressure loss is defined as

$$\frac{(P_4 - P_5) \times 100}{P_4} \tag{5}$$

Airflow rates through the miscellaneous passageways were computed using flow coefficients of 1 and compressible flow equations.

The gas properties, γ and $\mathscr{R}$, were adjusted to account for small amounts (less than 1 percent) of entrained water vapor present in the combustion air.

COMBUSTOR DESIGN CONCEPTS

During the course of the experimental investigation, the test apparatus was subjected to many changes. However, the fundamental design concepts and goals (ref. 2) that guided the initial design and test programs remained largely unchanged. A brief review of some of the important design concepts follows.

The diffuser and burner were integrated so that, instead of diffusing air to a low velocity and then accelerating it, they diffuse the air to the approximate velocity at which it flows around the burner snout. Reference 2 states that the diffuser length and effective diffusion angle were chosen to satisfy the following requirements:

(1) The rate of diffusion be small enough to avoid flow separation

(2) The turning angles of the fan discharge and burner inlet, which are at different radii, be small enough to avoid flow separation

(3) Sufficient space be provided around the inside and outside of the diffuser for the installation of the required engine accessories and equipment

Approximately 10 percent of the airflow passes through the bleed diffuser. About one-half of the bleed flow is used to cool the inner cooling liner and the remainder enters the combustion zone by way of the bypass louver (fig. 9). On an engine, the bleed diversion would make use of the available space between the engine gas generator and the duct burner, thereby increasing the effective volume of the combustion chamber. Bleeding also removes low-velocity airflow from the inner diameter of the diffuser before the turn in the ducting is encountered, thereby minimizing the possibility of flow separation at this turn.

One-third of the air passes through the snout and primary and secondary liners. Snout air enters the combustion chamber through radial swirlers and cooling passageways. The air scoops in the primary liner turn the air into the combustion zone through smoothly contoured (number 1 and 2) scoops. There is some flow diffusion in these scoops.

Table II lists the effective flow area and discharge coefficients of the various passages into the combustor for the Model B combustor described in the APPARATUS section. The airflow splits shown in the table and in figure 16 are based on the following assumptions:

(1) The total pressure in the annular outer and inner shrouds (fig. 16) remains constant.

(2) Within the combustion chamber, the static-pressure variations are negligible.

(3) The total temperature of the shroud air remains constant.

(4) Frictional losses are negligible.

The total open area of 1010 square inches (6516 cm^2), which represents 54.13 percent of A_{ref} (table II), passes all the air except for the 8 percent removed by the bleed diffuser and distributed as shown in figure 16. The figure also contains pertinent dimensions of the ram-induction section of the combustor.

DUCT BURNER PERFORMANCE

General

The airflow conditions at which performance evaluations were conducted are test conditions 1, 2, 4, and 5 of table I. Condition 1 simulates an abnormal flight condition at which the lowest anticipated combustor pressure level is encountered. Condition 2 simulates a normal transonic climb flight condition, and condition 5 simulates a cruise-approach flight condition (overall fuel-air ratio of 0.050) and an initial cruise condition (overall fuel-air ratios of 0.016 to 0.020). Condition 4 (overall fuel-air ratios of 0.016 to 0.020) simulates a cruise condition at very high altitude. Test condition 3 was used only for combustion instability studies.

The objective of the test program was to develop a combustor that provided smooth and efficient combustion at three selected test conditions: normal transonic climb, cruise approach, and initial cruise. Of all the combustors tested, the Model B-NOTURB configuration appeared to best fulfill the objective. This configuration was singled out for exhaustive evaluation after completion of an exploratory test program in which many different combustor hardware components were evaluated. These exploratory tests were in themselves a major effort and are described under the heading COMBUSTION INSTABILITY.

Model B Configuration Without Turbulators

The subject configuration (Model B-NOTURB) is described in the APPARATUS and COMBUSTOR DESIGN CONCEPTS sections of the report. This configuration exhibited greater combustion stability than any other. In fact, this was the only configuration that provided reliably smooth combustion at the three selected test conditions described in the previous paragraph.

Figure 17 displays combustion efficiency data for conditions 1 and 2 over the range of fuel-air ratios of interest. Each part of figure 17 presents a family of curves in which each curve defines a fixed value of zone 1 fuel-air ratio. Several remarks apply to these and all other data being presented under the heading DUCT BURNER PERFORMANCE. No performance data are shown for those situations wherein combustion pressure oscillations were present. To point out where the unstable regime exists, a barrier (—|) has been placed on each combustion efficiency data curve that was shortened or interrupted because of combustion instability. Figure 17(b) illustrates the use of barriers to denote fuel-air ratio regions of combustion instability. This figure shows that even the Model B-NOTURB configuration would not provide smooth combustion at all possible fuel flow splits. However, at the required operating fuel-air ratio of 0.050, stable operation was obtained with zone 1 fuel-air ratio greater than 0.018.

Figure 18 displays combustion efficiency data for conditions 4 and 5. Forty zone 1 nozzles were used for these tests, whereas 20 nozzles were used in gathering the data of figure 17. At overall fuel-air ratios of 0.010 to 0.030, only zone 1 fuel was injected. The data for test conditions 4 and 5 are unique in that the reference Mach number M_{ref} was not properly controlled. The desired M_{ref} value of 0.175 could be maintained only at fuel-air ratios richer than 0.017. At fuel-air ratios less than 0.016 the exhaust nozzle, with all nozzle plugs (fig. 11) inserted, still provided too large an open area. Hence, at these lower values of fuel-air ratio, M_{ref} progressively increased as the fuel-air ratio was progressively decreased until finally, at a fuel-air ratio of 0.012, the M_{ref} became 0.19. In spite of the aforementioned M_{ref} excursion, combustion efficiency is observed in figure 18 to increase continuously as the fuel-air ratio is decreased from 0.026 to 0.012. Other than the situation just cited, airflow parameters (M_{ref}, pressure, and temperature) were held very close to the set values of table I.

The combustion efficiency data of figures 17 and 18 are discussed in greater detail later in the report.

Isothermal combustor pressure loss data (zero fuel flow) are presented on figure 19, and combustor pressure loss data for the combined effects of friction and heat addition are shown in figure 20. Figure 20 was constructed in such a manner (ref. 5) that the experimental data would be characterized by a linear relation of ordinate to abscissa for the wide range of temperature ratios T_5/T_4 encountered. Figure 21 presents pressure loss data for the diffuser only. The isothermal pressure loss for the diffuser-combustor combination is 6 percent at a reference Mach number of 0.15. This loss consists of 1.7 and 4.3 percent losses in the diffuser and combustor, respectively (figs. 21 and 19).

Diffuser pressure loss data, over the entire range of combustor outlet temperatures encountered, were very similar to the nonburning data of figure 21. The diffuser parameter that did change with variations in combustor heat release was the bleed fraction.

Figure 22 shows the diffuser bleed flow to increase nearly 50 percent when the overall fuel-air ratio rises from "idle" to "acceleration."

Comparison with Reference 2 Results

Reference 2 was prepared near the midpoint of the development program. Performance data reported in reference 2 are compared herein to the data obtained with the Model B-NOTURB configuration. For the sake of clarity, we are designating the reference 2 configuration as Model A-TURB and Model A-NOTURB depending on whether turbulators are present in the configurations under discussion.

Model A and B configurations were very similar. Primary liners and tailpipe liners (figs. 6, 9, and 10) were identical. Also the same fuel injectors (both zones 1 and 2) were used. Differences involving the secondary liner and the turbulators can be described by means of figures 4 and 7. In the Model A configuration,

(1) There are five turning vanes in each number 3 scoop. (Cut marks still visible on fig. 7 show where vanes were removed for the Model B configuration.)

(2) The outer secondary liner rotated one-half pitch (4.5^{o}) so that the number 3 scoops opposed those on the inner liner. (Number 3 o.d. and i.d. scoops are staggered on the Model B configuration.)

(3) The turbulators (when present) on the outer wall rotated one-half pitch so that they opposed the turbulators on the inner wall. (The old supports were not removed and are visible on fig. 7. Turbulators are staggered on the Model B configuration.)

Test procedures have undergone only minor changes since the reference 2 tests were conducted. The zone 1 fuel injection manifolding arrangements were unaltered. Airflow condition 4 was not evaluated in reference 2. In the present tests, the combustor pressure at test condition 5 was reduced from 2 to $1\frac{2}{3}$ atmospheres in order to reduce wear and tear on the test apparatus.

In general, the Model B-NOTURB configuration was judged to provide greater freedom from combustion instability than Model A-NOTURB configuration which, in turn, exhibited lesser tendency towards combustion instability than did Model A-TURB. The relative merits of the Model A and B configurations, from the standpoint of stability, are discussed in detail in the section entitled COMBUSTION INSTABILITY.

Combustion efficiency data are compared on figures 23 and 24. (The Model B-NOTURB data are from figs. 17(b) and 18(b).) At the transonic climb condition (fig. 23), Model B-NOTURB provides an efficiency of 92 percent compared to 95 and 89 percent for Model A with and without turbulators. At cruise condition (0.016 fuel-air ratio in fig. 24) the Model B-NOTURB configuration provides a combustion efficiency of 91 percent as compared to 93 and 88 percent for Model A with and without turbulators.

At cruise-approach condition (0.05 fuel-air ratio in fig. 24) Model B-NOTURB provides an efficiency of 99 percent compared to 91 and 95 percent for Model A with and without turbulators. The poor showing of the Model A-TURB configuration at an overall fuel-air ratio of 0.05 is accounted for as follows: Because of the turbulators a minimum of two-thirds of the fuel had to be injected at the zone 1 site in order to avoid combustion instability. This large quantity of fuel entering zone 1 adversely affects combustion efficiency values. (Figure 18(b) serves to illustrate the undesirable effect of too much zone 1 fuel.)

Figure 25 shows that isothermal pressure losses are somewhat smaller for the Model B configuration than for the Model A configuration. Similar results were obtained with combustion (see fig 26). The pressure loss difference between the two models is due largely to the removal of all guide vanes from the number 3 scoops located in the secondary liner. Figures 25 and 26 show that turbulators produce a sizable pressure loss.

In summary, the Model B configuration without turbulators (B-NOTURB) simultaneously exhibited better combustion efficiency, smaller pressure losses, and greater combustion stability than the Model A-NOTURB configuration. The Model A-TURB configuration had the best efficiency of the three, except at cruise approach. However, this configuration suffered from a tendency toward combustion instability.

Effect of Turbulators on Performance

In the previous section of this report, combustion efficiency of the Model A configuration was shown to improve when turbulators were added. Hence, turbulators would be expected to improve combustion efficiency of the Model B configuration. And they did. The influence of turbulators on the combustion efficiency of the Model B configuration is shown in table III. These data are from figures 27 and 28 for Model B-TURB and from figures 17 and 18 for Model B-NOTURB. The data selected for table III are those provided by the optimum fuel flow splits between zones 1 and 2. Both figures 27 and 28 show how very important is the proper selection of the fuel flow split. The largest observed effect was at test condition 4 and an overall fuel-air ratio of 0.020 (fig. 28(a)). Combustion efficiency dropped from 90 percent to 74 percent when 40 percent of the total fuel was shifted from zone 1 to zone 2. A possible explanation is as follows: The zone 1 fuel burned near the zone 1 nozzles. Then the gases were quenched by fresh air coming through the downstream scoops. The resulting chilled gases were not a good environment in which to inject relatively small amounts of zone 2 fuel. Hence, the zone 2 fuel did not burn well. Even at overall fuel-air ratio values as great as 0.025, combustion efficiency was decreased by the injection of any zone 2 fuel (figs. 28(a) and (b)).

For an overall fuel-air ratio of 0.05, figures 27 and 28 indicate that the optimum flow split is obtained by placing about one-third of the fuel in zone 1 and two-thirds of the fuel in zone 2. That this is not always possible is illustrated by means of figure 27(a). Therein, when the zone 1 fuel-air ratio was 0.016 or 0.018, combustion instability prevented the attainment of an overall fuel-air ratio of 0.05. However, an increase of fuel-air ratio in zone 1 to 0.02 is shown to permit both smooth and efficient combustion at an overall fuel-air ratio of 0.05.

More data were obtained with turbulators (figs. 27 and 28) than without turbulators (figs. 17 and 18), the reason being that the Model B-TURB configuration yielded the best combustion efficiency values obtained during the investigation. Hence, a serious effort was made to find a way by which smooth combustion could be obtained at the cruise-approach test condition (overall fuel-air ratio of 0.05 on fig. 28(b)). Unfortunately, no way was found.

The significance of the tailed data symbols (figs. 27 and 28) involves data accuracy. These particular data points were gathered near the midpoint of the exploratory test program. Specifically, these data were taken some 8 months and numerous test apparatus changes prior to the taking of the more comprehensive set of data shown on the figures. Both sets of data were given equal weight in this analysis, an action bolstering the data accuracy statements made in appendix B.

Combustor pressure loss data (figs. 29 and 30) differ only in magnitude from the data of figures 19 and 20 obtained on the Model B-NOTURB configuration. As expected, the turbulators increased pressure loss both with and without combustion. The greatest effect was at a temperature ratio of 5 and a M_{ref} of 0.144, where the difference amounted to 10 percent of the pressure loss or 1 percent of the combustor total pressure.

Diffuser performance was unaffected by the presence of turbulators; hence, the data curves on figures 21 and 22 can be made to apply to the Model B-TURB configuration.

It may be feasible from a design standpoint to connect the turbulators to an actuating device and thereby move them out of the stream in accord with the dictates of the combustion stability maps. If this could be done, the Model B configuration would provide stable combustion at the test conditions of interest and would provide combustion efficiency values of 95 percent or better at the key simulated flight conditions of transonic climb, cruise approach, and initial cruise (table III). Also, removal of the turbulators, at times when they are not needed, would keep friction losses to a minimum.

Correlation and Interpretation of Combustion Efficiency Values

The combustion efficiency data of figures 17, 18, 27, and 28 are presented in figure 31 as a function of the ramjet correlation parameter $p^{0.3}T/V^{0.8}$. The terms p, T,

and V refer to the inlet air reference quantities of pressure, temperature, and velocity. Reference 6 utilized the parameter to correlate empirical data for a combustor employing V-gutter flameholders. (The parameter was found to provide a better fit to the present data than the correlation parameter pT/V described in ref. 6 and commonly used for turbojet combustors.) Figure 31 is very useful in rating the severity of the four airflow conditions. In particular, the figure shows the desirability of not operating the combustor at the abnormal flight condition (airflow condition 1). At this condition, combustion efficiency is below 90 percent.

Test condition 4 simulates a higher altitude than condition 5 (see table I). Thus, figure 31 shows that the combustion efficiency is decreased as the simulated cruise altitude is increased. At a fuel-air ratio of 0.02 and with turbulators present, the decrease is very sizable (4 percent) and typifies the loss to be expected during a long flight when the aircraft is operated in accordance with the Breguet formula (constant angle of attack and constant Mach number).

Figure 31 shows that turbulators improve combustion efficiency at both fuel-air ratios (0.020 and 0.050). The reasons for the improved combustion efficiency may differ for the two values of fuel-air ratio. At a fuel-air ratio of 0.05, most of the fuel enters the combustor by way of the zone 2 fuel injectors. The turbulators do several things that could foster burning of this fuel. In addition to promoting turbulence, the turbulators sweep fresh air into the active combustion zone located immediately downstream of the spray bars. Also, some of the zone 2 fuel (that is injected along the liner walls) is picked up by the turbulators and turned into the center of the combustion zone. There is little wonder that the combustion intensity and efficiency are improved by the mixing action of the turbulators. Such is not the case at a fuel-air ratio of 0.020. No fuel is being injected through the zone 2 spray bars. Sufficient air was provided in the ram-induction section of the combustor to burn the zone 1 injected fuel. Injection of air into these reacting gases when they are in the final phases of burning would tend to quench the reaction and lower the conversion of chemical to sensible enthalpy. Hence, we need to look elsewhere for the reason behind the observed beneficial effects of the turbulators. Figure 32 shows typical radial temperature profiles taken at the nozzle throat when turbulators are not present. The large gradients suggest that no great amount of mixing took place in the tailpipe between the combustion products and the air passing around the ram-induction region. Assuming the occurrence of complete chemical reaction in the upstream portion of the combustion chamber, a measured combustion efficiency of well below 100 percent would be expected if the bypass air did not mix with the combustion products (see appendix C). It is entirely possible that much of the measured combustion inefficiency occurring at simulated cruise flight conditions can be attributed not to any defect of the ram-induction zone, but to the inadequate mixing rate encountered in the tailpipe. Comparable temperature profile data with turbulators in place were not obtained.

Effect of Zone 1 Fuel Nozzle Arrangement on Performance

As described in the APPARATUS section of this report, there were five fuel injection arrangements used in zone 1. The data presented thus far were obtained with only two of the arrangements, namely 20 and 40 secondary nozzles. Data figures 17 and 27 (conditions 1 and 2) were obtained with 20 secondary nozzles, and data figures 18 and 28 (conditions 4 and 5) were obtained with 40 secondary nozzles.

At airflow conditions 4 and 5, the five arrangements by which fuel could be injected into zone 1 had little effect on combustion instability. This was not so at airflow conditions 1 and 2. Charts in the next section (COMBUSTION INSTABILITY) show a clear preference for an arrangement containing only 20 secondary nozzles. Since several fuel-injection arrangements exist for use at conditions 4 and 5, a study was made to select the most desirable arrangement or arrangements. Figure 33 presents combustion efficiency data for zone 1 fuel arrangement numbers 2 to 5. (The first arrangement (see APPARATUS section), which uses only the 40 primary nozzles, was not tested because the fuel flow rate obtainable from this arrangement is so small as to be of interest only for relight tests.) For each part of the figure a single curve was faired through all the data. Within the limits of experimental error (appendix B) the data from all four zone 1 fuel-injection arrangements tested fit the curve shown.

There appears to be no real need for all five options. Zone 1 fuel manifolding could be made quite simple by eliminating the primary fuel system (low-flow-rate system) and using the option of 20 or 40 secondary nozzles to provide the necessary turndown of fuel flow rate. Therefore, tests were conducted to ensure that unsatisfactory blowout limits or other unanticipated factors would not stand in the way of the simple 20-40 option. Figure 34 shows blowout and relight data for 20 zone 1 secondary nozzles and for 40 zone 1 primary nozzles. Although the fuel flow rates were so small that data error may be large, the very satisfactory blowout and relight results provided by the 20 secondary nozzle arrangements suggest elimination of both the primary fuel system and the complex dual-orifice injection. Modulation of fuel flow at low values of ΔT presented no problems during the blowout and relight tests.

Hardware Cooling, Cleanliness, and Durability

Wall cooling presented no problems for the present configuration. The coolant flow to the inner and outer tailpipe liners is shown in figure 35. At an overall fuel-air ratio of 0.050, almost one-tenth of the total airflow is utilized for tailpipe cooling. Wall temperature data are shown in figure 36. Maximum measured temperatures on the inner and outer liners are 1100° and 1540° F (593° and 838° C), respectively. The presence

of turbulators had no significant effect on wall temperatures. A heat-transfer analysis is presented in reference 2 for outer liners, and the predicted results are shown in figure 36(b). Combustor firewall (face) temperature data are presented in figure 37. No overheating was observed on the firewall or on other combustor hardware.

The combustor liners, scoops, and tailpipe liners appeared to be in excellent mechanical condition at the termination of the test program. All the aforementioned parts had been subjected to over 200 hours of hot testing in addition to over 200 hours of cold flowing. Furthermore, the test apparatus was subjected, hundreds of times, to violent mechanical vibrations produced by the combustion instability phenomena. No visual indication of metal fatigue was observed.

Durability of the fuel nozzles was satisfactory. (Reference 2 describes modifications made to strengthen both zone 1 nozzles and zone 2 spray bars.) Except for traces of soot, carbonaceous material did not form on nozzles or other flame tube parts. At no time in the entire program were fuel nozzle coefficients observed to have changed. The zone 2 nozzles (spray rings) were never cleaned nor were spray patterns examined. However, as the test program progressed, more and more attention was given to the quality of the spray patterns of the zone 1 nozzles. (This attention was motivated by the belief that certain combustion instability behavior could be related to fuel distribution.) About a year before the termination of the test program, the nozzles were observed to be streaking badly. Complete dismantling and cleaning eliminated all signs of streaking. Periodic inspection of the spray patterns during the final year of tests showed that the patterns progressively deteriorated; however, the amount of deterioration was judged to be small and harmless for the Model B configuration. Photographs (fig. 38) taken at the end of the test program shows spray patterns after 150 hours of intermittent testing involving 40 startup and shutdown cycles.

COMBUSTION INSTABILITY

Instability Maps and a General Explanation of Instability Behavior

Combustion instability maps obtained for the Model B-TURB configuration are presented in figure 39 for all five test conditions of table I. The procedure for gathering and presenting these data is described in the section PROCEDURE. Zone 1 fuel-air ratio is based on zone 1 fuel flow and total airflow. All maps shown in figure 39 were obtained with the combustion-instability-prone turbulators present. Figure 39(a) can be used to describe several features of the observed pressure oscillations. When no primary fuel was flowing, a smooth-combustion corridor existed. This corridor is bounded on the upper-left side by 75- to 80-hertz waves and on the right side by waves of various

frequencies ranging from 100 to 165 hertz. The corridor extends up and beyond an overall fuel-air ratio of 0.050. An upper bound to the corridor may exist; however, the apparatus was seldom tested at overall fuel-air ratios in excess of 0.050. (The solid symbols in fig. 39(a) indicate the existence of smooth combustion at the symbol locations shown.) Note that the corridor is closed off by a barrier of 80- and 165-hertz instability when the zone 1 primary fuel is present (fig. 39(b)) even in relatively small quantity (a primary fuel-air ratio of 0.006). The next several paragraphs discuss the nature of the combustion instability and the significance of the demarcation lines shown in figure 39.

An anomaly in the data was observed at test condition 4. As noted on figures 39(f) and (g) the demarcation line in one region of the map appeared to be dependent on the Mach number at the exhaust nozzle throat. As Mach number increased, the instability-free region of the map decreased. The pressure oscillations when the nozzle was at a choked or nearly choked condition were longitudinal.

Typical pressure wave data are shown in figure 40. Interpretation of these data was made with the aid of reference 7. The waves were judged to be of two types: traveling longitudinal waves (at frequencies usually below 100 Hz) and transverse waves (at frequencies usually above 100 Hz). The transverse waves were observed as standing waves in certain instances. At other times, they may have been either spinning or standing. The transverse waves existed as either first-, second-, or third-mode waves and were in the vicinity of 180, 300, or 450 hertz, respectively. Occasionally, a complex combination of longitudinal and transverse waves existed, but usually the waves could be easily cataloged. For any given wave type, the wave frequency was observed to increase somewhat when the inlet-air temperature was increased. While they are not noted as such on the figures, the 145- to 180-hertz waves on figures 39(a) to (d) are first-mode transverse, the 323- to 350-hertz waves on figures 39(e) and (f) are second-mode transverse, and the 440- to 470-hertz waves on figures 39(g) and (h) are third-mode transverse. In general, no particular significance has been attached herein to wave type or mode. Wave characteristics that affect hardware vibration are frequency, pressure amplitude, and wave shape (rate of pressure change with time).

At frequencies below 100 hertz, the intensity of the wave at the demarcation lines in figure 39 was sufficiently small that the wave was inaudible. When the frequency increased to about 120 hertz, the instability could be heard and could also be observed on the accelerometers attached to the test apparatus. At these relatively low frequencies, the test apparatus vibrated near 800 hertz, which was the frequency of its vibration with smooth combustion or with airflow alone. As the gas-pressure frequency increased further, the waves began to lose their sinusoidal shape. The curves in figure 40(a) are more irregular than those normally encountered at the frequency noted. For frequencies in the general region of 300 to 500 hertz, the noise was loud and the test apparatus

shook badly. At these higher frequency conditions, the waves contained spikes and the accelerometer "g" values often were more than double the value for smooth combustion. Sometimes the test apparatus would shake at the frequency, or twice the frequency, of the pressure waves.

Peak-to-peak pressure amplitudes of longitudinal waves, when driven to their maximum intensity, were approximately 10 percent of the mean pressure for frequencies in the vicinity of 100 hertz. Some transverse waves, when driven to their maximum intensity showed peak-to-peak pressures in excess of 40 percent of the mean pressure. (Normally, high-intensity waves were avoided in order to preserve the physical integrity of the test apparatus.)

For transverse waves, hysteresis between entering and exiting the instability zone was approximately the width of the shaded area shown in the combustion instability maps. Hysteresis of the low-frequency, longitudinal waves was often considerably greater than the width of the shading.

Figure 39 shows that the optimum zone 1 fuel manifolding arrangement depends on test conditions. For example, at test condition 5, one arrangement is as good as another, while at test condition 4 a 40-secondary-nozzle arrangement is preferred. At the very important simulated transonic climb condition (test condition 2), only the 20-secondary-nozzle system provided a smooth combustion corridor to the desired overall fuel-air ratio of 0.050.

The purpose of generating instability maps at test condition 3 was to aid in establishing simple relations between combustion instability and combustor inlet velocity, pressure, and temperature. A comparison of the various parts of figure 39 indicates that smooth combustion was promoted by increasing reference Mach number (compare test conditions 3 and 4), increasing combustor pressure (compare test conditions 4 and 5), and decreasing inlet air temperature (compare test conditions 2 and 3).

The removal of the turbulators, while providing an almost inperceptible change in the instability maps at test condition 2, eliminated the instability barrier at test condition 5. The resulting improvement in combustion stability can be observed by comparing figures 18(b) and 28(b). Figure 18(b) shows smooth combustion at an overall fuel-air ratio of 0.050 for a wide range of zone 1 fuel-air ratio. Figure 28(b) shows the impossibility of attaining an overall fuel-air ratio of 0.050 when turbulators are present.

In a preceding paragraph, mention was made that the demarcation line between smooth and unstable combustion was a reasonably sharp line - particularly in the case of transverse waves. It is also of interest that, in figure 39(d), three different zone 1 fuel manifold arrangements yielded the same demarcation line and a fourth zone 1 manifold arrangement exhibited a totally different behavior. These and the other previously described observations regarding the sensitivity of combustion instability to zone 1 manifolding arrangements pose an important question. How does the quality of the zone 1

spray pattern affect the demarcation lines? Streaks form easily in these nozzles because the spray cones are very thin and hence readily affected by minute deposits on critical surfaces. The data of figure 39 were obtained with fairly clean nozzles and uniform sprays (figs. 38(a) and (b)). Data obtained about 1 year earlier are shown in figure 41. Subsequent examination showed that the nozzles were streaking badly. The demarcation lines of figure 41 closely match those of figure 39. The somewhat narrower corridor of figure 41(a) is attributed to spray streaking. Also two sets of data are shown in figure 41(a). The sets were taken on different days. Repeatability of the instability maps was demonstrated in numerous other instances not reported herein.

The Model A configuration (ref. 2) was sensitive both to changes in manifolding and to streaking. Toward the end of tests described in reference 2 the demarcation lines on the instability maps were shifting. The changes were very noticeable at test condition 2. The instability worsened. Eventually the maximum overall fuel-air ratio that could be attained was only about 0.030 at test condition 2. Originally, overall fuel-air ratios of 0.050 had been attained (fig. 23). At this time the zone 1 fuel nozzle had experienced about 200 hours of exposure to the airstream. Nozzle streaking was becoming very pronounced in nearly all nozzles. (There was no change in nozzle flow coefficient.) It was at this time (midway in the present test program) that the Model B configuration was first tested.

Techniques of Combating Combustion Instability

Combustor pressure oscillations plagued this project from the beginning. Numerous methods of suppressing the waves were attempted. Some of the actions taken and their influence on combustion stability are described in the next several paragraphs. The actions are grouped according to the particular pieces of hardware involved.

Acoustic dampers. - The efforts expended on acoustic dampers were not successful. The Model B configuration contained acoustic dampers on both inner and outer walls of the tailpipe. Reasons are as follows: These dampers (figs. 9 and 10) were designed, built, and tested during the initial efforts to suppress the oscillations (ref. 2). They provided very little suppression, but they did provide adequate cooling while consuming less cooling air than was used by the original design (see ref. 2). Also, the damping outer liners (fig. 10) were less subject to warpage than the original liners and hence were easier to replace when damaged. During the present investigation, the inner liner underwent one modification. Thimbles, 21/32 inches (1.7 cm) in diameter, were inserted into each of the 1-inch (2.54-cm) diameter standpipes of figure 9. The inserts had the same length as the original standpipes. The modifications had no detectable effect.

Next, a set of full-length liners was fabricated of perforated steel plate (fig. 42). Inner and outer liners were tested together in a configuration that otherwise embodied the Model B-TURB components. A description of these liners, including the technique for calculating absorption, is provided in appendix D. Because of the large amount of liner open area, the cooling air did not always go where it was most needed. Hot spots occurred. Various arrangements for guiding the cooling air behind the liners were tested. Cooling airflow distribution had a small effect on combustion instability; however, there was no indication that the perforated plate liners provided greater stability than those of the Model B-TURB configuration.

The final attempt to acoustically dampen the waves utilized the secondary liner design of figure 43. This liner, in addition to the perforations, embodied twice as many number 3 scoops as the basic liner (fig. 7). Both liners introduced about the same quantity of air into the zone 1 combustion chamber. Tests were made in conjunction with the tailpipe liners of figures 9 and 10. The combined effect of perforations and scoop changes on combustion stability could not be detected.

Scoops and baffles. - Various scoop configurations were tested. Some had a pronounced influence on combustion instability; others had little effect.

It was hoped that introducing additional air to the upstream combustion zone might inhibit combustion instability. Scoops were added to the primary liner immediately upstream of the number 1 scoops. The added scoops, shown in figure 44, passed about 0.6 as much air as the swirlers. Except for these scoops, the hardware consisted of the Model B configuration. The major effect of the scoops was to lower combustion efficiency 2 to 5 percent. There was little effect on combustion stability. No other attempts were made to improve combustion stability by modifications to the primary liners.

However, numerous changes were made to the secondary liner region. Generally, it was found undesirable to sharply turn large quantities of air into this region of the combustion chamber. Figure 45 shows how 80 large scoops were positioned in the location usually occupied by the secondary liner. These scoops intercepted about twice the amount of air as the number 3 scoops of the Model B configuration. Second-mode, transverse instability was abruptly encountered at test condition 2 at overall fuel-air ratios as small as 0.009 (40 zone 1 primary nozzles). The presence of the large scoops resulted in isothermal combustor pressure losses that were the largest encountered in the program, 40 percent greater than that of the Model B configuration.

Next, five baffle plates were added in hopes of stopping the transverse instabilities associated with the zone 1 fuel system. The configuration as tested is shown in figure 45. The baffles produced no observable effect on instability with this configuration or with another configuration tested later in the program. Cross-firing was no problem and the baffles did not warp badly.

Another variation of the Model B configuration was the elimination of all liners and scoops in the secondary liner region. The effect on combustion instability was similar to the removal of turbulators, namely, the transverse instability barrier was virtually eliminated. However, fuel injected through the zone 1 nozzle could not be consumed efficiently when the zone 1 fuel-air ratio exceeded about 0.012. Hence, some air diversion into the secondary liner region was a necessity for good combustion. Several attempts were made to provide the proper amount of air with the right amount of turning. From this effort, the secondary liner arrangement of the Model B configuration evolved. Along the way, several other secondary liner schemes were tried. One of these, shown in figure 43, has already been discussed. Another configuration is shown in figure 46. It differed from the Model B configuration only in the number 3 scoop geometry. The scoop airflow rate was halved and the flow direction turned sharply. This change produced instability maps that differed little from those for the Model B configuration; however, combustion efficiency values were several percent lower.

Another configuration contained both the figure 43 liner and the figure 44 scoops but otherwise consisted of the Model B configuration. Strong pressure oscillations existed at all fuel-air ratios in excess of 0.044 at test condition 2, however, this configuration had one particularly desirable feature: All zone 1 fuel manifolding arrangements yielded the same combustion instability behavior. Apparently, the figure 44 scoops and the relatively large pressure drop of the system provided more air and stronger mixing downstream of the zone 1 nozzles than the Model B configurations. Hence, breakup of the fuel sprays was faster. The implication exists that this configuration may not be sensitive to nozzle streaking.

The original number 4 scoops, called vortex generators, are shown in figure 47. Their testing is described in reference 2. Their behavior was very similar to that of turbulators. Exhaustive testing would have been required to pinpoint differences between the two types of scoops. Tests were conducted (ref. 2) with one-half the normal number of turbulators. The combustion stability and combustion efficiency results were as expected - about halfway between those for no turbulators and those for all 80 turbulators. (Figure 47 also shows the number 3 scoops of the secondary liner prior to removal of the trailing edge to prevent thermal cracking (ref. 2) and prior to removal of the turning vanes.)

Manifolding arrangements, fuel nozzles, and supply systems. - Zone 1 manifolding arrangements were important and were discussed previously with the aid of the instability maps of figure 39.

Four different types of zone 1, simplex atomizing nozzles were evaluated at test condition 2. Nominal flow rate was 30 gallons per hour (120 liters/hr) at 100 psi (6.8 atm). Spray patterns were as follows:

Hollow cone	80° full angle
Hollow cone	60° full angle
Semisolid cone	80° full angle
Semisolid cone	60° full angle

Only 20 of each type were available; hence, there were no zone 1 fuel manifolding options. The test results indicate no appreciable changes in combustion stability associated with nozzle spray angle or solidity of spray. These relatively inexpensive nozzles produced combustion efficiency values equally as good as those obtained with the regular nozzles.

In one series of tests, all zone 2 nozzles in line with the turbulators (i. e., 40 nozzles on both o. d. and i. d.) were capped. No changes in stability were observed. Efforts in reference 2 to influence combustion stability by unbalancing the flow to the zone 2 spray bars also proved ineffective.

Several tests indicated that feedback loops involving the fuel systems were an unlikely source of combustion instability in this combustor. One test involved fuel line capacitance. The relatively large fluid volume of each fuel system could conceivably promote instability. If fluid volume were a factor, a volume change would likely affect the behavior of the combustion instability. The effective volume could be changed, without changing fuel flow rate, by making simultaneous adjustments to the bypass-type pressure regulator and throttle valve. (A maximum effective volume occurs when the throttle valve is wide open.) Combustion instability behavior was never observed to change during tests of the type just described. In a second series of tests, dynamic pressure sensors located in the zone 1 secondary fuel manifold showed that the maximum peak-to-peak pressure amplitudes were not at the frequency observed within the combustor. Rather, the observed fuel pressure frequencies (200, 600, and 800 Hz, ref. 2) appeared to be related to the seven-barrel fuel pump which was driven by a 1780-rpm motor. The dominant fuel pressure fluctuations were observed at both stable and unstable combustion conditions. Finally, the amount of feedback is decreased by fuel injector pressure drop. Pressure drops in this apparatus ranged to 900 psi (620 N/cm^2). Also, in many cases either considerably different nozzle pressure drops or fuel manifolding arrangements had no observable effect on instability maps. (For example, compare the three different zone 1 fuel injection arrangements that provided 40 zone 1 flame sources, fig. 39(d).)

Bleed diffuser and centerbody cavity. - A feedback loop involving the bleed diffuser (fig. 3) could conceivably be involved in a combustion-driven oscillation. Also the centerbody cavity (volume and/or length) could influence the instabilities. Several tests

were required to eliminate both possibilities. A description follows.

In the first test, the air was ducted from the exit of the bleed diffuser directly to the bypass louver and cooling louvers (figs. 5, 9, and 48). Hence, the diffuser bleed air could not "see" the centerbody cavity. The ducting, if anything, caused a slight worsening of the oscillatory condition. In the second test, the aforementioned duct work was removed and the bleed diffuser was blocked. Air for the bypass louver and tailpipe cooling was introduced through a 14-inch (35-cm) diameter pipe that extended 6 feet (1.8 m) upstream of the diffuser dome (fig. 3). The pipe was capped at the forward end. Air entered on the cylindrical wall through a helical arrangement of 260 holes distributed along the 1.8-meter length of the pipe extension. Some of the holes are visible in figure 48. Hole diameter was 1.2 inches (3 cm). The hole arrangement was intended to eliminate any feedback of pressure waves traveling upstream through the diffuser and inlet plenum. The modified centerbody produced no observable change in combustion-oscillatory behavior.

Facility and test apparatus interface. - The diffuser-combustor assembly is in intimate contact with the air-inlet and gas-exhaust facilities. These facilities did not appear to be significantly involved in the combustion instability problem. (A somewhat different viewpoint is presented in ref. 2.) A discussion pertaining to feedback loops and noise involving the inlet plenum follows. This material also provides evidence that the combustion instability is not associated with radial velocity profile changes that were induced at the diffuser inlet.

The combustor was operated with the exhaust nozzle both choked and unchoked. The behavior of the combustion instability was nearly independent of the Mach number at the exhaust-nozzle throat. (Exceptions were noted in figs. 39(f) and (g).)

Tests conducted near the end of the experimental work of reference 2 seemed to indicate that the combustion instability could be linked to the inlet facility rather than to the combustor. Hence, an endeavor was made to isolate the combustor from the inlet facility. Diffuser-mounted vanes were selected as a means of studying the interface between inlet plenum and test apparatus. Typical vanes are shown in figure 49. The plane at which the vanes were mounted was about 8 inches (20 cm) downstream of the minimum flow area. The vanes were mounted individually on the outer casing wall. They could be rotated to set values ranging from 0° to 60°. The larger angles provided near-sonic flow at the blades. The blades tested in reference 2 extended two-thirds of the distance across the annulus, causing radial velocity profile to be shifted radially inward. During the present investigation both the old vanes and a new set were tested. The new set spanned the entire passageway. The purpose of the vanes, in the present investigation, was threefold. They were used to produce a large pressure drop (choked flow) and thereby to destroy any combustion-driven feedback loop involving the inlet plenum. Secondly, the effects of deliberately generated noise (turbulence) on combustion were

studied. Thirdly, radial velocity profile effects were examined.

Piezoelectric pressure sensors were mounted along the inlet plenum and diffuser-combustor walls. Pressure disturbances were found to travel freely through the combustor, diffuser, and inlet plenum. The march of a traveling longitudinal wave could be easily followed by inspection of chart data similar to that shown in figure 40. For these studies, at least six pressure transducers were located longitudinally along the test apparatus from the front of the inlet plenum to the end of the tailpipe.

Most of the facility-apparatus interface tests, both in this study and in reference 2, were conducted at test condition 2. This condition permitted a study of both longitudinal and transverse instability, and results were very responsive to zone 1 fuel manifold arrangement (fig. 39(d)).

In order to study the feedback loop possibility, a perforated plate was bolted to the feathered vanes. The plate completely filled the flow area shown in figure 49. Choked flow existed immediately downstream of the 3/16-inch (0.5-cm) diameter perforations. These small holes resulted in a noise level no greater than that of the vaneless diffuser. The plate was tested in conjunction with three different combustor configurations. When combustion instability occurred, flow conditions were such that pressure waves did not pass the barrier. The results showed that the location of the demarcation lines on the instability maps was unchanged by the presence of the plate. The tuning of the longitudinal waves was observed to be somewhat sharper when the plate was present. Hence, a feedback loop involving the combustor and the inlet plenum was an unlikely source of combustion instability in this combustor.

The plate was removed, and combustion instability was mapped for various positions of blade angle. Tests were made both with the long vanes and with the short vanes. During the present investigation, these vane tests were conducted many times with many different combustor configurations. No effect of vane length or vane angle (or even the presence of the vanes themselves) on combustion instability was detected. The perforated plate concentrated the flow along the outer wall (fig. 50). The short vanes had the opposite effect. In neither case did the profile become sufficiently extreme that flow separation was detected. Both the long vanes and the vaneless diffuser provided profiles intermediate to those exhibited by the short vanes and the perforated plate; however, the vaneless diffuser provided a higher velocity flow along the inner wall (fig. 50). The tests showed that the radial velocity profile variations encountered did not materially influence combustion instability in the duct burner.

The error introduced into pressure amplitude measurements by apparatus vibration is shown in figure 51. The upper curve of figure 51 shows the signal produced by a piezoelectric pressure transducer when it was vibrated at 800 hertz on a bench calibration stand upon which an accelerometer was mounted. The lower curve shows the signal produced by the same transducer when mounted on the combustor casing alongside an

accelerometer. The data of figure 51 indicate that for a given accelerometer value the pressure level produced in the combustor is approximately equal to the noise produced on a vibration stand. Hence, when air is flowing at test condition 4 (fig. 51) and the accelerometer is registering about 9 g's, the pressure level of 0.2 psi (0.015 atm) registered by the pressure transducer may be largely noise associated with vibration of the instrument. These values are typical of the data obtained both with no combustion and with smooth combustion. (The ordinate of fig. 51 is the noise (hash) shown on the pressure transducer traces of fig. 40.)

The noise level (turbulence) of the inlet plenum and the test apparatus was observed to change quite drastically as the vane angle was increased. For example, in one set of tests the pressure (noise) signal increased approximately fourfold when the vanes were rotated from a feathered position to a 60° position. Accelerometer values doubled. That these relatively large changes in turbulence level had no noticeable effect on the instability maps is evidence of the extent to which inlet-plenum noise and combustion instability were unrelated. No evidence was found during the present investigation that showed any relation between inlet-plenum noise and combustion instability.

Much time and effort were devoted to a study of the possible effect of the air-supply and gas-exhaust systems on combustion instability. An examination of all the results has led the authors to this conclusion - the instability problem is within the diffuser-combustor apparatus and is not materially affected by the test facility.

SUMMARY OF RESULTS

Numerous hardware changes were made to a full-scale duct burner in an effort to suppress combustor pressure oscillations while simultaneously maintaining good performance characteristics. The following results were obtained:

1. A configuration (Model B-NOTURB) evolved which provided smooth combustion at three prescribed, simulated flight conditions. Combustion efficiency was 92 percent at transonic climb, 99 percent at cruise approach, and 91 percent at cruise.

2. The addition of number 4 air scoops (Model B-TURB) improved the mixing process and raised the combustion efficiency 3 to 4 percent at transonic climb and cruise conditions; however, combustion oscillations existed at the cruise-approach condition when the scoops were present.

3. Other characteristics of the Model B configuration were

(a) Diffuser pressure loss was 1.7 percent and isothermal combustor pressure loss was 4.3 percent. These values were obtained at a combustor reference Mach number of 0.15.

(b) The flight-weight combustion chamber liners proved to be well cooled and showed no signs of metal fatigue. Neither temperature sensors nor postrun inspection showed evidence of hot-spot damage. The hardware experienced over 200 hours of hot testing and over 200 hours of cold flowing. Furthermore, the test apparatus was subjected hundreds of times to combustion instability which often produced violent and noisy vibrations for periods of several seconds each.

(c) A simplified fuel injection arrangement replaced the dual-orifice atomizers with simplex atomizers. Blowout and relight performance, as well as combustion efficiency, were in no way penalized by changing to the less complex injection scheme.

4. At certain test apparatus conditions, even the Model B-NOTURB combustor would exhibit pressure oscillations. The oscillations occurred at very specific values of zones 1 and 2 fuel flow rates for the five selected sets of combustor inlet air parameters (pressure, temperature, and velocity) tested. The repeatability of the demarcation line dividing smooth and oscillatory combustion was demonstrated by comparing data taken over a span of nearly 1 year.

5. No other combustor configuration tested in this apparatus has provided, in a reproducible manner, stable combustion at all three prescribed simulated flight conditions.

6. During the course of the investigation, certain general observations were made regarding the pressure waves. The pressure waves ranged from 70-hertz longitudinal waves to 470-hertz third-mode transverse waves. Specific waveforms were associated with specific sets of operating conditions and combustor configurations. Peak-to-peak pressure amplitudes of the waves, when driven at maximum intensity, were approximately 10 percent of the mean pressure for the longitudinal waves and in excess of 40 percent of the mean pressure for the transverse waves.

7. Four separate efforts to combat the pressure oscillations by means of acoustic damping liners were unsuccessful.

8. Tests showed that the combustion instability could not be linked to the facility or to the bleed diffuser and centerbody cavity. Also, longitudinal baffles in the forward portion of the combustor were of no help.

9. For the range of test conditions that were investigated, smooth combustion was promoted by

(a) Increasing combustor reference Mach number

(b) Increasing combustor pressure

(c) Decreasing combustor inlet-air temperature

(d) Proper selection of the number of zone 1 fuel injection sources

(e) Proper selection of fuel flow split between zones 1 and 2

10. Oscillatory combustion was promoted by

(a) Increasing the quantity, size, and turning angle of the number 3 and number 4 air scoops

(b) Zone 1 fuel nozzle streaking

CONCLUDING REMARKS

Combustion instability was of harmful consequence in a large, high-heat-release, diffuser-combustor combination that otherwise demonstrated excellent performance. Suppression of combustion instability was obtained by eliminating a particular set of isolated air scoops. These scoops, harmful only at certain test conditions, promoted combustion at all times. A mechanical linkage that would retract the air scoops when necessary would be very helpful. The combustor so constructed would exhibit combustion efficiencies of 95 percent or better at simulated transonic climb, cruise-approach, and initial cruise flight conditions. Isothermal pressure drop of the diffuser-combustor combination would be in the vicinity of 6 percent at a reference Mach number of 0.150.

Lewis Research Center,
National Aeronautics and Space Administration,
Cleveland, Ohio, September 29, 1970,
720-03.

APPENDIX A

SYMBOLS

A	area
C	specific heat (used also as a constant in appendix C)
C_d	discharge coefficient
F	gross stream thrust
f/a	fuel-air ratio (always based on the total airflow rate at the diffuser inlet)
g_c	gravitational constant
H	enthalpy
M	Mach number
P	total pressure
p	static pressure
Q	heat flow rate
$\mathscr{R}$	gas constant
ΔR	distance from wall to center of exhaust nozzle annulus
r	radial position
T	total temperature
ΔT_L	temperature loss
t	static temperature
V	velocity
W	fluid flow rate
γ	ratio of specific heats
η	combustion efficiency
ρ	mass density

Subscripts:

a	air, including entrained water vapor
exp	experimental
norm	normalized
ref	reference
t	total
2, 3, 4, 5	stations 2, 3, 4, 5 of figure 3

APPENDIX B

ERROR ANALYSIS

In order to estimate accuracy of combustion efficiency values obtained by the choked-nozzle technique, a numerical study of probable combustion efficiency error was undertaken. The approach used was to start with a set of actual performance program input data obtained at test condition 5. This data set was then submitted repeatedly as input to the performance analysis program. With each input, however, one of the parameters affecting combustion efficiency was assigned a 1-percent change from its original value. All other parameters were left unaltered. A sufficient number of inputs was prepared for each parameter to be varied first 1 percent below and then 1 percent above its original value. From the computed results the error in combustion efficiency η due to a 1-percent error in parameter χ_i (i.e., $\Delta\eta_i/\Delta\chi_i$) could be obtained. To arrive at probable efficiency error due to all parameters χ_i (i = 1, N), a statistical error formula was used, as shown:

$$\Delta\eta = \left[\sum_{i=1}^{N}\left(\frac{\Delta\eta_i}{\Delta\chi_i}\right)^2 \times \Delta\chi_i\right]^{1/2} \tag{B1}$$

where

$\Delta\eta$ 3σ variation of η

N number of parameters affecting η

$\Delta\chi_i$ 3σ variation of test parameter χ_i

Equation (B1) assumes normal distribution of error for each parameter. Table IV gives a summary of the error study. The parameters are listed in the first column. In the second column, headed $\Delta\chi_i$, are listed the best estimates available for the 3σ error of the individual test parameters. The fourth column shows the error in η due to a positive 1-percent error in any given parameter χ_i. The last column, headed $\Delta\eta_i$, lists the error in η that would be caused by any one parameter being measured with its individual 3σ error, with all other parameters being correct. This column identifies the three most critical parameters as nozzle throat area, nozzle throat pressure, and fuel flow rate.

Table V shows the overall η error that can be expected in the data, assuming normal distribution. The 1σ error of ± 0.73 percent agrees well with the reproducibility of test data. It should be pointed out that this analysis was performed for test condition 5. However, checks made on the η error due to the three most critical parameters at the other test conditions show the η error given in table V to be fairly representative.

APPENDIX C

RADIAL TEMPERATURE PROFILE EFFECT ON COMBUSTION EFFICIENCY

Since the choked nozzle instrumented with total-pressure rakes was actually measuring gross stream thrust at the throat section, the derived combustion efficiency values presented in this report also represent thrust efficiency. Contrasted to chemical combustion efficiency, which is based on an average exhaust gas temperature regardless of radial profile, the thrust-producing capability of the gases is affected by exhaust gas temperature profile. This profile effect will be illustrated in the succeeding paragraphs by comparing the thrust obtained assuming a flat temperature profile (fig. 52(a)) to the thrust due to a parabolic profile (fig. 52(b)) typical of test condition 4. Both profiles have the same average total temperature (i. e., the same chemical combustion efficiency).

Gross stream thrust in compressible flow is given as

$$F = pA + W\frac{V}{g_c} = pA\left(1 + \frac{\rho V^2}{pg_c}\right) = pA(1 + \gamma M^2) \tag{C1}$$

The term pA can be expressed in terms of throat temperature, Mach number, and total mass flow rate as

$$pA = \frac{W\sqrt{T} \times \sqrt{\frac{\mathscr{R}}{\gamma g_c}}}{M\sqrt{1 + \frac{\gamma - 1}{2} M^2}} \tag{C2}$$

permitting the stream thrust to be written as

$$F = W\sqrt{T}\left[\frac{(1 + \gamma M^2)\sqrt{\frac{\mathscr{R}}{\gamma g_c}}}{M\sqrt{1 + \frac{\gamma - 1}{2} M^2}}\right] \tag{C3}$$

Several observations can be made about equation (C3) which will greatly simplify the

final expressions used to compare the thrust efficiencies of the two exhaust temperature profiles.

For a fully choked exhaust nozzle the Mach number can be assumed to have a value of 1 across the nozzle annulus. For this case the term in brackets is a function only of the specific-heat ratio γ, which in turn varies with static gas temperature. For the flat temperature profile, then, this term will be constant across the annular duct. For the parabolic total-temperature profile the static gas temperature varies across the nozzle annulus. In this case the computed value of the bracketed term in equation (C3) was found to vary by about 1.5 percent across the annular duct. It can be shown, however, that the mean effective value of this term is only about 0.05 percent lower than for the flat profile. For the sake of simplicity the value for this bracketed term will be assumed to be the same constant for both profiles.

Based on the preceding observations the thrust equation reduces to

$$F = CW\sqrt{T} \tag{C4}$$

where C is the constant evaluated from the bracketed term in equation (C3). If T or W are functions of radial position, equation (C4) changes to

$$F = C\int_{R_i}^{R_o} \sqrt{T(r)}\,\frac{dW(r)}{dr}\,dr \tag{C5}$$

For the purpose of illustration, axisymmetric profiles are assumed, thus permitting only one cross section of the annulus of width $R_o - R_i = 2\,\Delta R$ to be considered. For the flat profile, shown in figure 52(a),

$$F = C\int_{-\Delta R}^{\Delta R} \sqrt{T}\,\frac{dW}{dr}\,dr = C\int_{-\Delta R}^{\Delta R} \sqrt{2500}\,\frac{dW}{dr}\,dr \tag{C6}$$

(Rankine units are used for temperature in eq. (C6).) Before the integral can be evaluated, the term dW/dr, representing the mass flow per unit radial width, must be determined. Data obtained from other combustors show dW/dr to be practically constant across the duct, even in cases where the temperature profile is peaked. Thus dW/dr can be replaced by the constant term $W/2\,\Delta R$. Equation (C6) now becomes

$$F = \frac{CW}{2\,\Delta R} \int_{-\Delta R}^{\Delta R} \sqrt{2500}\, dr \tag{C7}$$

Thus the flat profile thrust can be evaluated as

$$\left.\begin{aligned} F &= \frac{CW}{\Delta R} \times 50 \int_0^{\Delta R} dr = \frac{50\,CW}{\Delta R} [r]_0^{\Delta R} \\ \text{or} \\ F &= 50\,CW \end{aligned}\right\} \tag{C8}$$

For the parabolic temperature profile shown in figure 52(b) the gross thrust can be calculated by substituting the parabolic profile into equation (C5):

$$F = C \int_{R_i}^{R_o} \sqrt{\frac{2250}{\overline{\Delta R}^2}\left(1.445\,\overline{\Delta R}^2 - r^2\right)}\, \frac{dW}{dr}\, dr \tag{C9}$$

Again assuming dW/dr to be a constant equal to $W/2\,\Delta R$ and because of axial and radial symmetry across the annulus $R_o - R_i = 2\,\Delta R$

$$F = \frac{47.43}{\Delta R}\, \frac{CW}{2\,\Delta R}\, 2 \int_0^{\Delta R} \sqrt{1.445\,\overline{\Delta R}^2 - r^2}\, dr \tag{C10}$$

$$F = \frac{47.43}{2}\, \frac{CW}{\overline{\Delta R}^2} \left[r \sqrt{1.445\,\overline{\Delta R}^2 - r^2} + 1.445\,\overline{\Delta R}^2 \sin^{-1}\left(\frac{r}{1.202\,\Delta R}\right) \right]_0^{\Delta R} \tag{C11}$$

$$F = \frac{47.43}{2}\, \frac{CW}{\overline{\Delta R}^2} \left(0.667\,\overline{\Delta R}^2 + 1.445\,\overline{\Delta R}^2 \times 0.982\right) \tag{C12}$$

$$F = \frac{47.43}{2}\, CW(2.086) \tag{C13}$$

$$F = 49.47\ CW \tag{C14}$$

This value of thrust is 98.9 percent of the thrust value (eq. (C8)) for the flat profile. The 1.1-percent decrement in thrust is equivalent to a 1.1-percent decrement in pressure which has been shown (appendix B) to correspond to approximately a 3-percent loss in combustion efficiency as defined in this report. It is again emphasized that this penalty in efficiency is due to the profile effect alone.

APPENDIX D

ACOUSTIC LINER DESIGN

In an effort to dampen the various frequencies of combustion oscillations encountered in the duct burner, acoustic absorption liners (fig. 42) were designed for both the inner and outer walls. The absorption analysis is outlined in reference 8.

The specifications for these liners are as follows:

	Outer liner	Inner liner
Thickness:		
in.	0.125	0.125
cm	0.32	0.32
Annular gap:		
in.	0.95	1.312
cm	2.42	3.33
Hole diameter:		
in.	0.188	0.188
cm	0.48	0.48
Open area ratio, percent	13	13
Estimated velocity at liner hole:		
ft/sec	60	80
m/sec	18	24

Figure 53 shows the absorption coefficients computed for these liners as a function of velocity through the holes. The outer liner, designed to absorb frequencies in the neighborhood of 450 hertz, is shown to have an absorption coefficient of 0.5 or better at hole velocities near 60 feet per second (18 m/sec). The inner liner, designed for the lower frequencies of 200 to 300 hertz, shows absorption coefficients between 0.4 and 0.5. These values should have been sufficient to significantly dampen combustion oscillations in the 200- to 500-hertz range. The fact that this did not occur could be attributed to the following causes:

(1) The empirical model used in the absorption calculations did not fit the hardware conditions.

(2) The absorption capacity of the liners was never fully tested since maximum amplitudes were limited to 1 psi peak-to-peak by limiting fuel flow.
It is possible that the absorption would have been more significant at higher pressure amplitudes. High amplitudes, however, could not be tolerated in this combustor, and attempts to limit screech by absorption were discontinued.

REFERENCES

1. Dugan, James F., Jr.; Koenig, Robert W.; Whitlow, John B., Jr.; and McAuliffe, Timothy B.: Turbojet and Turbofan Engines for a Mach 3 Supersonic Transport. Paper 64-244, AIAA, June 1964.

2. Clapp, C. J.: Full Scale Turbofan Duct Burner Test Program. Rep. PWA-FR-2542, Pratt & Whitney Aircraft (NASA CR-54637), Mar. 18, 1968.

3. Mealey, Charles; and Kee, Leslie: A Computer-Controlled Central Digital Data Aquisition System. NASA TN D-3904, 1967.

4. Staff of the Lewis Laboratory: Central Automatic Data Processing System. NACA TN 4212, 1958.

5. Shapiro, Ascher H.: The Dynamics and Thermodynamics of Compressible Fluid Flow. Vol. I. Ronald Press Co., 1953.

6. Cervenka, A. J.; and Friedman, R.: Ram-Jet Performance. Adaptation of Combustion Principles to Aircraft Propulsion. Vol. II - Combustion in Air-Breathing Jet Engines. NACA RM E55G28, 1956, ch. XIV.

7. Blackshear, Perry L., Jr.; and Rayle, Warren D.: Oscillations in Combustors. Basic Considerations in The Combustion of Hydrocarbon Fuels with Air. NACA Rep. 1300, 1957, ch. VIII.

8. Anon.: A Study of the Suppression of Combustion Oscillations with Mechanical Damping Devices. Rep. PWA FR-2596, Pratt & Whitney Aircraft (NASA CR-90094), Nov. 20, 1967.

TABLE I. - TEST CONDITIONS

Test condition	Inlet-air pressure absolute, atm	Inlet-air temperature		Reference Mach number	Mass flow rate		Fuel-air ratio of emphasis	Simulated flight condition
		°F	K		lb/sec	kg/sec		
1	2/3	200	367	0.138	91	41	Near 0.050	---
2	1	285	414	.144	135	61	0.050	Transonic climb
3	1	550	561	.144	118	53	Near 0.050	---
4	1	550	561	.175	141	63	0.016 to 0.020	Cruise[a]
							Near 0.050	---
5	$1\frac{2}{3}$	550	561	.175	230	105	0.016 to 0.020	Cruise[b]
							0.050	Cruise approach

[a]At 75 000 ft (23 km).
[b]At 65 000 ft (20 km).

TABLE II. - FLOW AREAS OF MODEL B CONFIGURATION

Flow area	Discharge coefficient, C_d	Percentage of open area,[a] $\frac{AC_d \times 100}{A_{ref}}$	Percentage of total airflow, $\frac{AC_d \times 100}{A_{ref}} \times \frac{92.00}{54.13}$
Swirler	0.8	3.35	5.69
Firewall cooling:			
Firewall face	.6	.48	.80
Firewall:			
Inside diameter		.31	.52
Outside diameter		.36	.60
Firewall support:			
Inside diameter		.31	.52
Outside diameter		.37	.62
Number 1 cooling slots:			
Inside diameter	.75	.74	1.26
Outside diameter	.75	.87	1.47
Number 1 and 2 scoops	.71	4.76	8.08
Number 2 cooling slots:			
Inside diameter	.75	.89	1.51
Outside diameter	.75	1.47	2.50
Number 3 scoops	.88	6.42	10.92
Number 3 scoop bypass	.94	33.80	57.50
Total		54.13	[b]92.00
Number 4 scoops (turbulators)	.90	5.60	------

[a]Based on an A_{ref} of 1865 in.^{2} (12 020 cm^2).
[b]An additional 8 percent enters diffuser bleed.

TABLE III. - COMPARISON OF COMBUSTION EFFICIENCY FOR MODEL B CONFIGURATION WITH AND WITHOUT TURBULATORS

Airflow condition	Overall fuel-air ratio	Turbulators	Combustion efficiency, percent
1	0.050	Present	90
		Absent	83
2	0.050	Present	95
		Absent	92
4	0.016	Present	91.0
		Absent	90.0
	0.050	Present	99.0
		Absent	98.0
5	0.016	Present	95
		Absent	91
	0.050	Present	No data[a]
		Absent	99

[a]Combustor pressure oscillations present.

TABLE IV. - SUMMARY OF COMBUSTION EFFICIENCY ERROR

Parameter χ_i	3σ Error in χ_i, $\Delta\chi_i$, percent	$\Delta\chi_i^2$, percent	$\frac{\Delta\eta_i}{\Delta\chi_i}$ (a)	$\left(\frac{\Delta\eta}{\Delta\chi_i}\right)^2$	$(\Delta\eta_i)^2$, percent	3σ Error in η due to $\Delta\chi_i$ only, $\Delta\eta_i$, percent
Air orifice pressure	±0.5	±0.25	-1.0	1.0	±0.25	±0.50
Air orifice delta pressure	±.5	±.25	-.8	.64	±.16	±.40
Air orifice temperature	±1.0	±1.0	.45	.202	±.202	±.45
Fuel flow rate	↓	↓	-.9	.81	±.81	±.90
Fuel temperature			-.45	.202	±.202	±.45
Combustor inlet temperature			-.38	.144	±.144	±.38
Nozzle throat pressure	±.33	±.109	2.70	7.29	±.795	±.89
Nozzle throat area	±.5	±.25	2.70	7.29	±1.82	±1.35
Specific-heat ratio at nozzle throat	±.5	±.25	1.0	1.0	±.25	±.5
Fuel heating value	±.5	±.25	-.9	.81	±.202	±.45

[a]Sign indicates direction of η error due to a positive χ_i error.

TABLE V. - ERROR OF COMBUSTION EFFICIENCY DATA

Standard deviation	$\pm\sigma$	$\pm2\sigma$	$\pm3\sigma$
Percent of data	68.3	95.5	99.8
Error in combustion efficiency, percent	±0.73	±1.46	±2.2

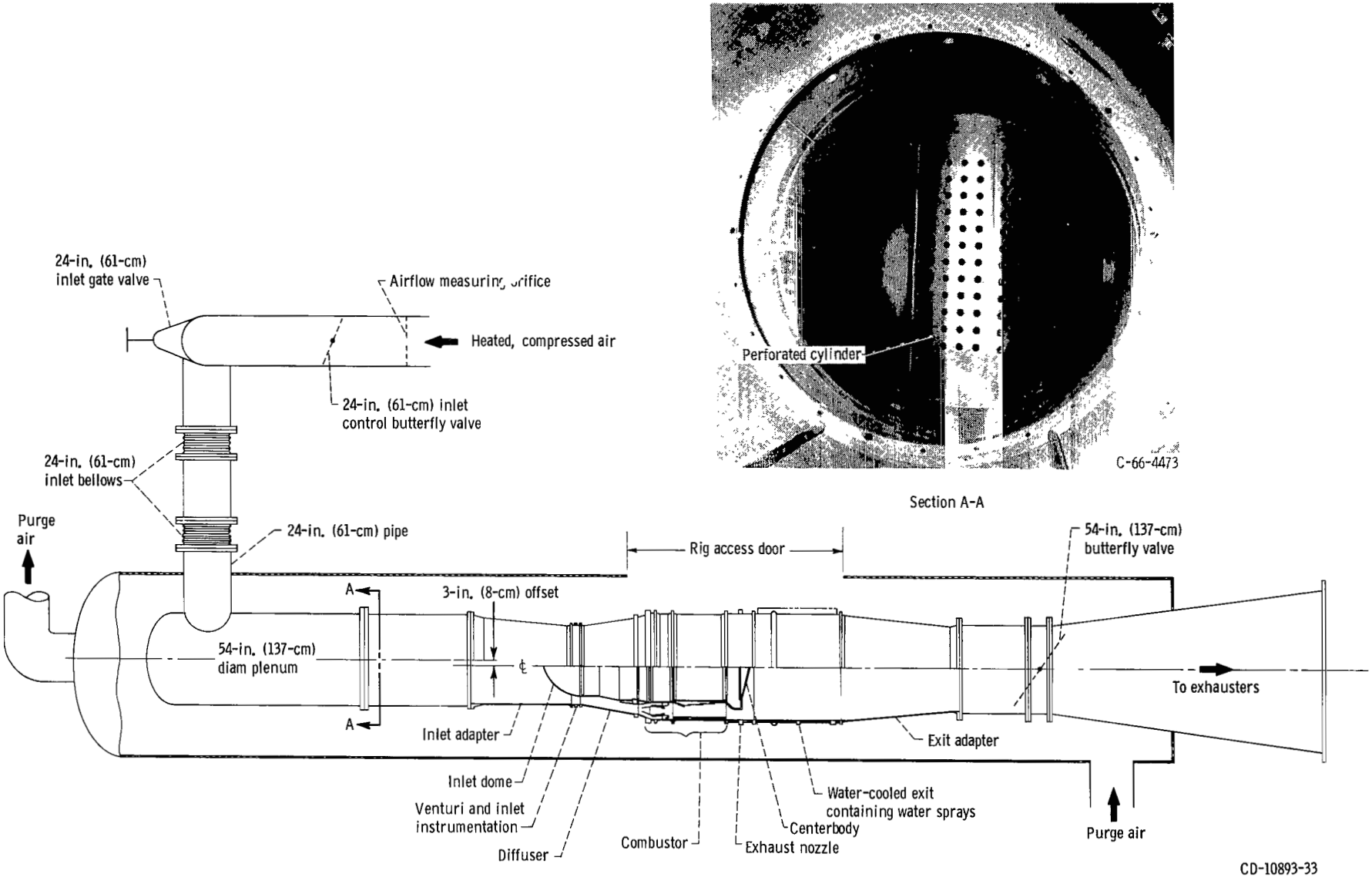

Figure 1. - Duct burner mounted on test facility.

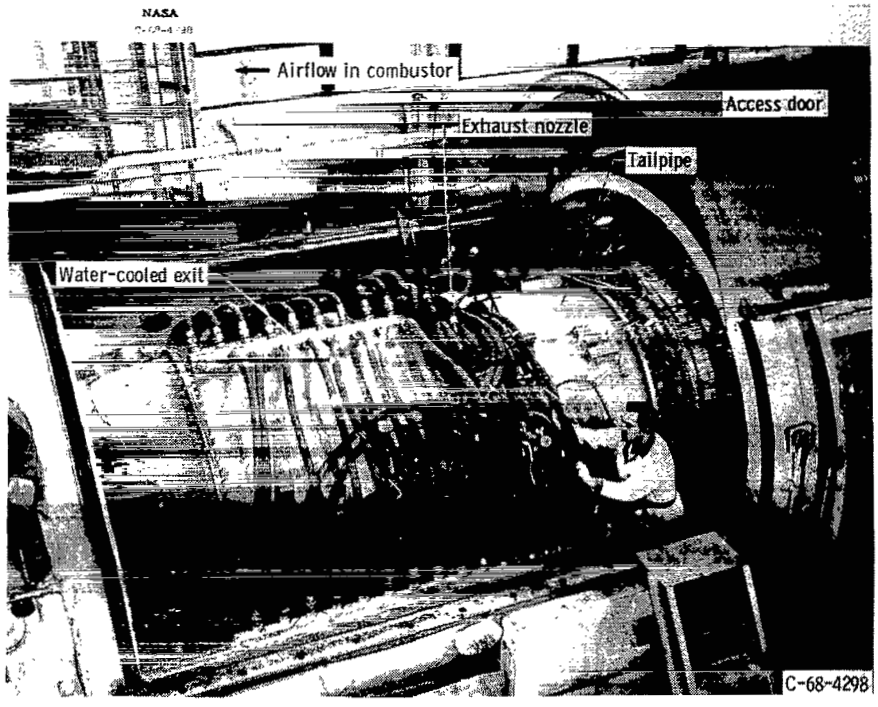

Figure 2. - Test apparatus assembly viewed through open access door.

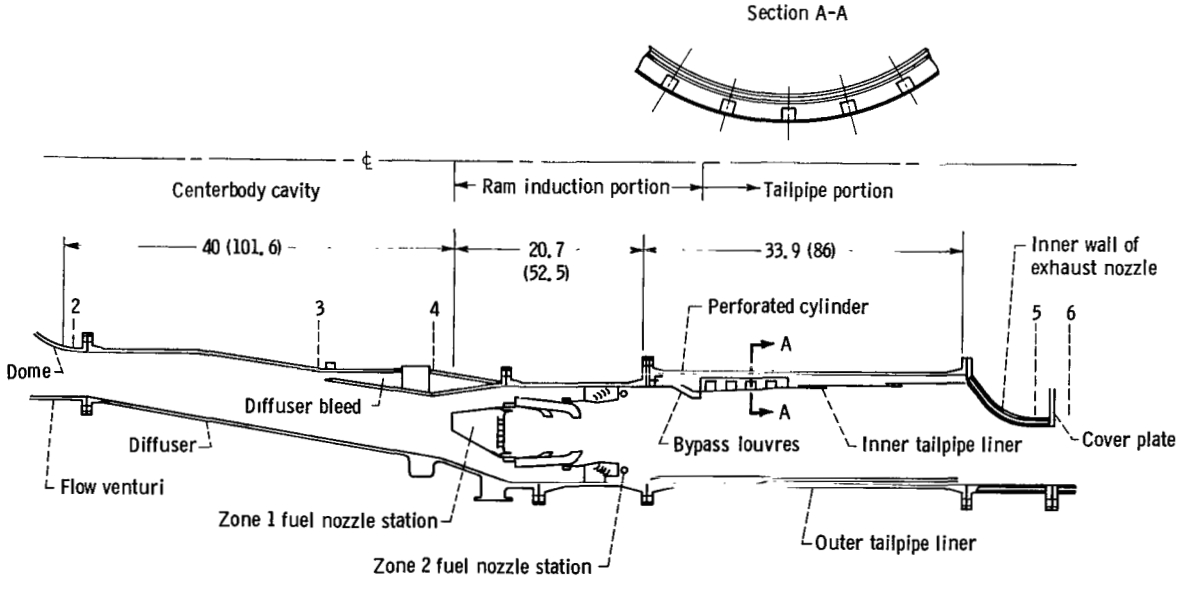

Figure 3. - Cross section of duct burner. (Dimensions are in inches (cm).)

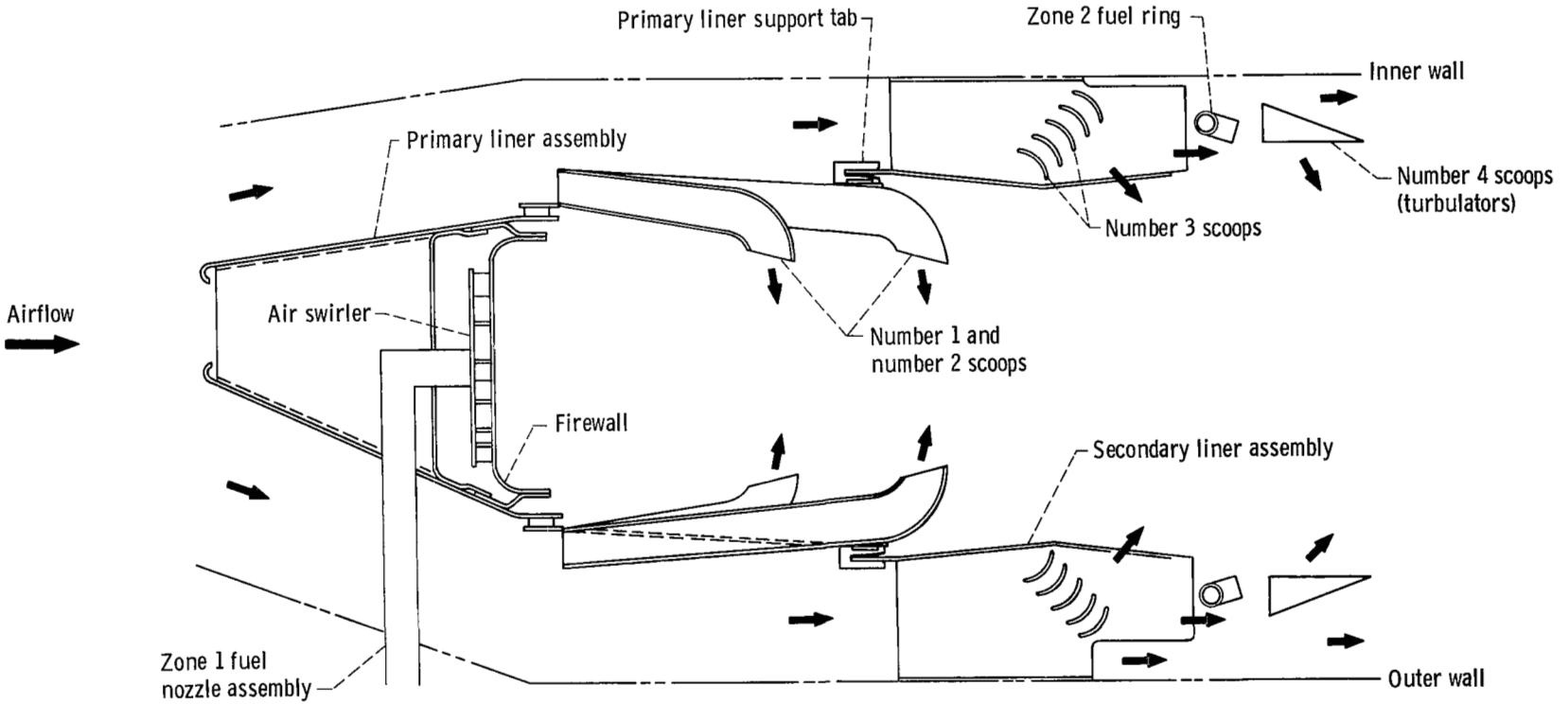

CD-10895-33

Figure 4. - Cross section of ram-induction portion of duct burner.

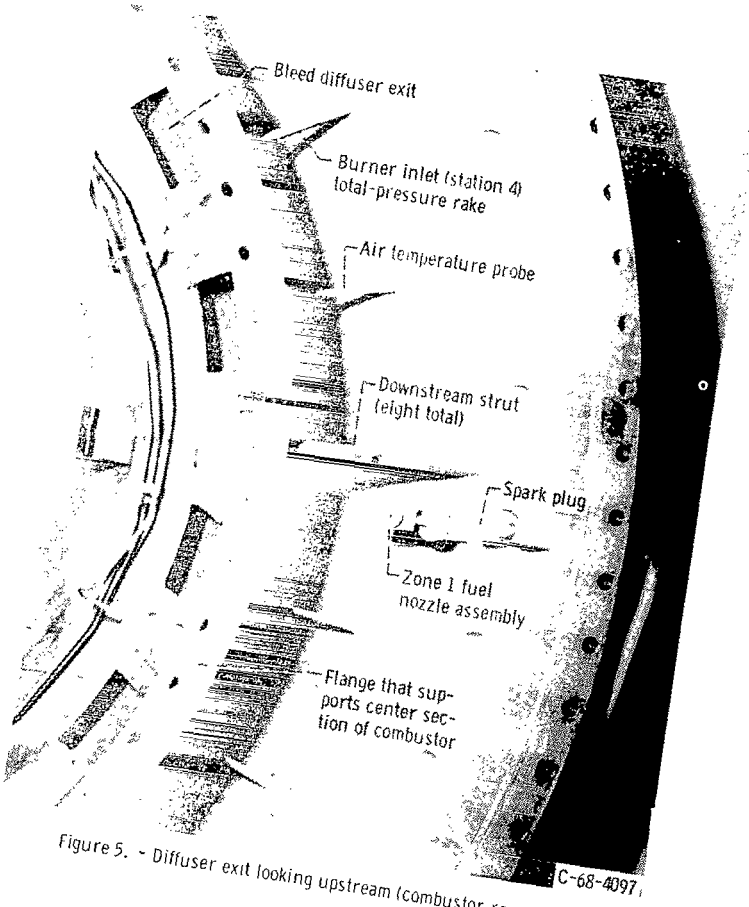

Figure 5. - Diffuser exit looking upstream (combustor removed).

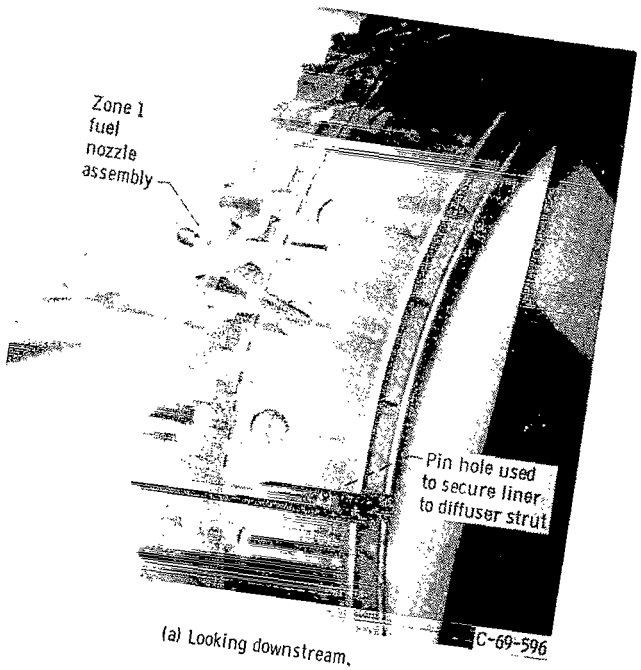

(a) Looking downstream.

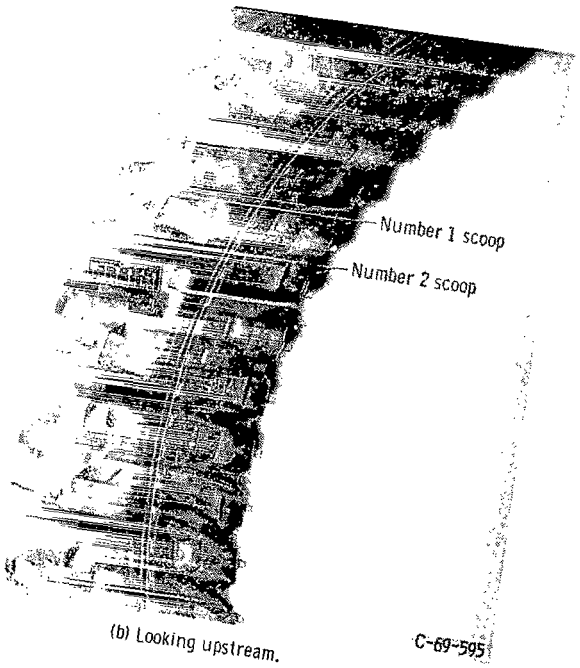

(b) Looking upstream.

Figure 6. - Primary liner.

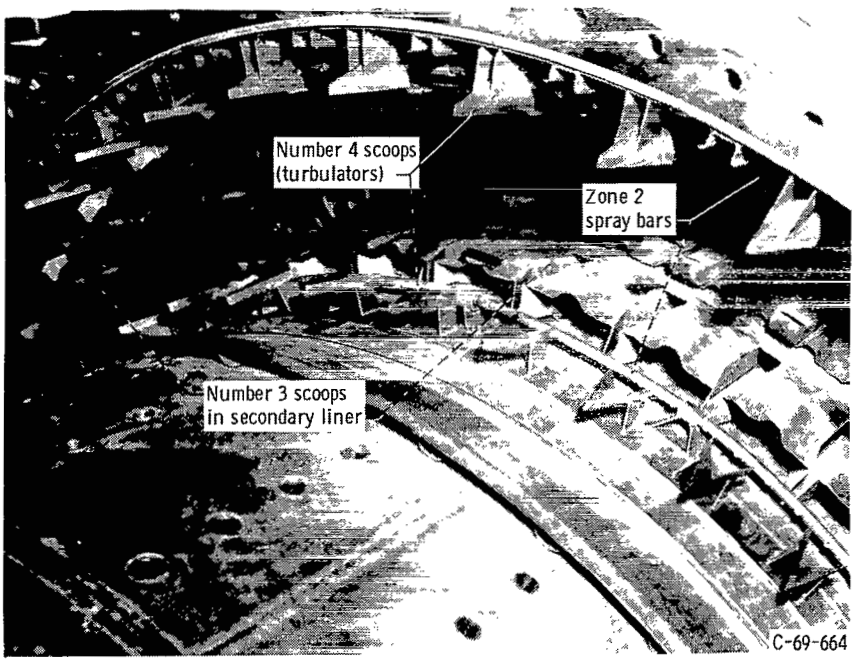

Figure 7. - Oblique view of combustor.

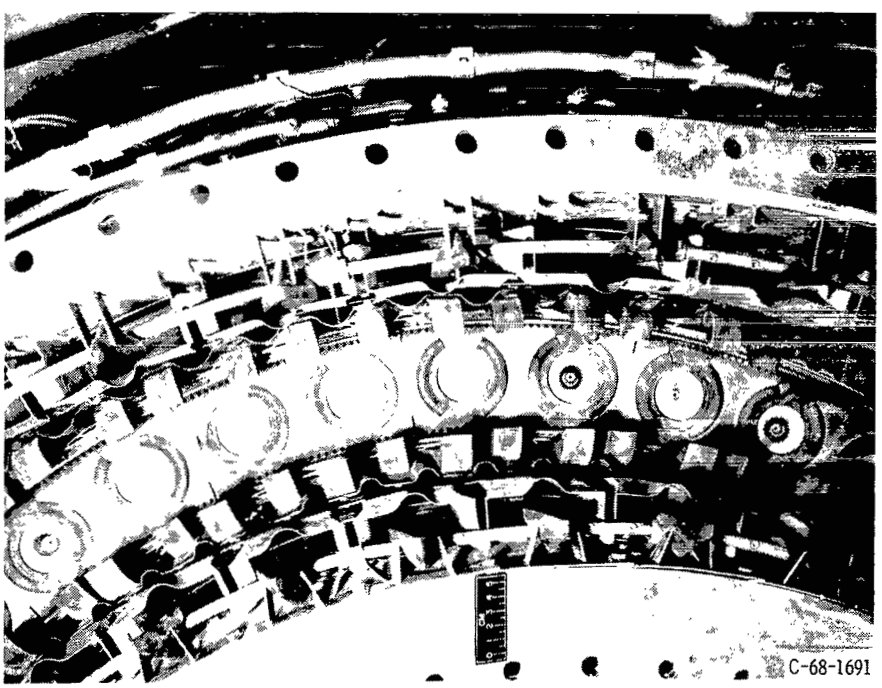

Figure 8. - Looking upstream at scoop assembly.

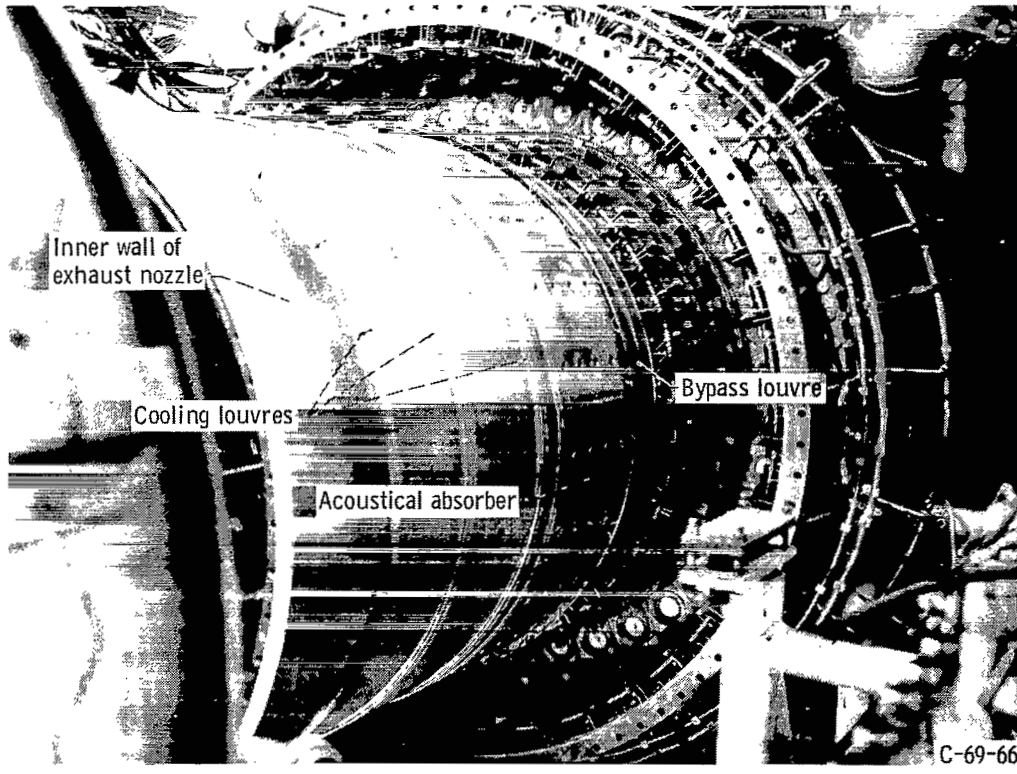

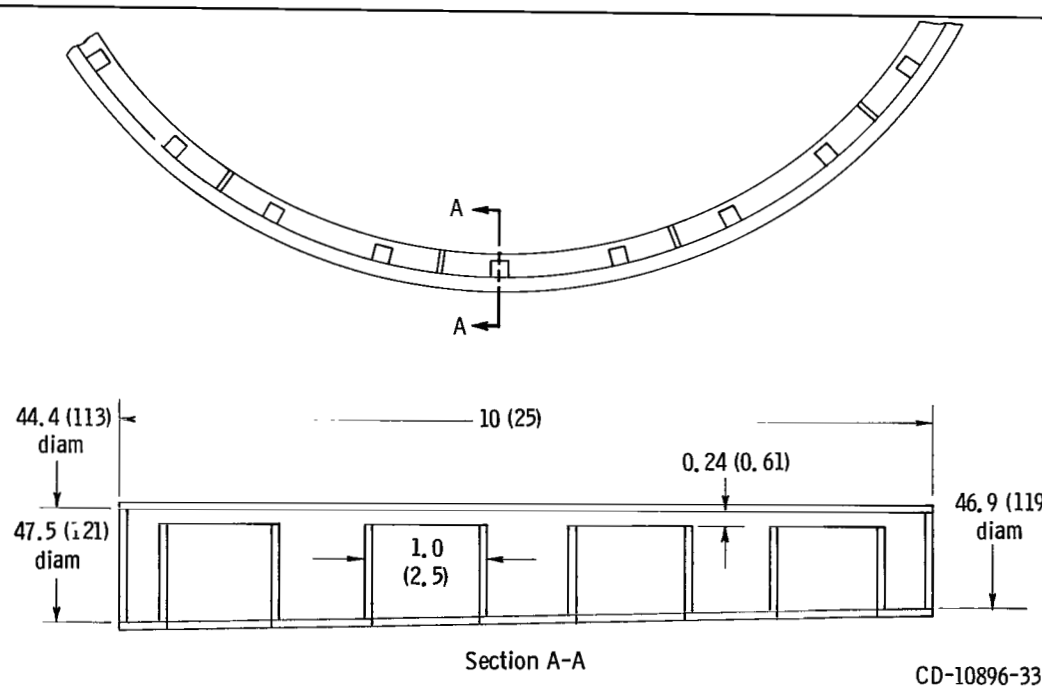

Figure 9. - Inner tailpipe liner. (Dimensions are in inches (cm).)

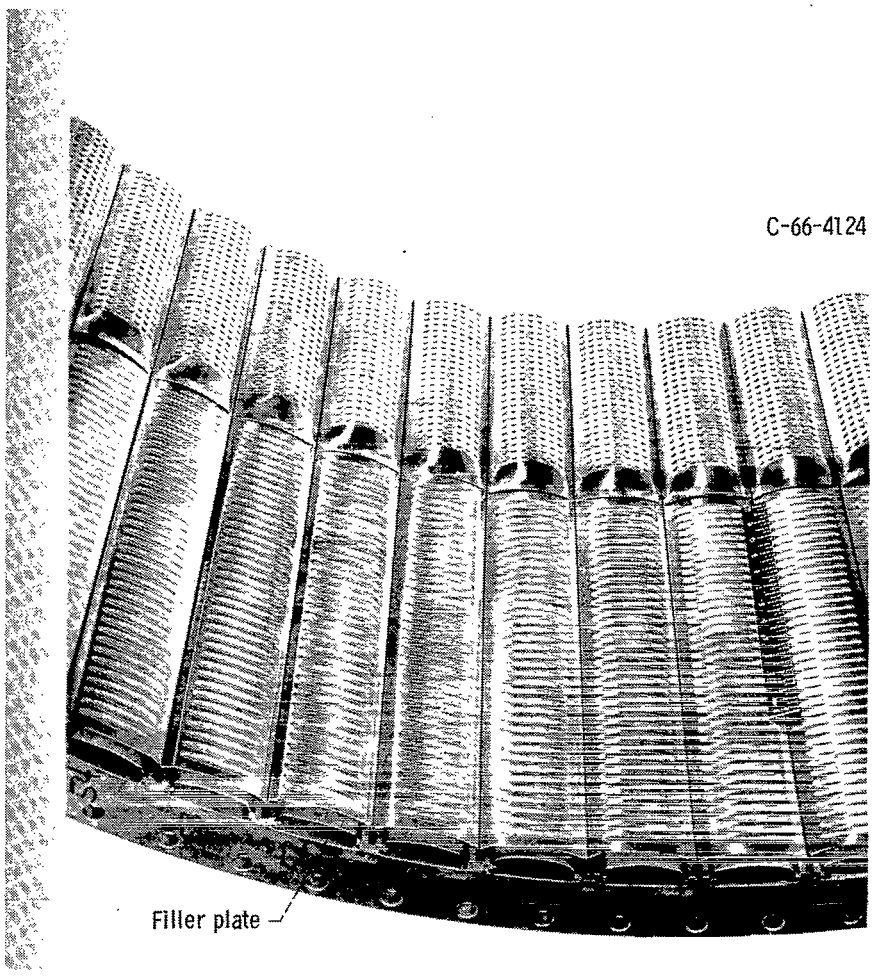

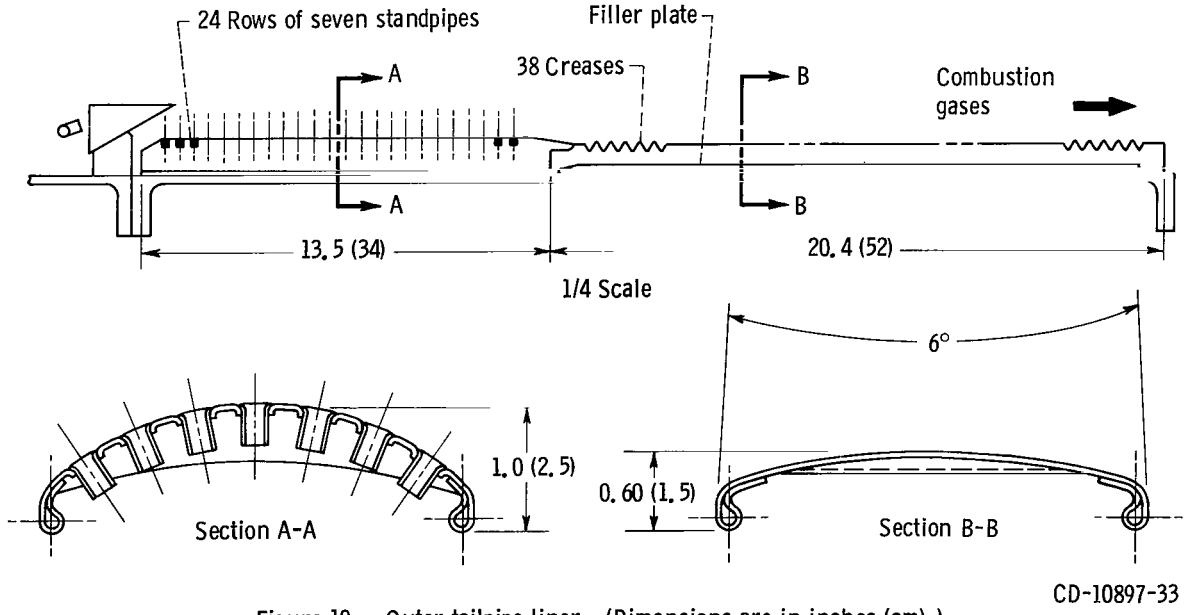

Figure 10. - Outer tailpipe liner. (Dimensions are in inches (cm).)

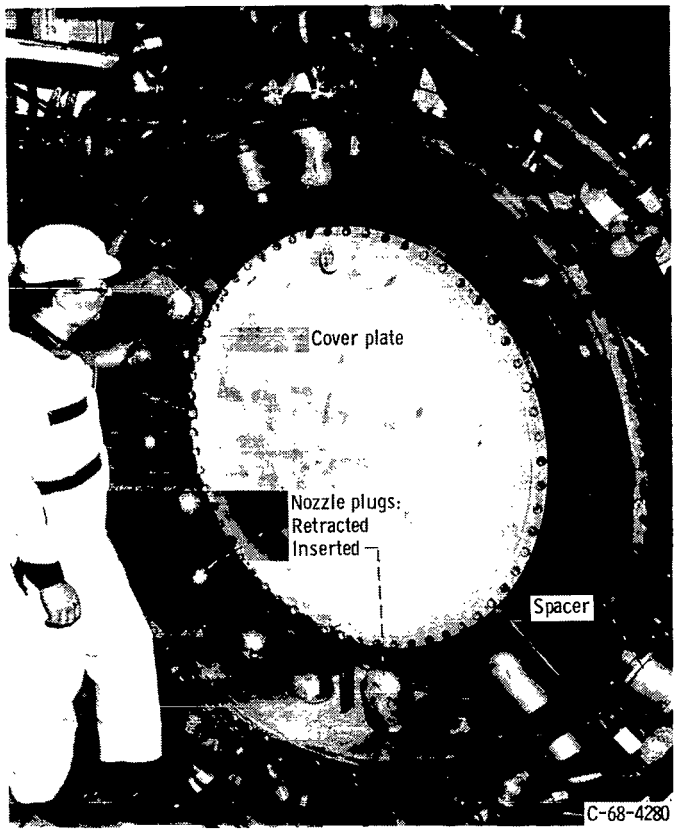

Figure 11. - Exhaust nozzle.

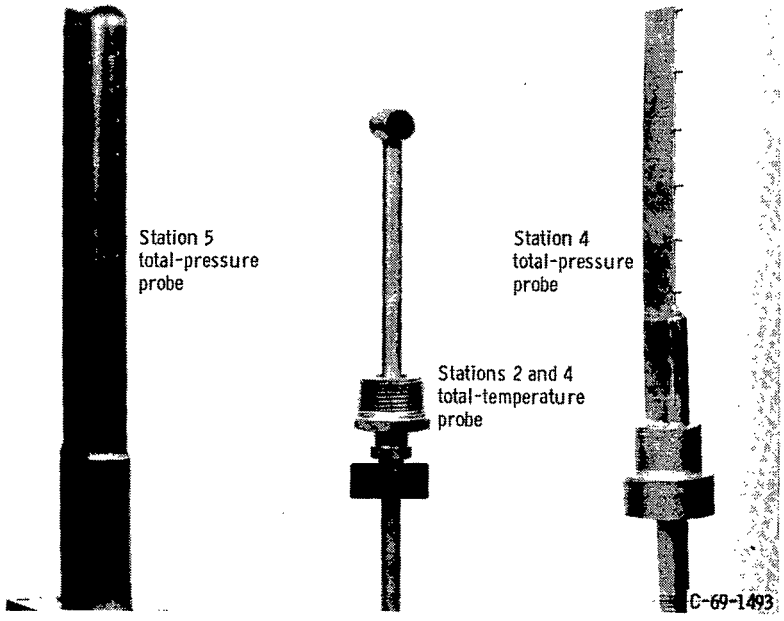

Figure 12. - Typical, fixed-position sensors.

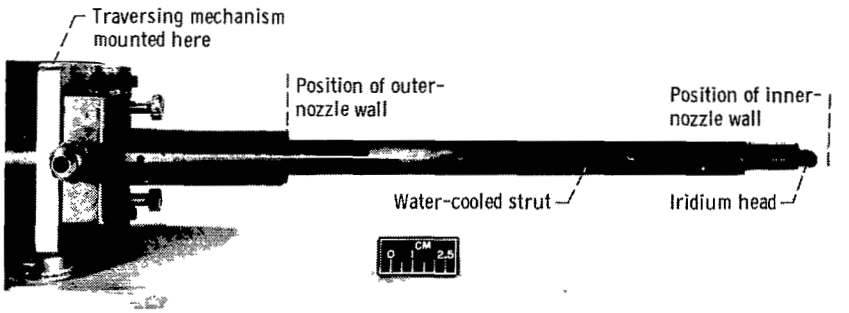

Figure 13. - Traversing thermocouple and total-pressure probe shown in the fully inserted position.

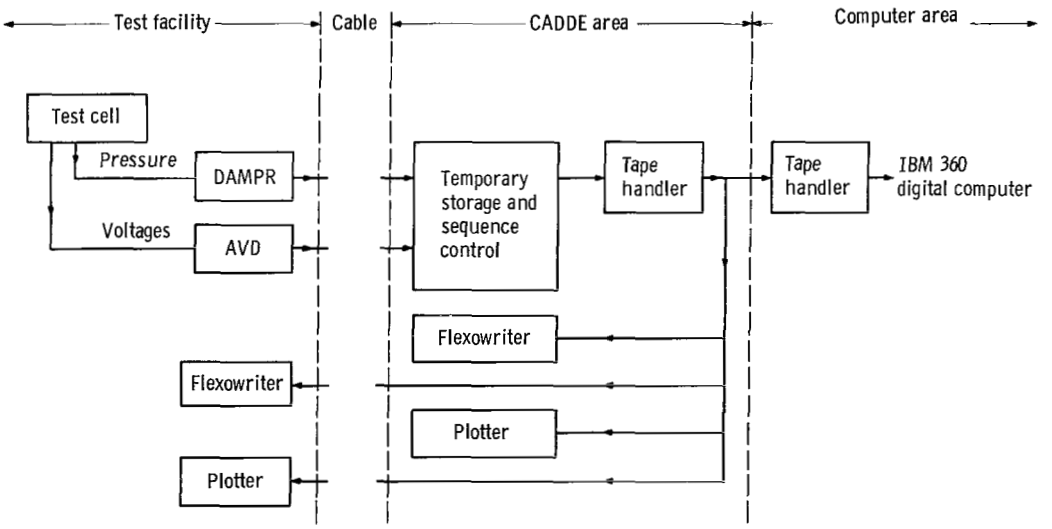

Figure 14. - Data recording system.

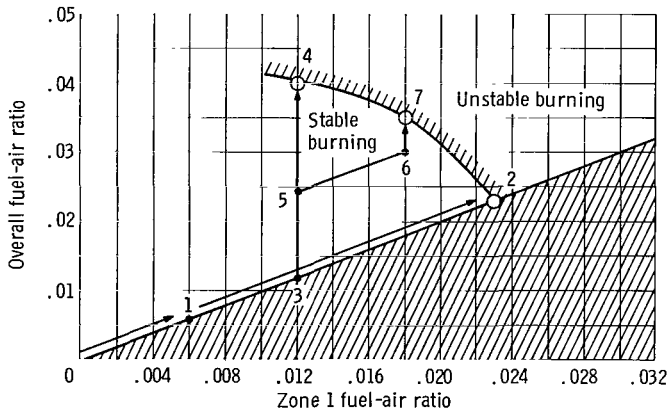

Figure 15. - Procedure for construction of an instability map. (This example is described in the section PROCEDURE.) Zone 1 primary fuel-air ratio, 0.006.

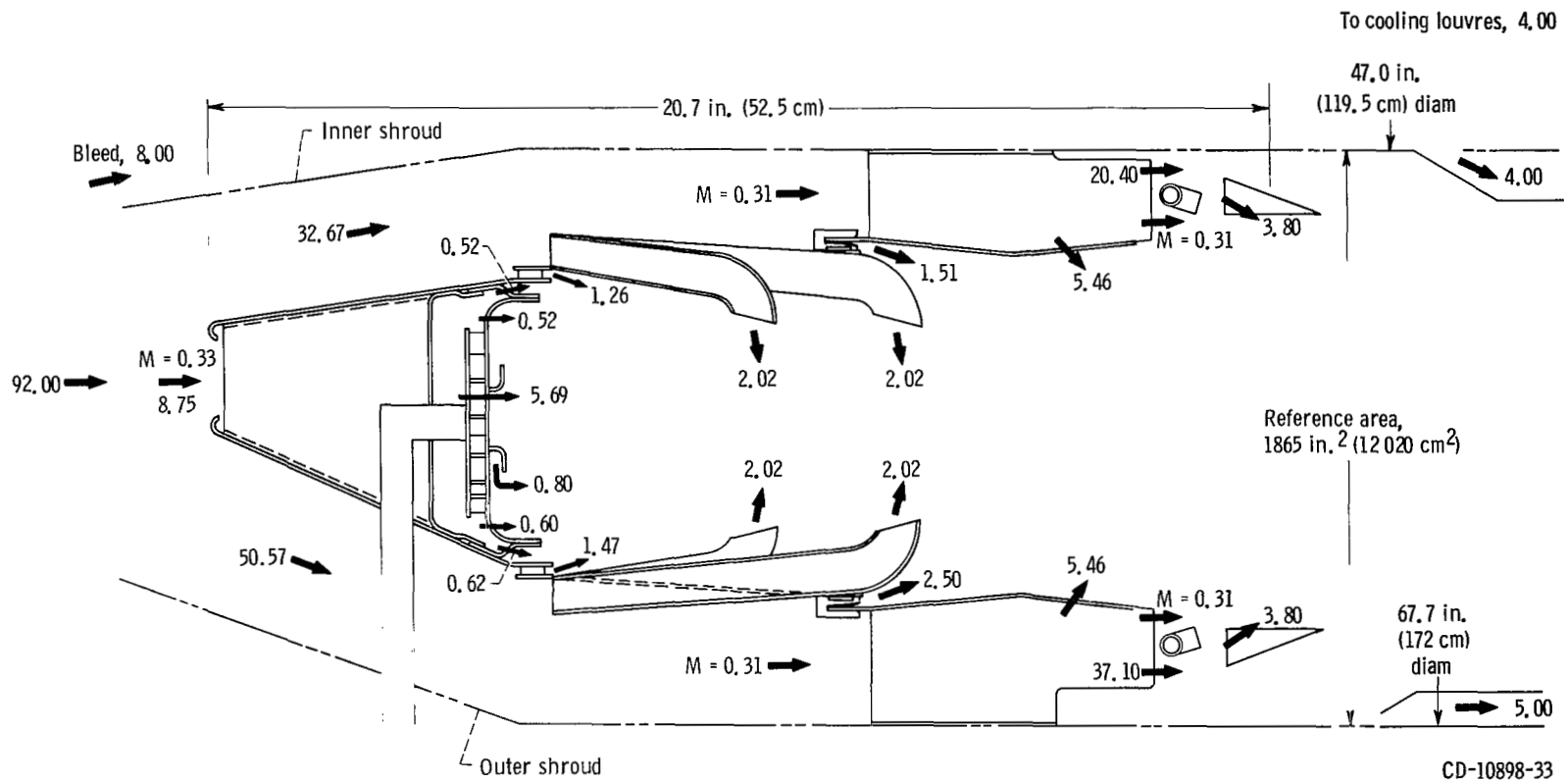

Figure 16. - Airflow splits within the combustor. Airflows given in percentage of total fan discharge. Mach number values on diagram are denoted by M.

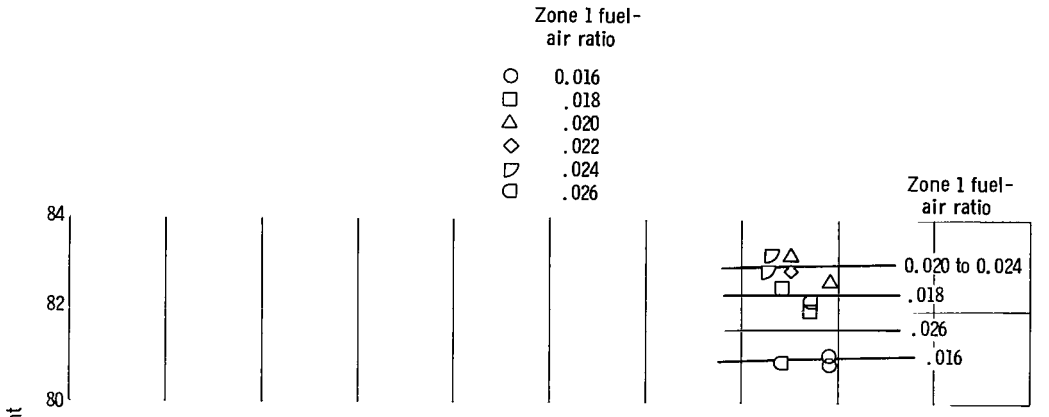

(a) Test condition 1. Combustor inlet values: pressure, 2/3 atmosphere; temperature, 200° F (367 K); reference Mach number, 0.138.

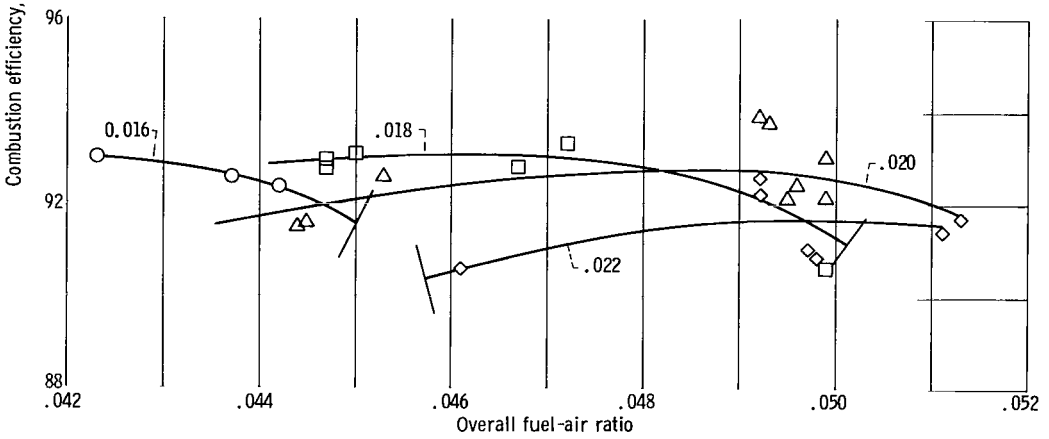

(b) Test condition 2. Combustor inlet values: pressure, 1 atmosphere; temperature, 285° F (414 K); reference Mach number, 0.144.

Figure 17. - Combustion efficiency at transonic climb conditions for Model B-NOTURB configuration. Twenty secondary fuel nozzles. Barriers (⊣) on the curves indicate location of incipient combustor pressure oscillations.

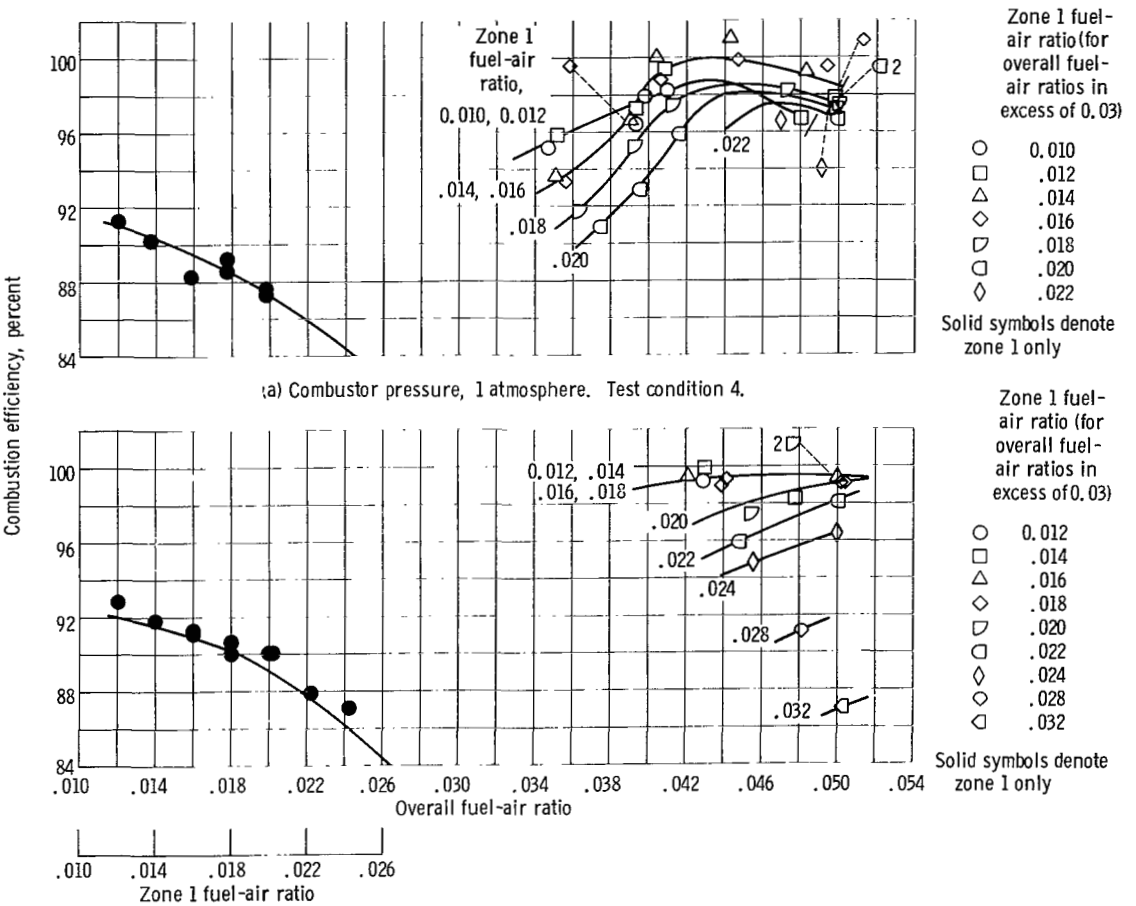

(b) Combustor pressure, 1.7 atmospheres. Test condition 5.

Figure 18. - Combustion efficiency at simulated cruise and simulated cruise-approach conditions for Model B-NOTURB configuration. Forty secondary nozzles. Reference Mach number, 0.175; inlet total temperature, 550° F (561 K). Barriers on curves (—|) indicate location of incipient combustor pressure oscillations.

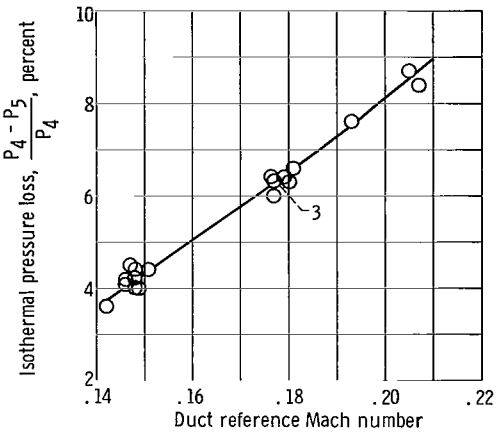

Figure 19. - Isothermal combustor pressure loss for Model B-NOTURB configuration. Zero fuel flow.

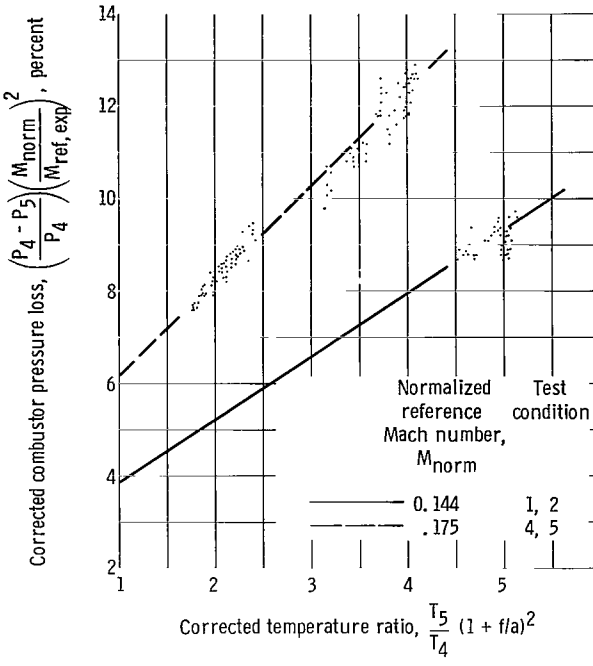

Figure 20. - Normalized combustor pressure losses for Model B-NOTURB configuration. Intercepts on Y-axis are from figure 19.

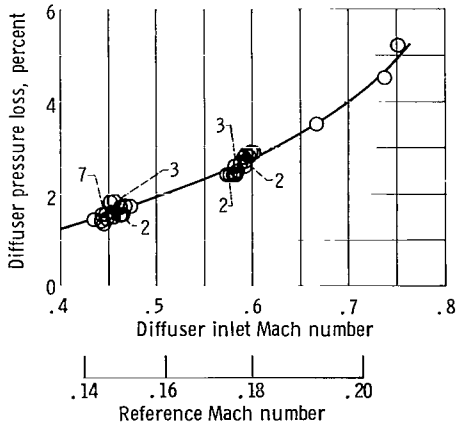

Figure 21. - Diffuser pressure loss. Test conditions 1 to 5; no combustion.

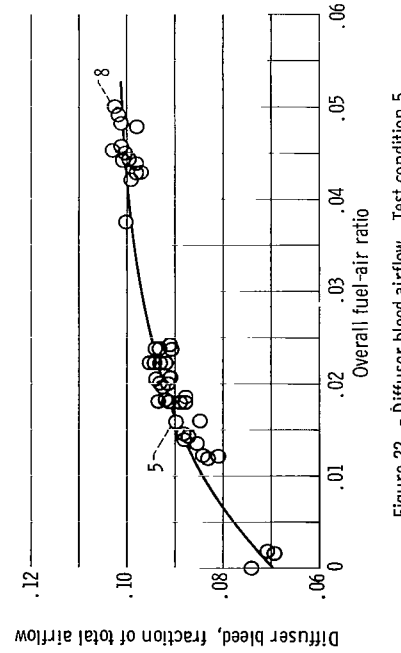

Figure 22. - Diffuser bleed airflow. Test condition 5.

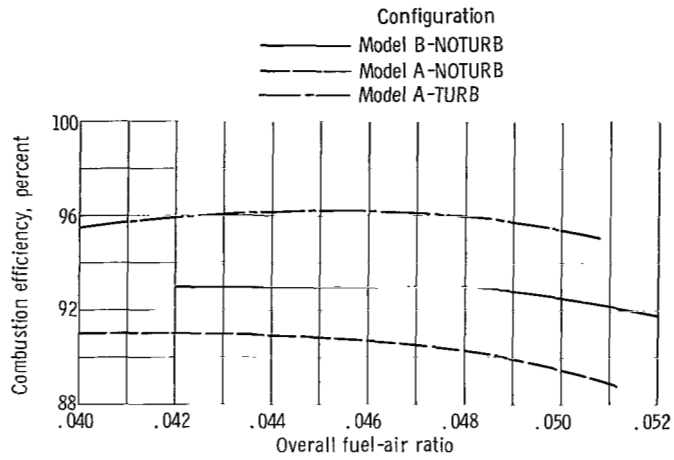

Figure 23. - Comparison of combustion efficiency data of Model A and Model B combustors at test condition 2. Twenty secondary zone 1 nozzles. Model A data are from reference 2.

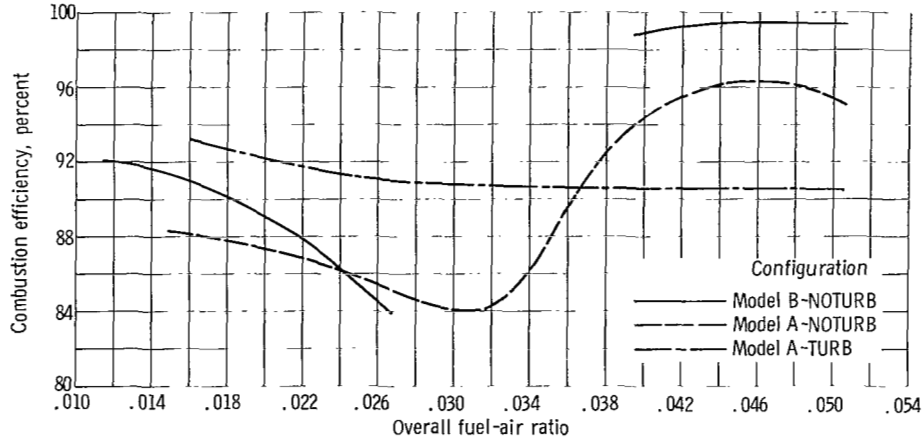

Figure 24. - Comparison of combustion efficiency data of Model A and Model B combustors at test condition 5. Forty secondary zone 1 nozzles. Model A data are from reference 2.

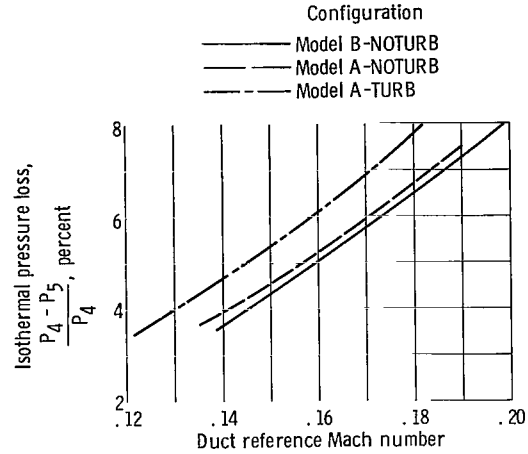

Figure 25. - Comparison of isothermal pressure loss data of Model A and Model B combustors. Model A data are from reference 2.

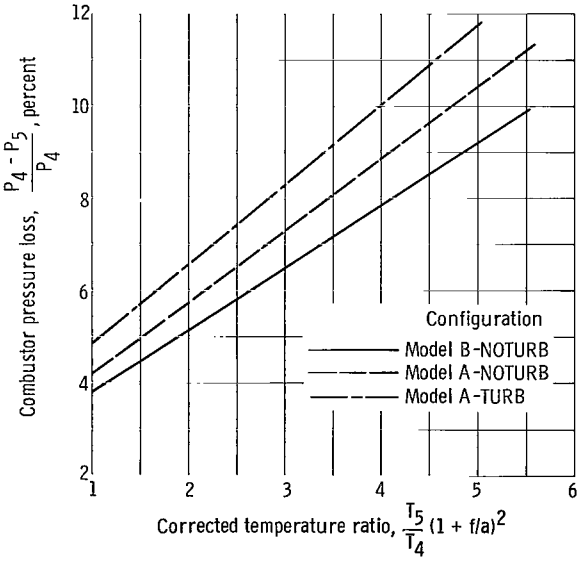

igure 26. - Comparison of pressure loss with heat addition for Model A and Model B combustors. Reference Mach number, 0.144. Model A data are from reference 2.

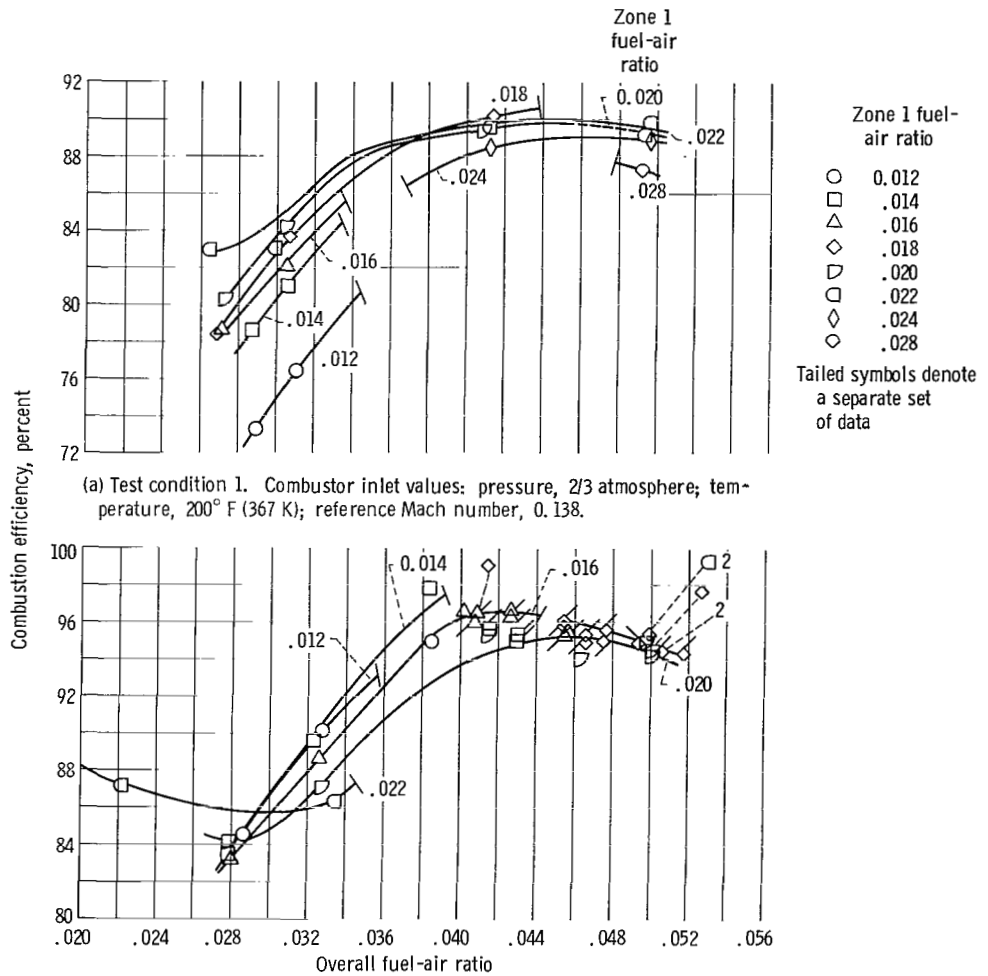

(a) Test condition 1. Combustor inlet values: pressure, 2/3 atmosphere; temperature, 200° F (367 K); reference Mach number, 0.138.

(b) Test condition 2. Combustor inlet values: pressure, 1.0 atmosphere; temperature, 285° F (414 K); reference Mach number, 0.144.

Figure 27. - Combustion efficiency at transonic climb conditions for model B-TURB configuration. Twenty secondary fuel nozzles. Barriers on curves (⊣) indicate location of incipient combustor pressure oscillations.

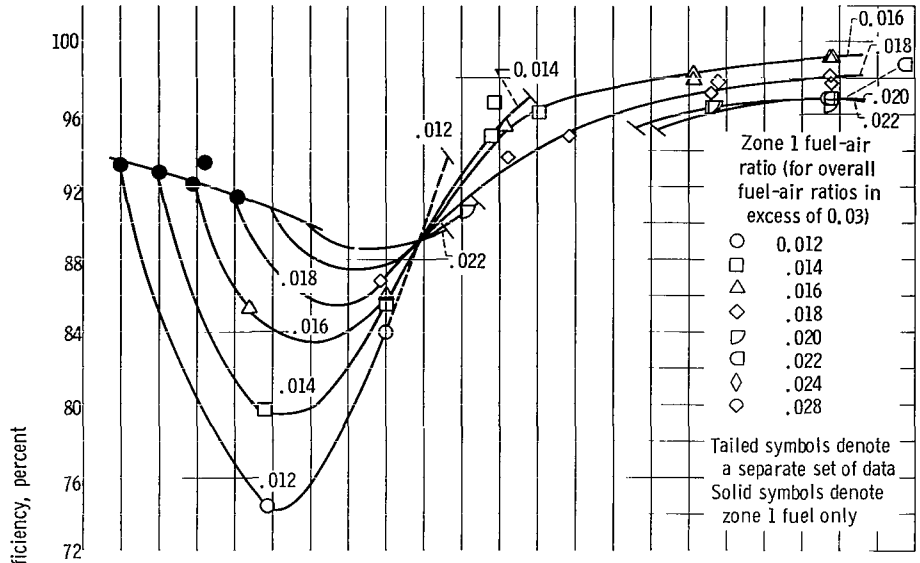

(a) Combustor pressure, 1 atmosphere. Test condition 4.

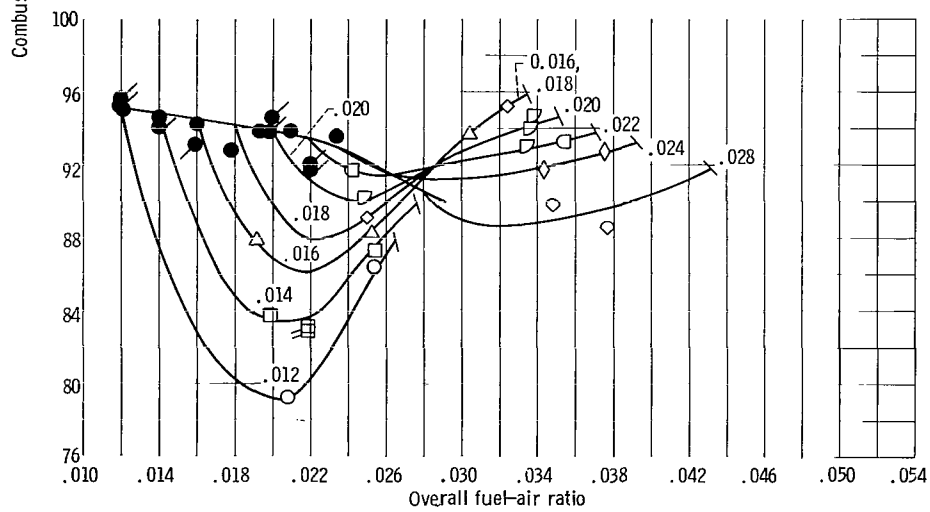

(b) Combustor pressure, 1.7 atmospheres. Test condition 5.

Figure 28. - Combustion efficiency for simulated cruise and simulated cruise-approach conditions for Model B-TURB configuration. Forty secondary nozzles. Reference Mach number, 0.175; inlet total temperature, 550° F (561 K). Barriers on curves (⊣) indicate location of incipient combustor pressure oscillations.

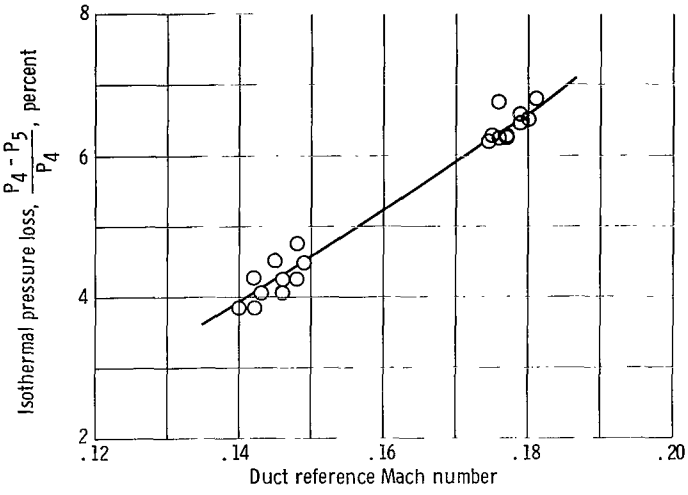

Figure 29. - Isothermal combustor pressure loss for Model B-TURB configuration.

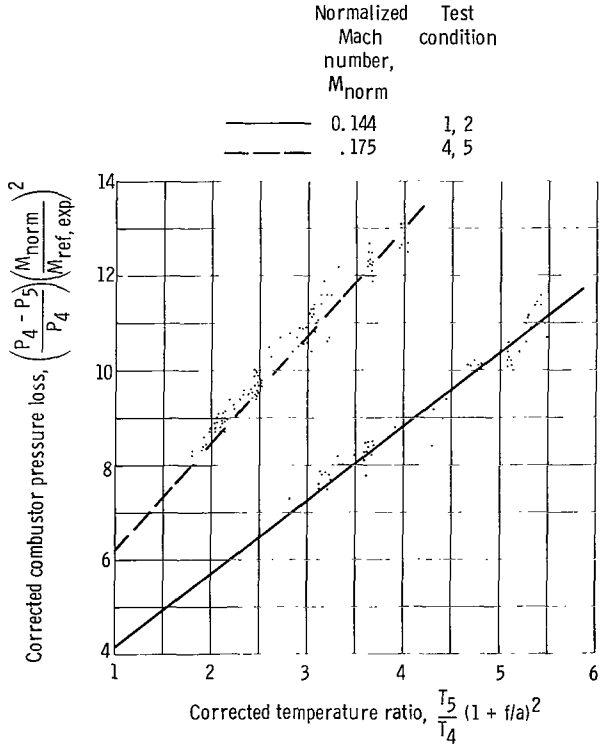

Figure 30. - Normalized combustor pressure loss for Model B-TURB configuration. Intercepts on Y-axis are from figure 29.

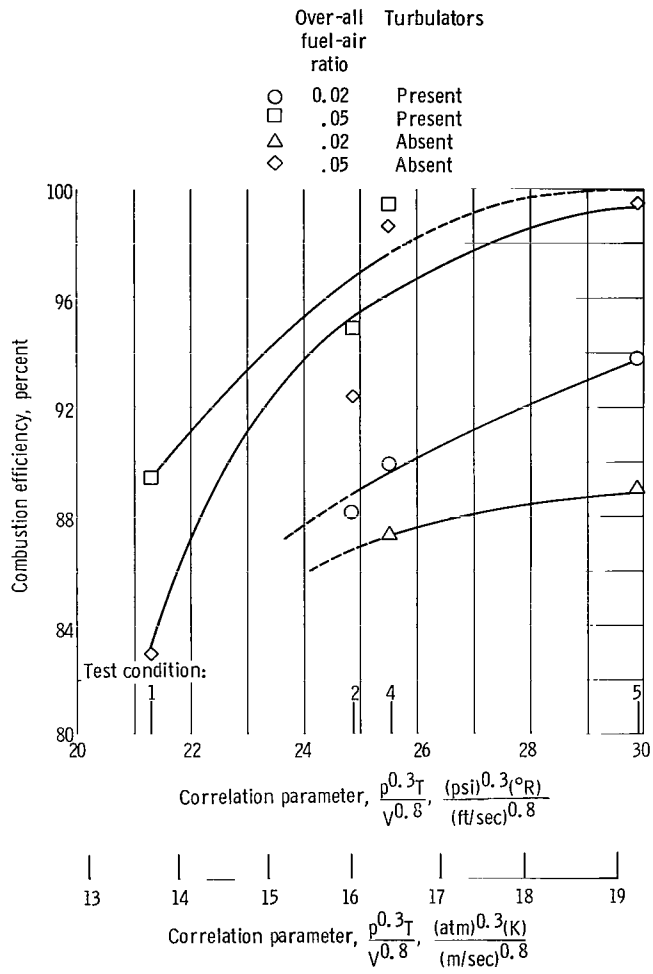

Figure 31. - Influence of inlet-air parameters on combustion efficiency. Fuel flow splits chosen for maximum value of combustion efficiency. Correlation parameter composed of inlet-air pressure, temperature, and velocity.

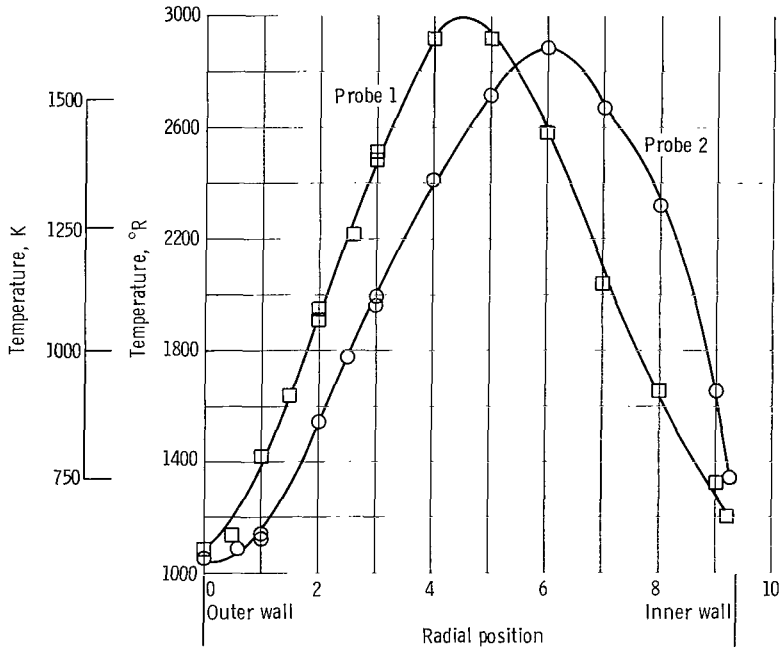

Figure 32. - Combustor exit temperature profile for Model B-NOTURB configuration at test condition 4. Overall fuel-air ratio of 0.018 provided by 40 secondary fuel nozzles. Probes are 37° apart and are located in annulus at nozzle throat.

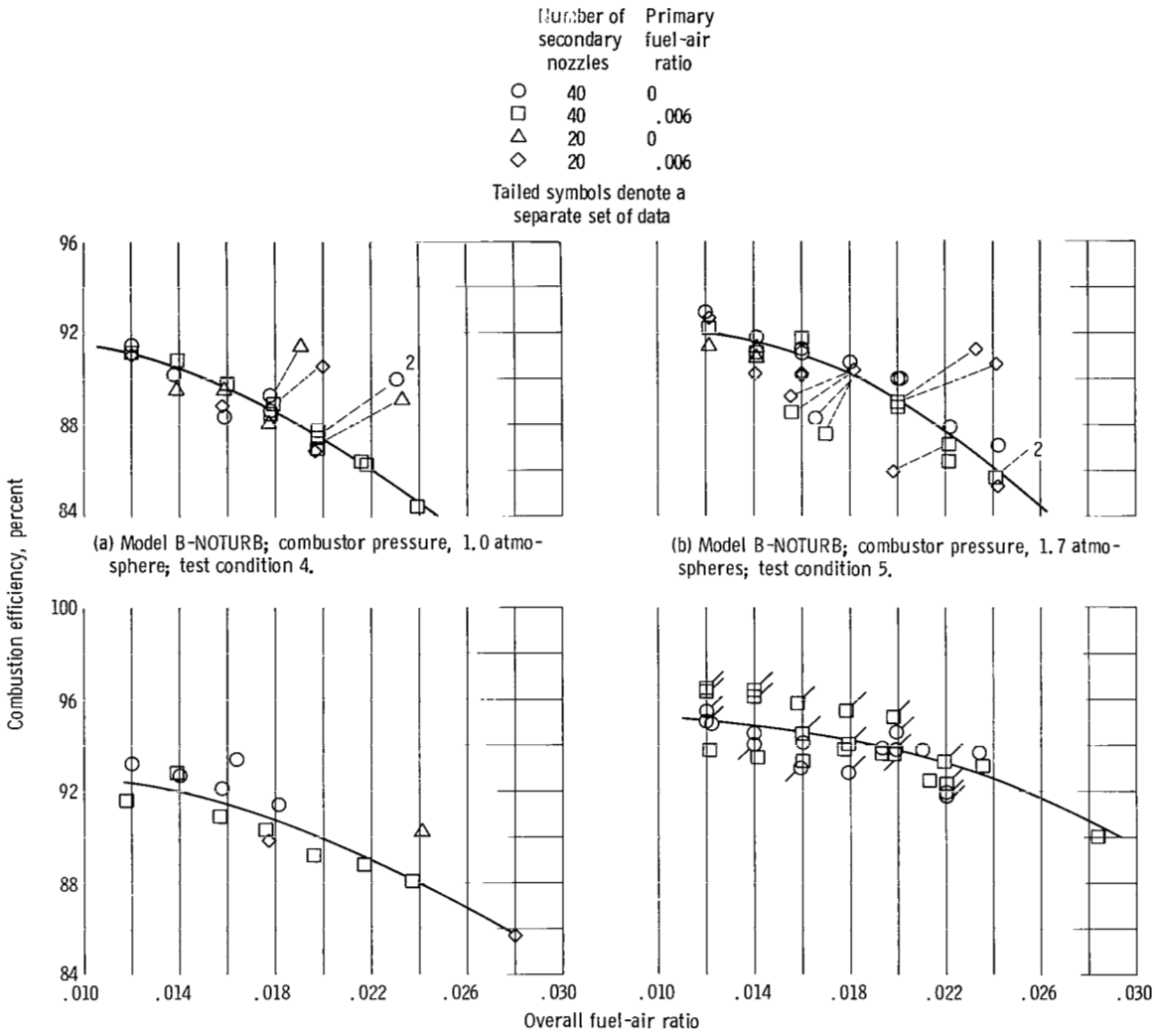

(a) Model B-NOTURB; combustor pressure, 1.0 atmosphere; test condition 4.

(b) Model B-NOTURB; combustor pressure, 1.7 atmospheres; test condition 5.

(c) Model B-TURB; combustor pressure, 1.0 atmosphere; test condition 4.

(d) Model B-TURB; combustor pressure, 1.7 atmospheres; test condition 5.

Figure 33. - Combustion efficiency at simulated cruise conditions. Reference Mach number, 0.175; inlet total temperature, 550° F (561 K). No zone 2 fuel.

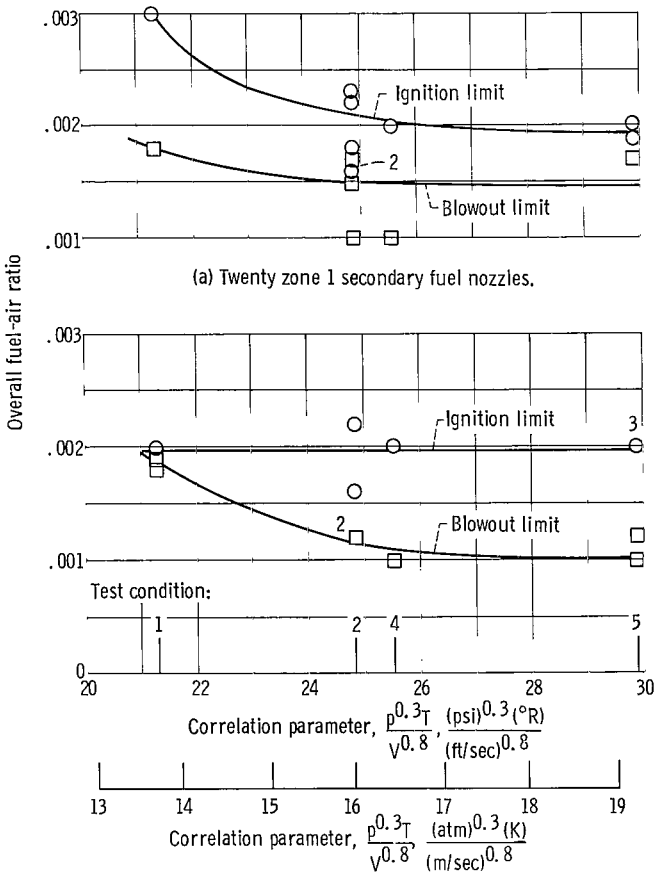

Figure 34. - Blowout and relight data obtained by slowly changing fuel flow rate while maintaining a constant test condition. Correlation parameter composed of inlet-air pressure, temperature, and velocity.

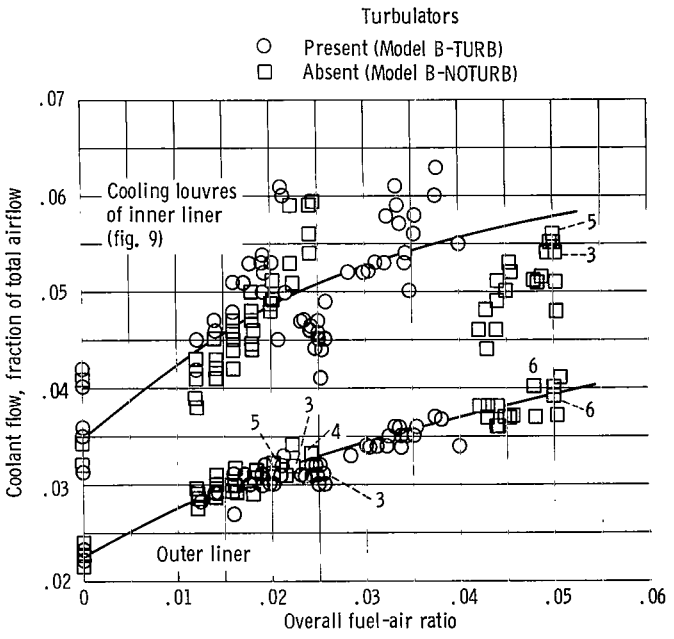

Figure 35. - Cooling liner airflow rates obtained at test condition 5.

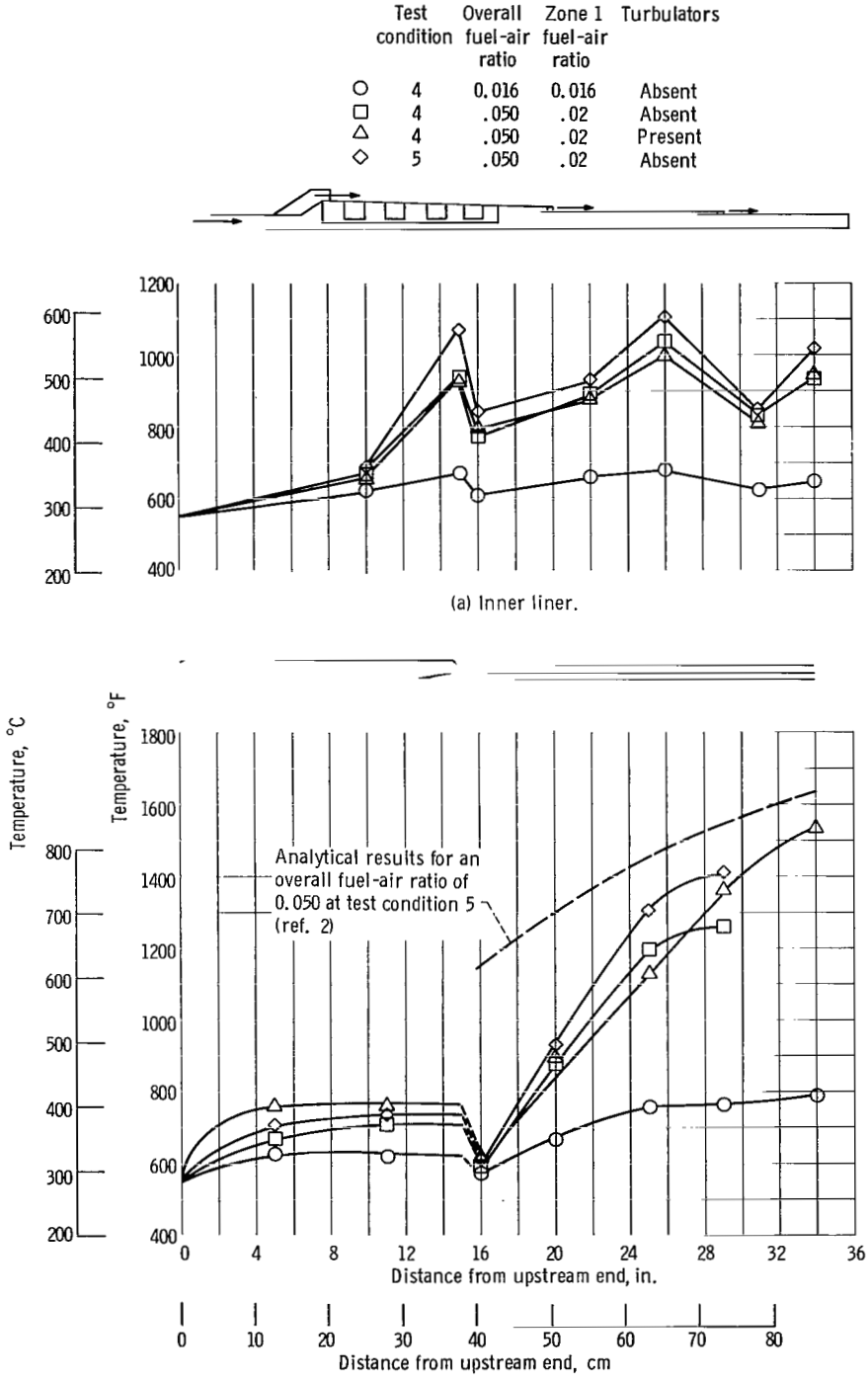

(a) Inner liner.

(b) Outer liner.

Figure 36. - Wall temperature profile of tailpipe liners.

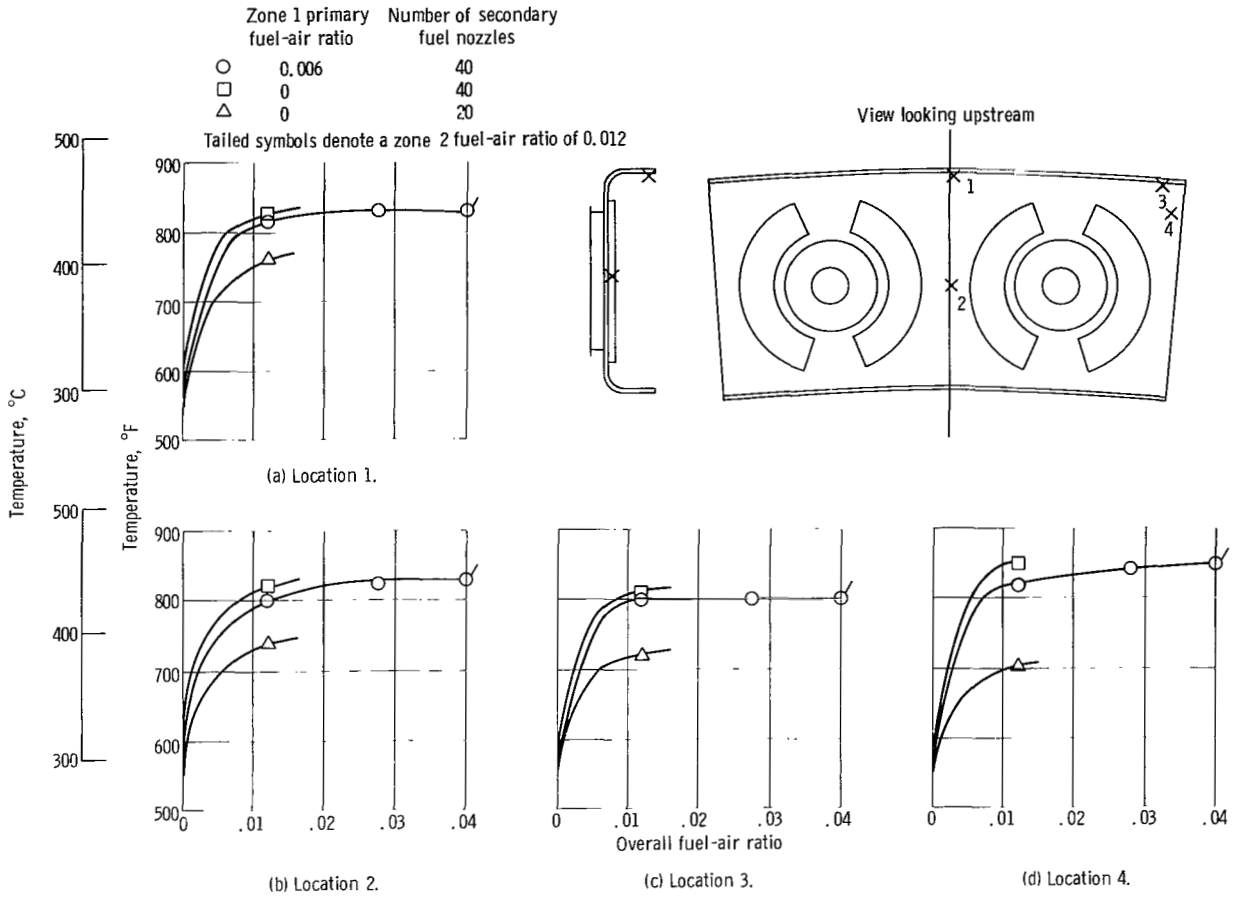

Figure 37. - Combustor firewall temperature at test condition 5. Unless stated otherwise, only zone 1 fuel injectors used.

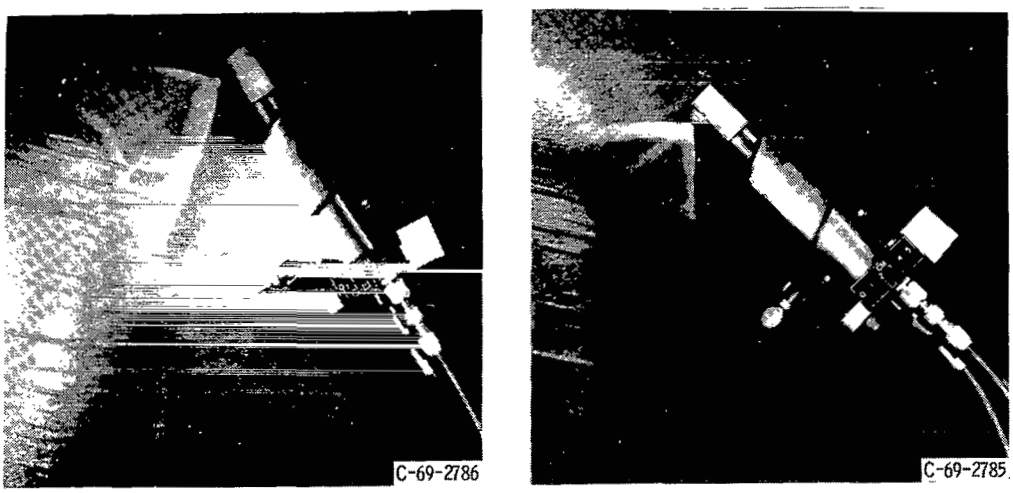

(a) Zone 1 secondary nozzle flowing at 500 psi (33 atm) and showing essentially no streaking.

(b) Zone 1 nozzle demonstrating moderate amount of streaking.

Figure 38. - Typical spray patterns after 1 year of intermittent use.

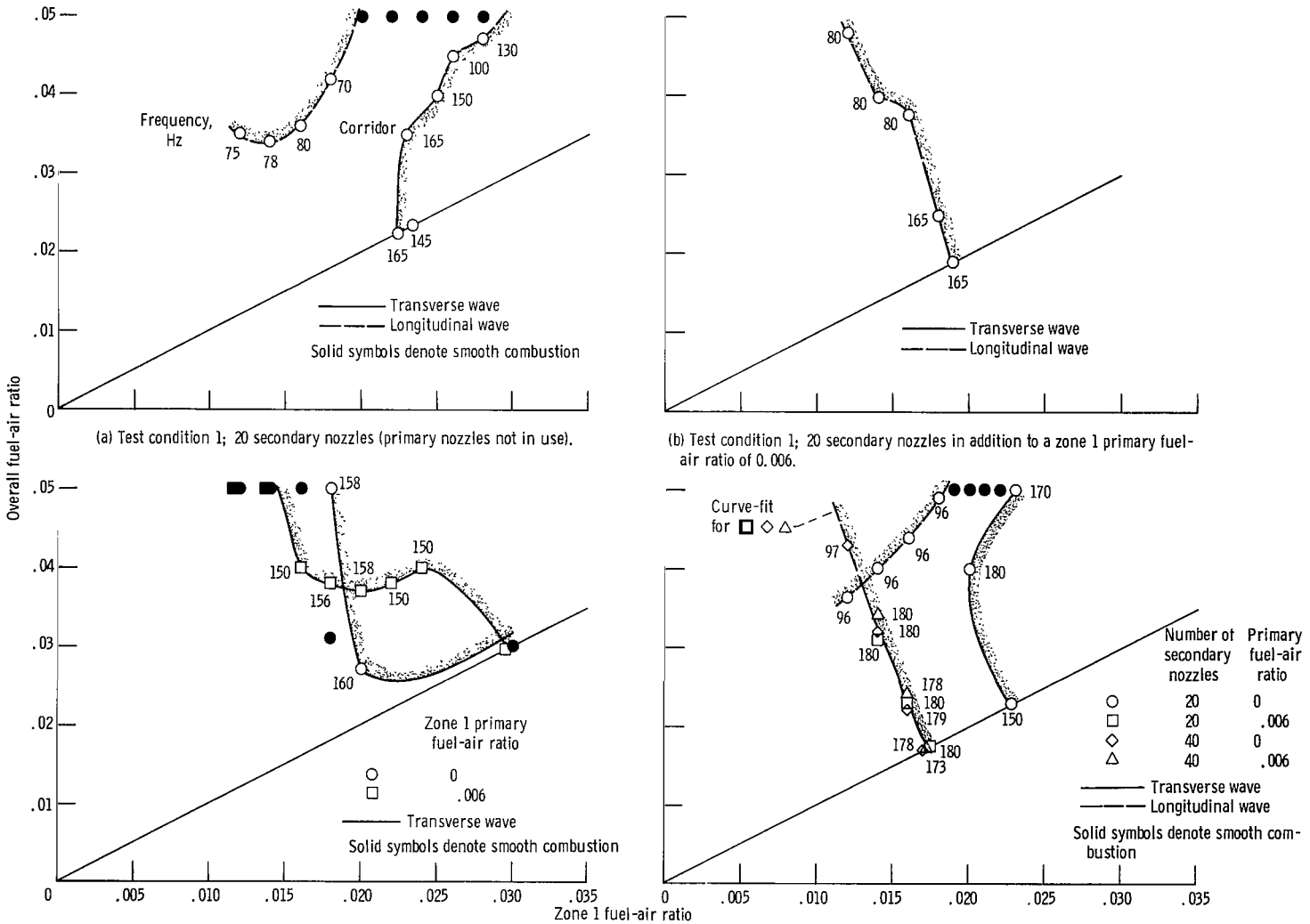

(a) Test condition 1; 20 secondary nozzles (primary nozzles not in use).

(b) Test condition 1; 20 secondary nozzles in addition to a zone 1 primary fuel-air ratio of 0.006.

(c) Test condition 1; 40 secondary nozzles.

(d) Test condition 2.

Figure 39. - Combustion instability maps for Model B-TURB configuration.

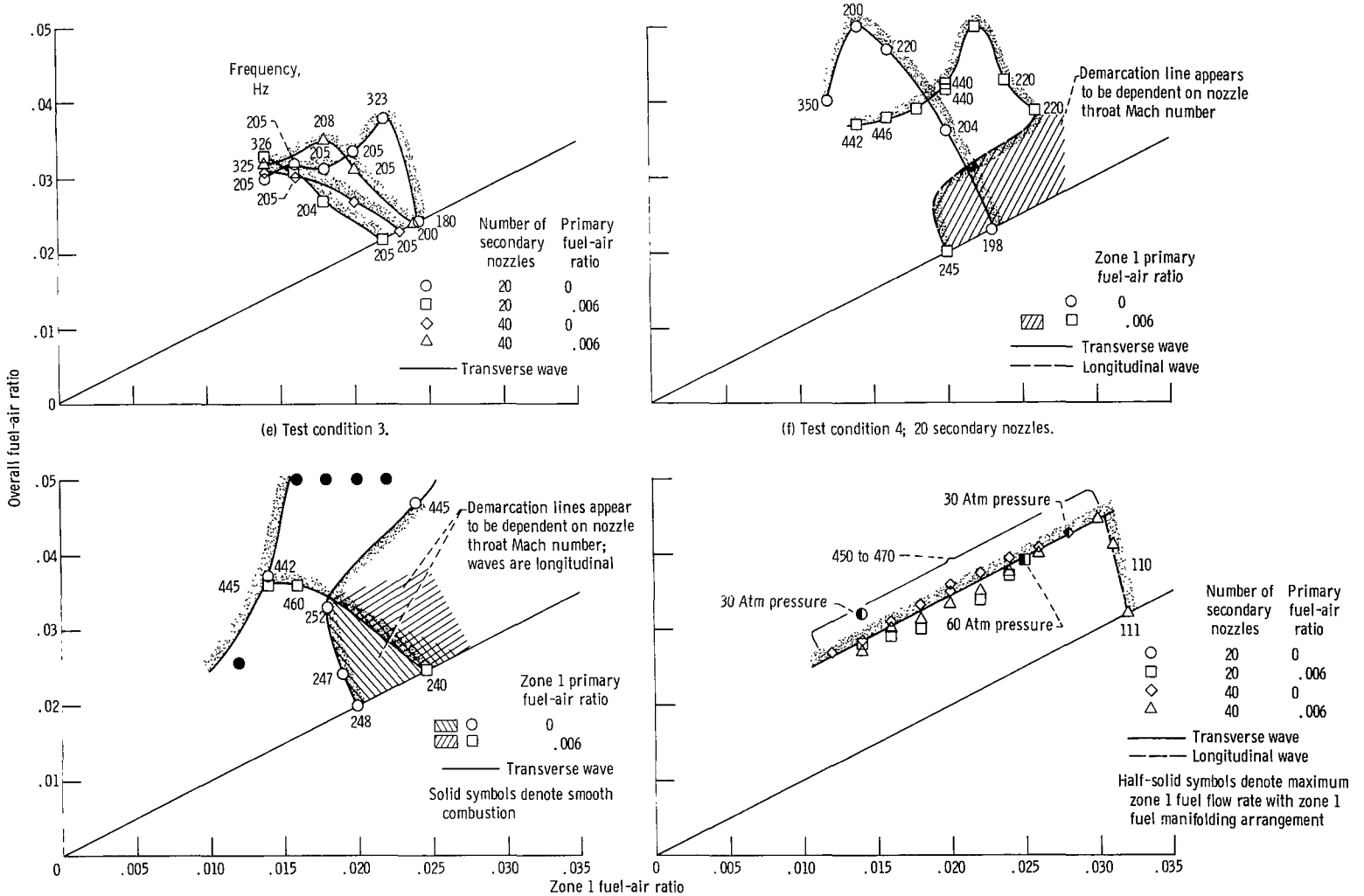

(e) Test condition 3.

(f) Test condition 4; 20 secondary nozzles.

(g) Test condition 4; 40 secondary nozzles.

(h) Test condition 5.

Figure 39 . - Concluded.

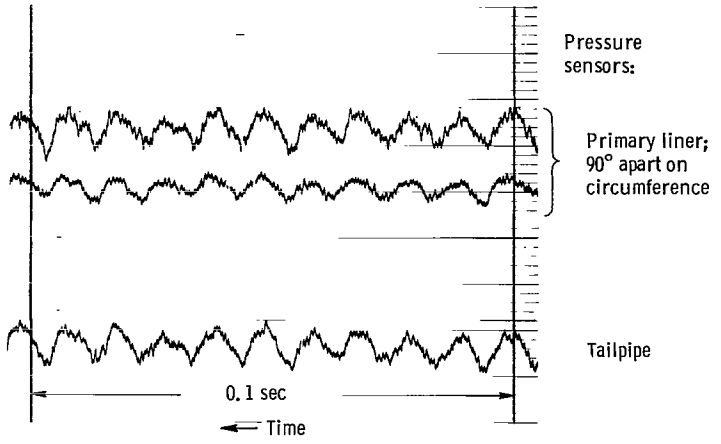

(a) Longitudinal, 98-hertz pressure waves; combustor inlet-air temperature, 285° F (414 K).

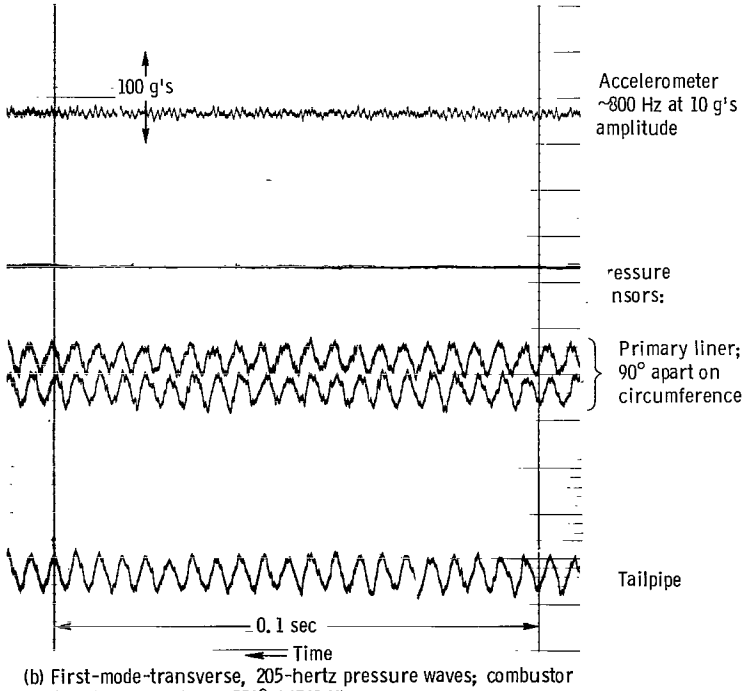

(b) First-mode-transverse, 205-hertz pressure waves; combustor inlet-air temperature, 550° F (561 K).

Figure 40. - Oscillatory behavior of gas-pressure sensors and a test apparatus accelerometer. Pressure amplitude of gases in primary liner region, approximately 1/20 atmosphere peak-to-peak (all pressure scales are the same size and are inverted).

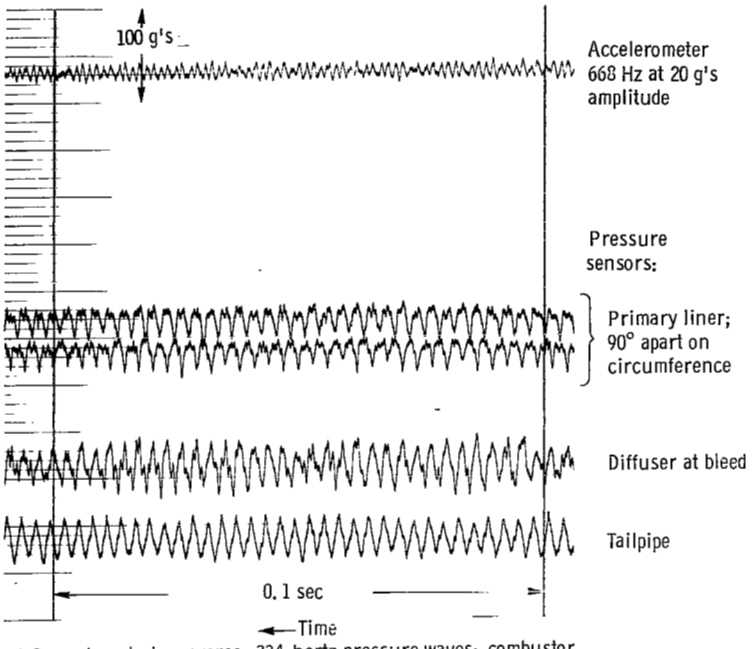

(c) Second-mode-transverse, 334-hertz pressure waves; combustor inlet-air temperature, 550° F (561 K).

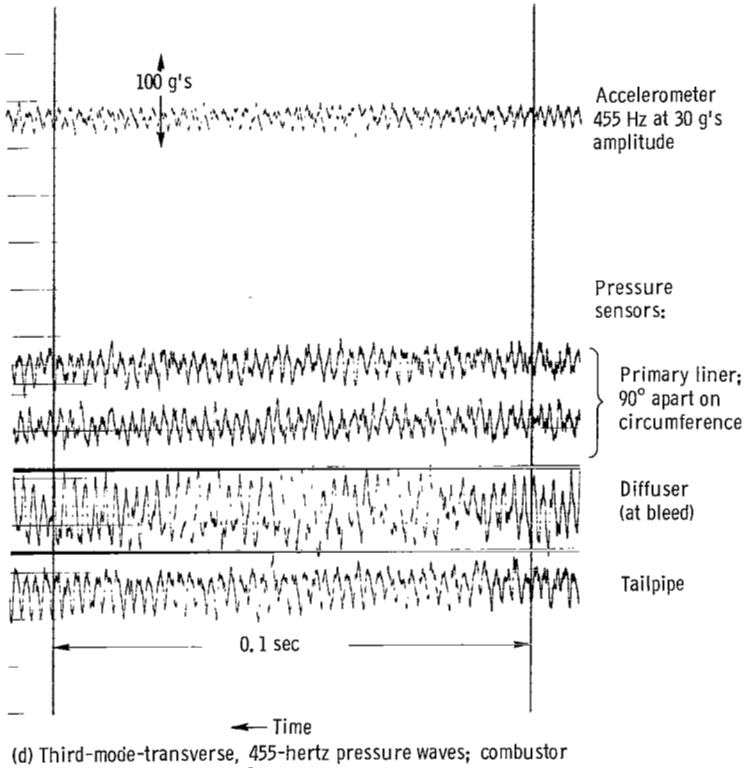

(d) Third-mode-transverse, 455-hertz pressure waves; combustor inlet-air temperature, 550° F (561 K).

Figure 40. - Concluded.

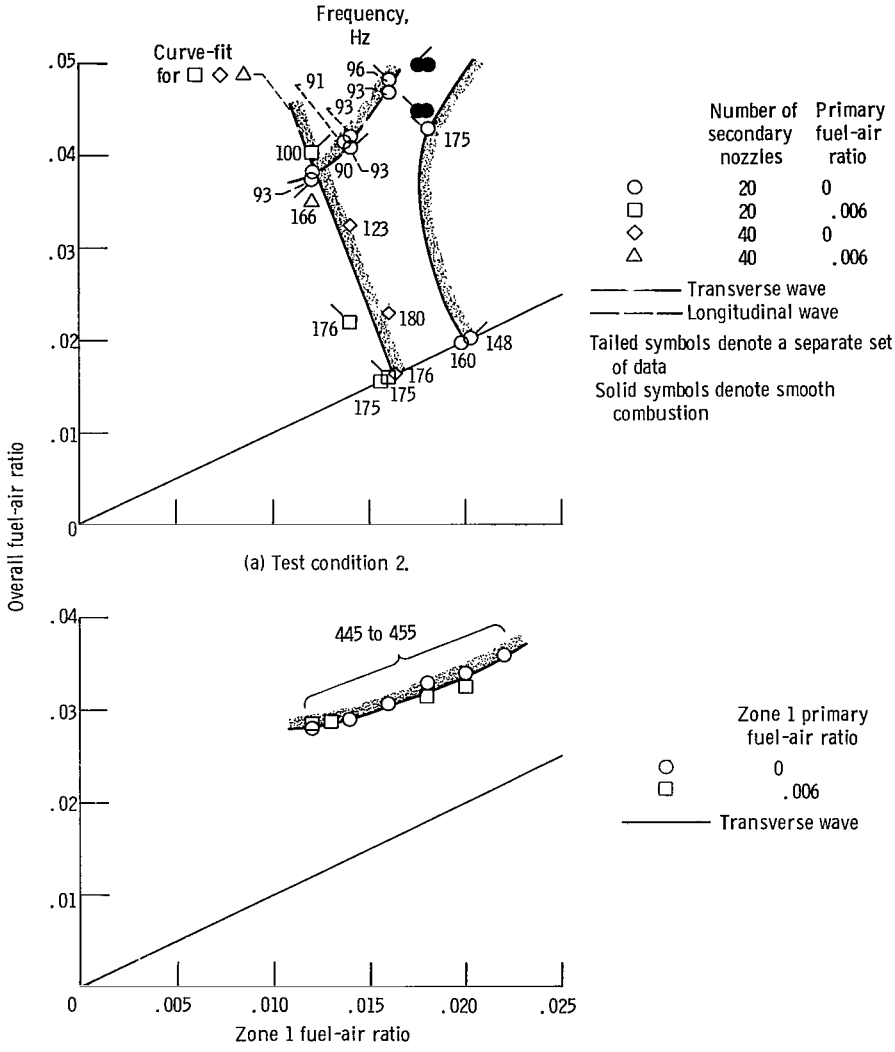

(a) Test condition 2.

(b) Test condition 5; 40 secondary nozzles.

Figure 41. - Combustion instability maps for Model B-TURB configuration when zone 1 fuel nozzles were producing streaked sprays.

(a) Outer liner.

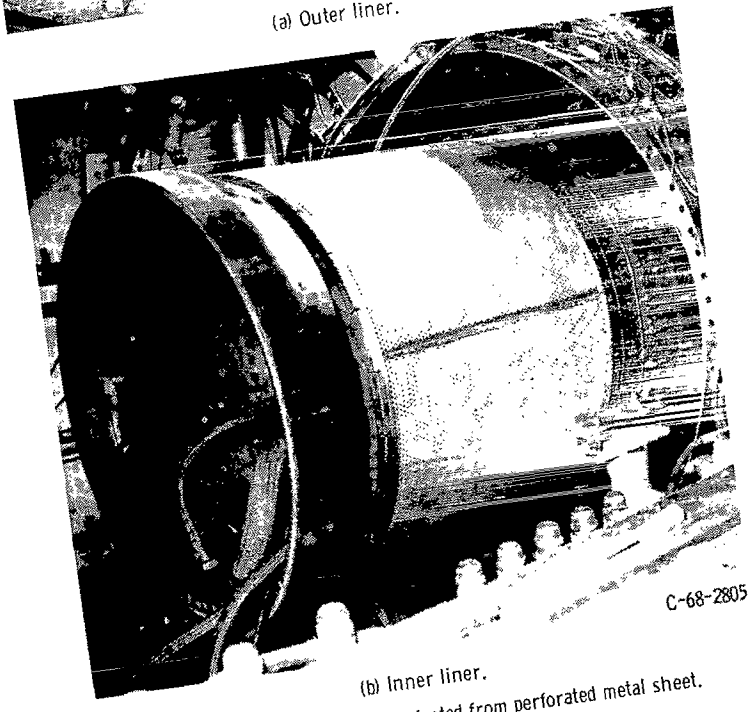

(b) Inner liner.

Figure 42. - Tailpipe liners fabricated from perforated metal sheet.

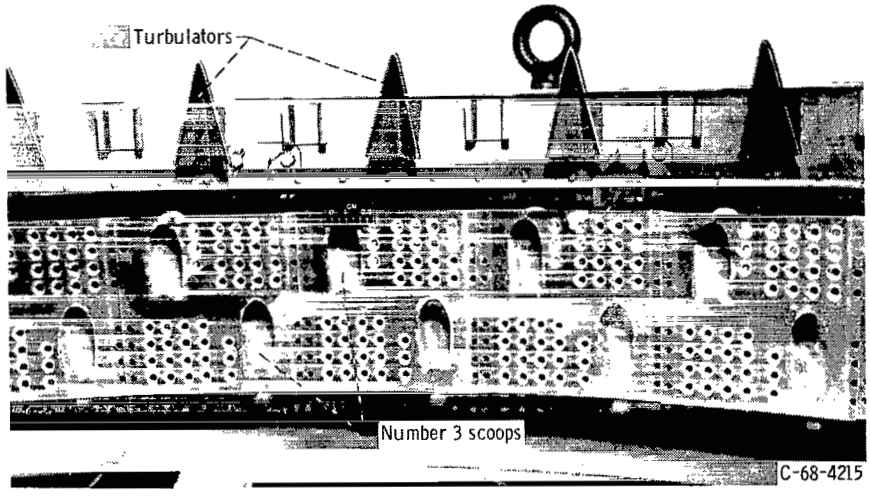

(a) Outer liner.

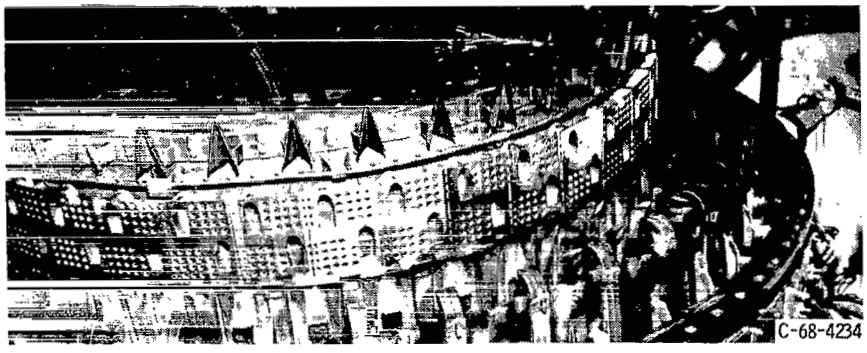

(b) Inner liner.

Figure 43. - Redesigned secondary liner.

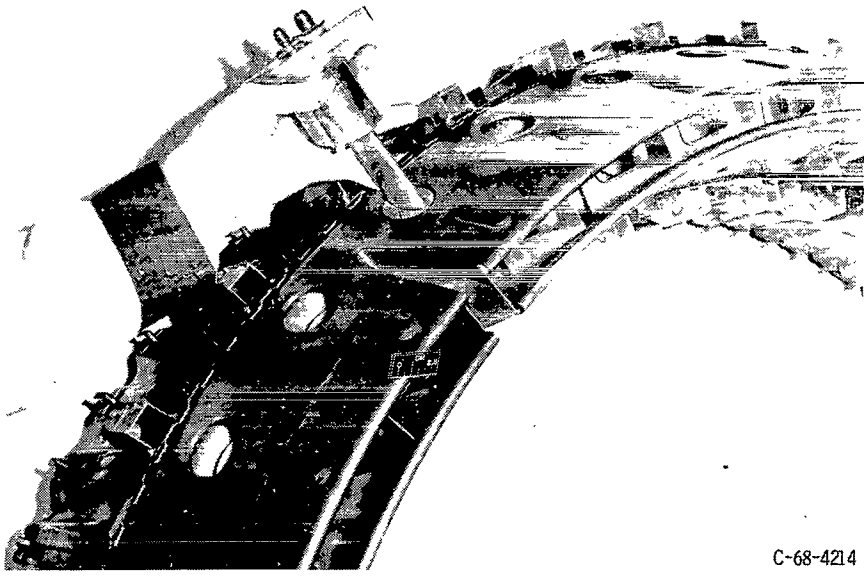

C-68-4214

(a) Looking downstream.

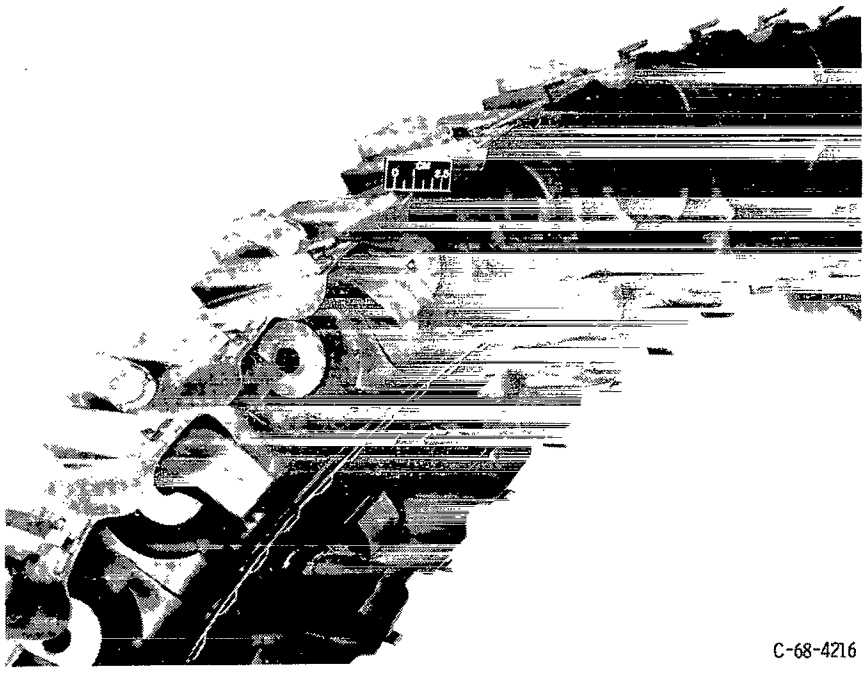

C-68-4216

(b) Looking upstream.

Figure 44. - Primary liner modification showing the scoops that were added immediately upstream of the number 1 scoops.

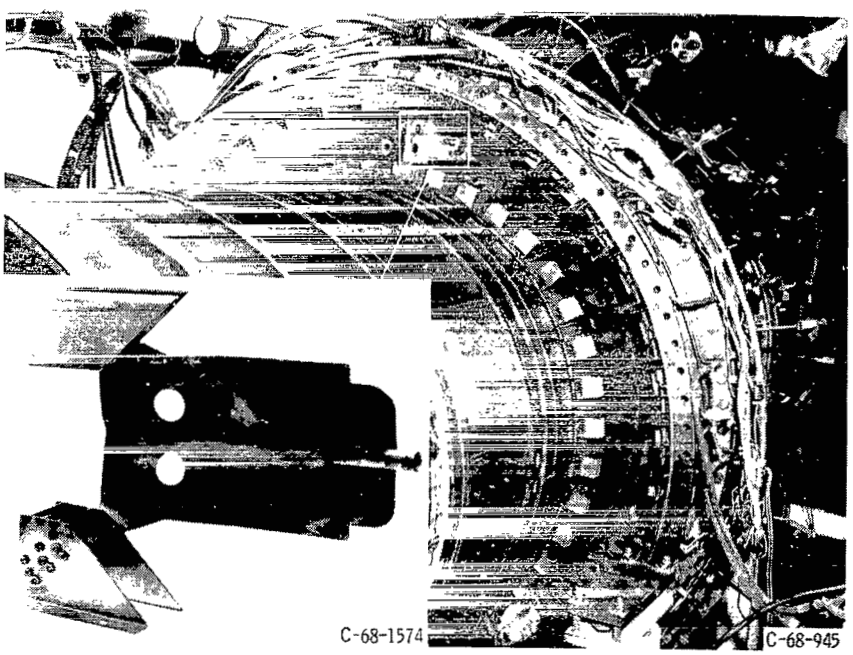

Figure 45. - Baffle plates and large secondary scoops.

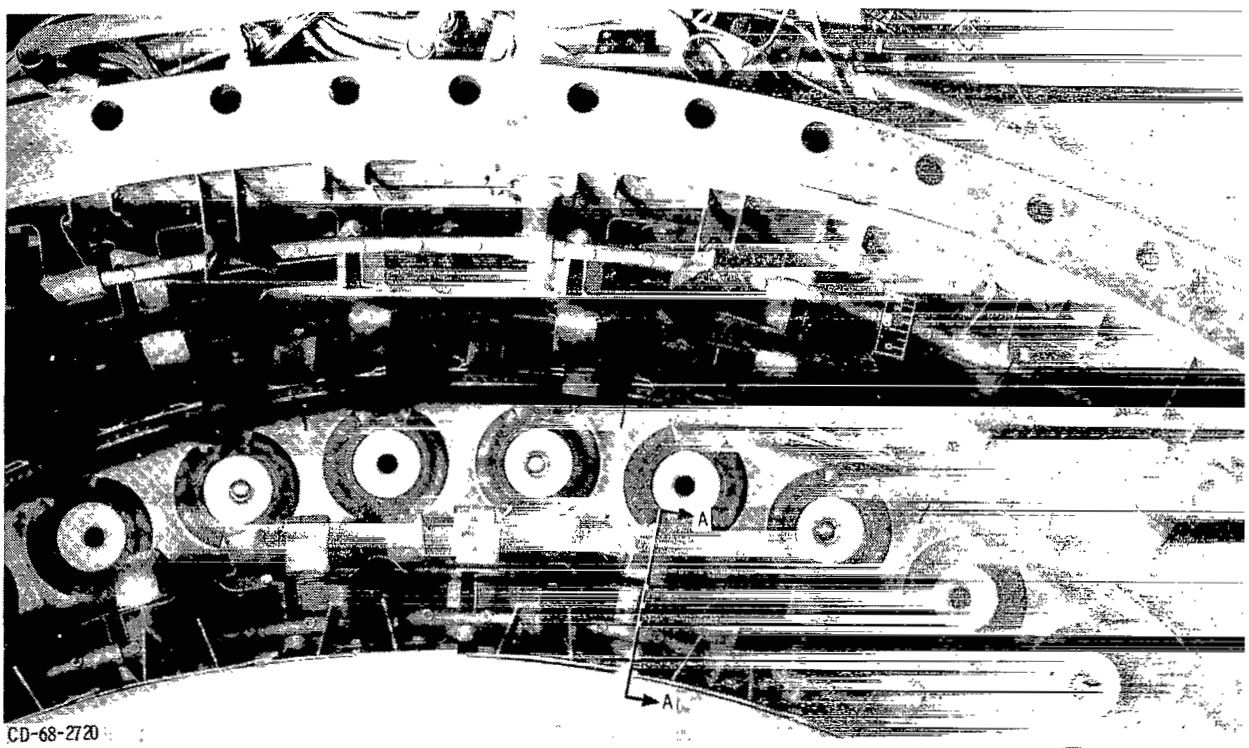

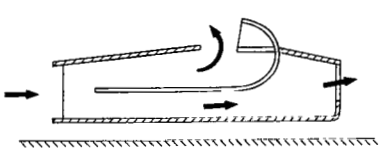

Section A-A

CD-10899-33

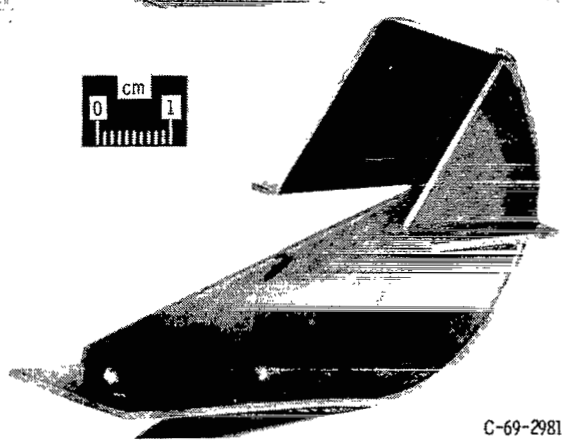

C-69-2981

Figure 46. - Reverse scoops in number 3 position.

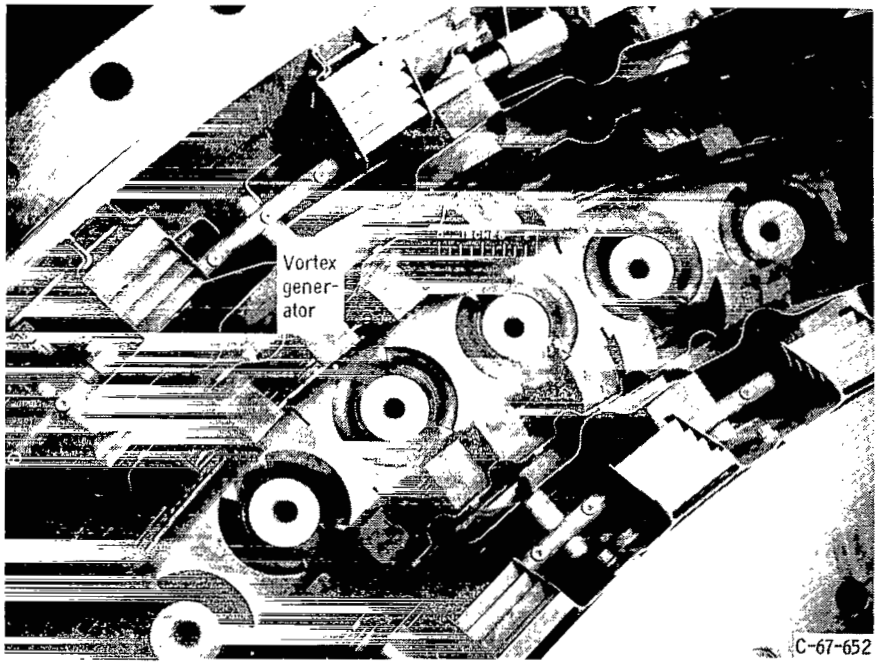

Figure 47. - Original number 4 scoops (vortex generators).

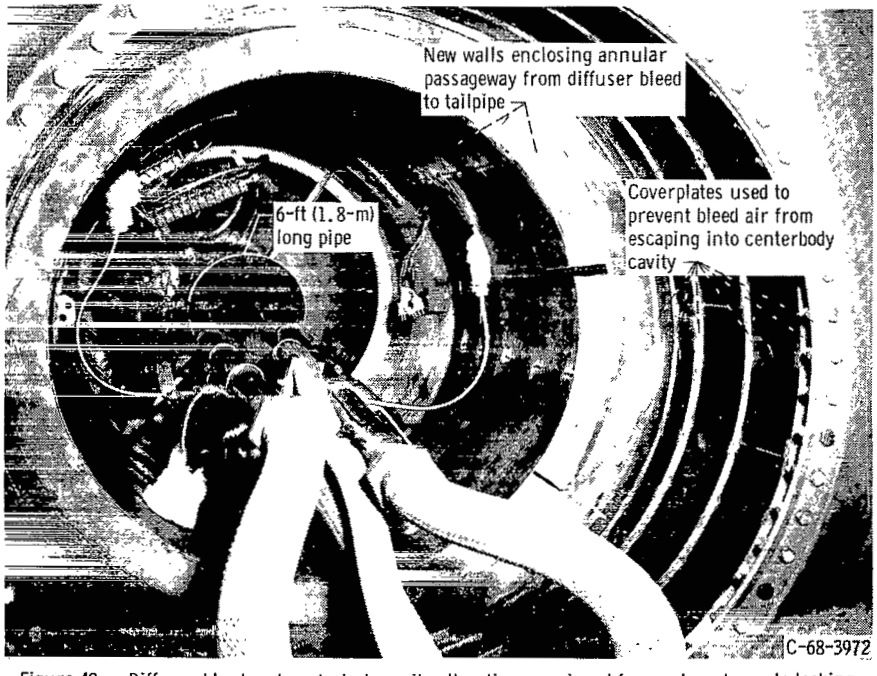

Figure 48. - Diffuser bleed and centerbody cavity alterations as viewed from exhaust nozzle looking upstream.

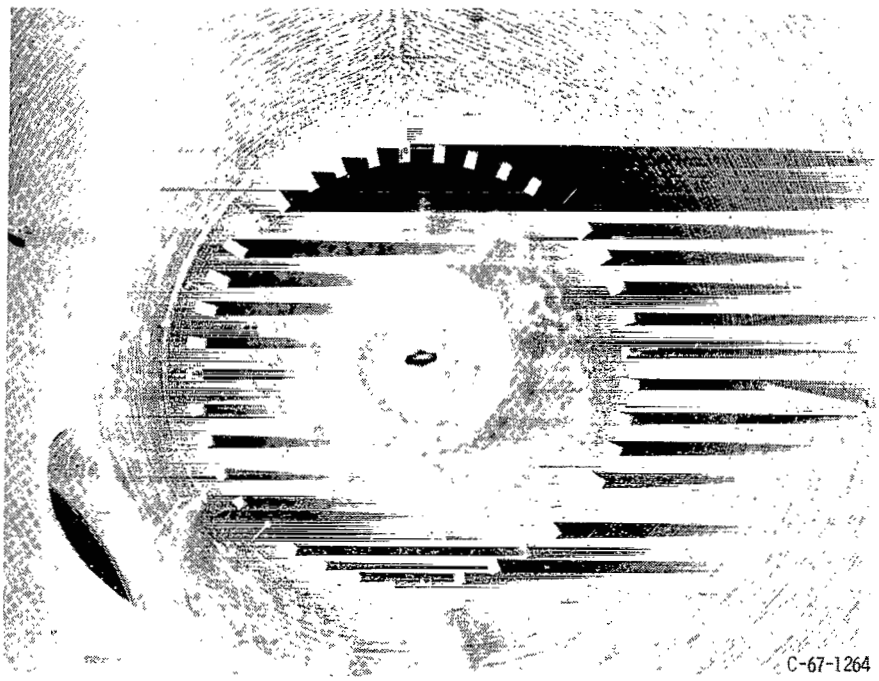

Figure 49. - Looking downstream at diffuser vanes. Vane setting, 60°.

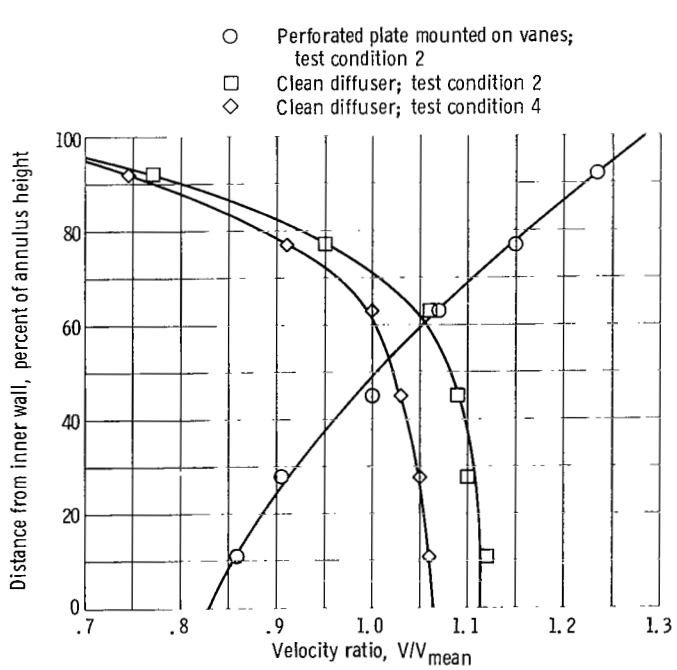

Figure 50. - Radial velocity profiles at diffuser exit.

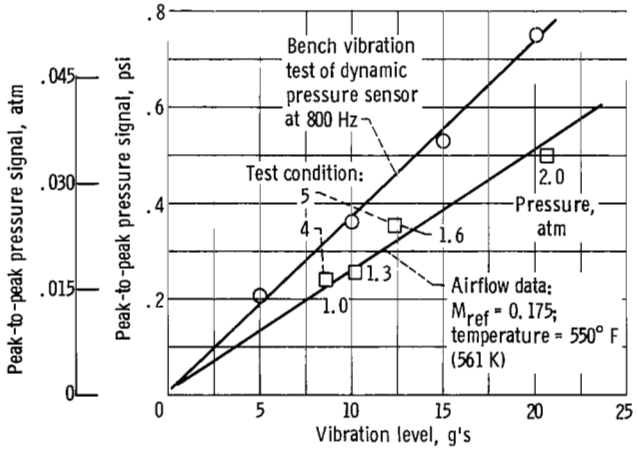

Figure 51. - Noise data for a dynamic pressure sensor. Accelerometer mounted alongside pressure transducer. Airflow data obtained with instruments mounted on combustor casing at primary-liner location.

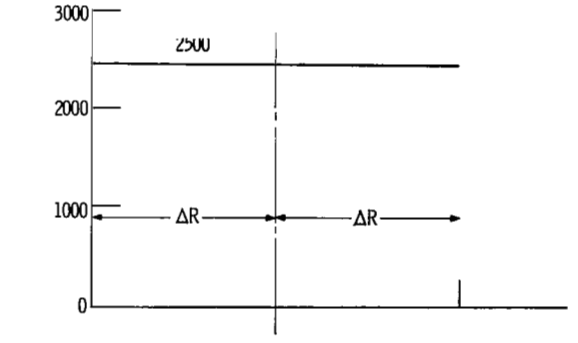

(a) Average exhaust temperature of 2500° R with a flat profile. T(r) = 2500° R; T_{av} = 2500° R.

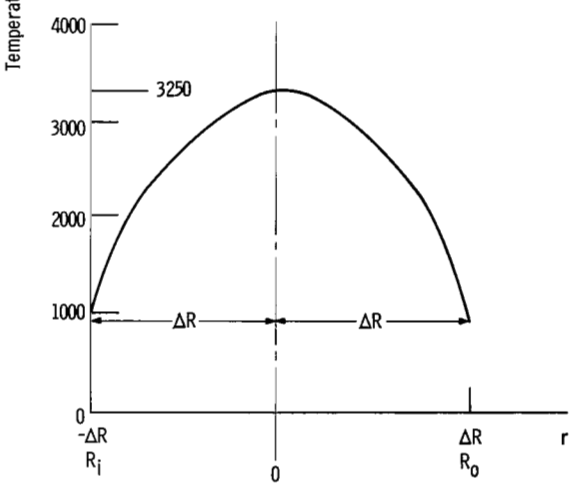

(b) Average exhaust temperature of 2500° R with a parabolic profile. $T(r) = \frac{2250}{\overline{\Delta R}^2}(1.445\,\overline{\Delta R}^2 - r^2)$ degree Rankine units, T_{av} = 2500° R.

Figure 52. - Gas temperature profile models. See appendix C.

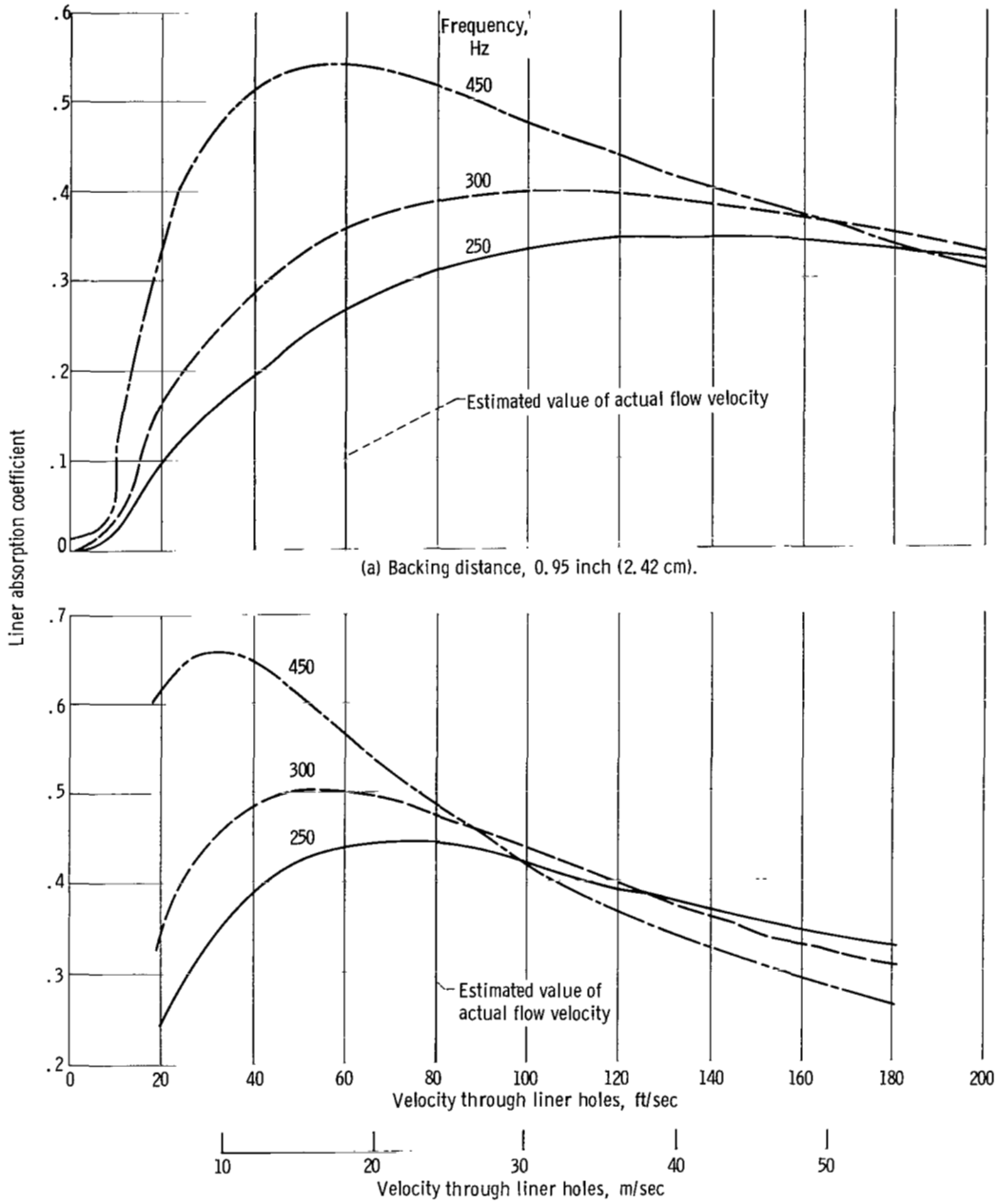

Figure 53. - Effect of velocity through the liner holes on analytical value of absorption coefficient. Pressure, 1.7 atmospheres; temperature, 1010° R (561 K); pressure amplitude, 175 decibels; wall thickness, 0.125 inch (0.32 cm); liner hole diameter, 0.187 inch (0.48 cm); open area ratio, 0.13.

NASA-Langley, 1971 —— 33 E-5679

03U 001 53 51 3DS 71043 00903
AIR FORCE WEAPONS LABORATORY /WLOL/
KIRTLAND AFB, NEW MEXICO 87117

ATT E. LOU BOWMAN, CHIEF,TECH. LIBRARY

"The aeronautical and space activities of the United States shall be conducted so as to contribute . . . to the expansion of human knowledge of phenomena in the atmosphere and space. The Administration shall provide for the widest practicable and appropriate dissemination of information concerning its activities and the results thereof."

—NATIONAL AERONAUTICS AND SPACE ACT OF 1958

NASA SCIENTIFIC AND TECHNICAL PUBLICATIONS

TECHNICAL REPORTS: Scientific and technical information considered important, complete, and a lasting contribution to existing knowledge.

TECHNICAL NOTES: Information less broad in scope but nevertheless of importance as a contribution to existing knowledge.

TECHNICAL MEMORANDUMS: Information receiving limited distribution because of preliminary data, security classification, or other reasons.

CONTRACTOR REPORTS: Scientific and technical information generated under a NASA contract or grant and considered an important contribution to existing knowledge.

TECHNICAL TRANSLATIONS: Information published in a foreign language considered to merit NASA distribution in English.

SPECIAL PUBLICATIONS: Information derived from or of value to NASA activities. Publications include conference proceedings, monographs, data compilations, handbooks, sourcebooks, and special bibliographies.

TECHNOLOGY UTILIZATION PUBLICATIONS: Information on technology used by NASA that may be of particular interest in commercial and other non-aerospace applications. Publications include Tech Briefs, Technology Utilization Reports and Technology Surveys.

Details on the availability of these publications may be obtained from:

SCIENTIFIC AND TECHNICAL INFORMATION OFFICE

NATIONAL AERONAUTICS AND SPACE ADMINISTRATION

Washington, D.C. 20546